UNIVERSITY OF SASSARI

DISSERTATION OF THE DEGREE OF PhD SCHOOL
IN NATURAL SCIENCE
UNIVERSITY OF SASSARI, 2010
XXII CYCLE

INTERDISCIPLINARY STUDIES FOR THE KNOWLEDGE OF THE GROUNDWATER FLUORIDE CONTAMINATION IN THE EASTERN AFRICAN RIFT: MERU DISTRICT – NORTH TANZANIA

Candidate:
Daniele Pittalis

Supervisor:
Prof. Marco Apollonio

Tutor*:*
Prof. Giorgio Ghiglieri

Co-Tutor:
Prof. Giacomo Oggiano

Dedicated to my love:

Angela

For a lot of beautiful sensations and mainly because… I love you
thank you, Ange

Groundwater studies do not create more water, but good information can prevent costly mistakes and can help increase the efficiency of resource use.

Sustainable Development of groundwater resources in southern and eastern Africa- Regional Technical co-operation project RAF/8/029

LIST OF CONTENENTS

1. INTRODUCTION AND OBJECTIVES

Water contamination is a global problem that affect development and sub-development countries. Particularly groundwater pollution, as a result of human activities and natural contamination, has become one of the most debated environmental issues.
At the United Nations Millennium Summit in 2000 and during the 2002 World Summit on Sustainable Development in Johannesburg, world leaders from rich and poor countries, recognized the vital importance of surface and subterranean fresh water to human development, and committed themselves to a precise, time-bound agenda for addressing the world's current and future water resource and sanitation needs.
This promise was reported onto the Millennium Declaration, among the Millennium Development Goals (MDGs). The MDGs are an eight-point[1] road map with measurable targets and clear deadlines for improving the lives of the world's poorest people. World leaders have agreed to achieve the MDGs by 2015 to:

- Integrate the principles of sustainable development into country policies and programs; reverse loss of environmental resources.
- Reduce by half the proportion of people without sustainable access to safe drinking water.
- Achieve significant improvement in lives of at least 100 million slum dwellers, by 2020.

Since, the issues of sustainability and maintenance of quality of drinking water supplied is an area of concern for countries where groundwater is a main source of drinking water, safe drinking water supply has been enlisted as one of the ten targets of Millennium Development Goals (MDGs), to halve by 2015 the proportion of people without sustainable access of safe drinking water.
In 2005, for example, slightly more than one third of the urban population in developing regions lived in slum conditions, with the associated problems of inadequate water and sanitation facilities, and lack of social infrastructure, including for health and education. Water use has grown at more than twice the rate of the population for the past century. Although there is not yet a global water shortage, about 2.8 billion people, representing more than 40 per cent of the world's population, live in river basins with some form of water scarcity (UN, 2008). More than 1.2 billion of them live under conditions of physical water scarcity, which occurs when more than 75 per cent of the river flows are withdrawn. Consequently, especially for rural people, more difficult access to reliable water supplies and high vulnerability to short and long-term drought (figure1.1).

[1] The 8 MDGs are: 1- End hunger; 2 - Universal education; 3 - Gender Equity; 4 - Child health; 5 - Maternal health; 6 - Combat HIV/AIDS; 7 - Environmental sustainability; 8 - Global partnership.

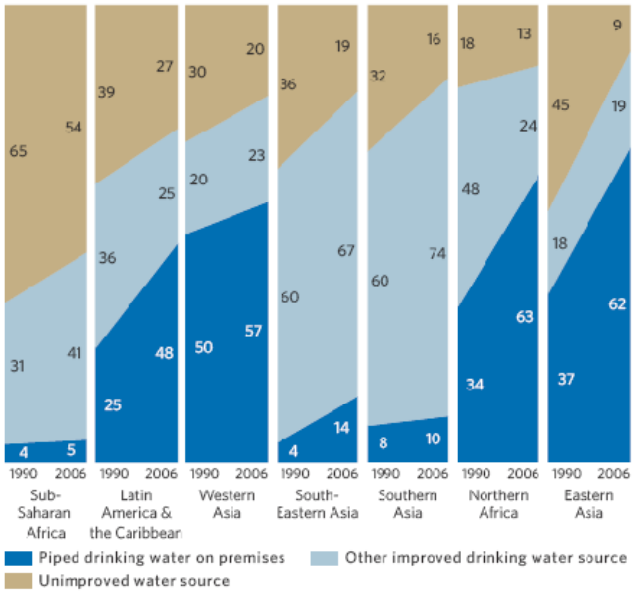

Figure 1.1 – Proportion (%) of rural households using piped water, other improved sources and unimproved sources, 1990 and 2006 (rearranged from UN, 2008)

Fifty per cent of rural dwellers relied on other improved drinking water sources, such as public taps, hand pumps, improved dug wells or springs (a small proportion of this population relied on rainwater). Nearly one quarter (24 per cent) of the rural population obtained their drinking water from 'unimproved' sources: surface water such as lakes, rivers, dams or from unprotected dug wells or springs. But even using an improved water source is no guarantee that the water is safe: when tested, the drinking water obtained from many improved sources has not met the microbiological standards set by WHO (UN, 2008).

As reported in United Nations 2009, 884 million people worldwide still rely on unimproved water sources for their drinking, cooking, bathing and other domestic activities (figure 1.2). Of these, 84 per cent (746 million people) live in rural areas.

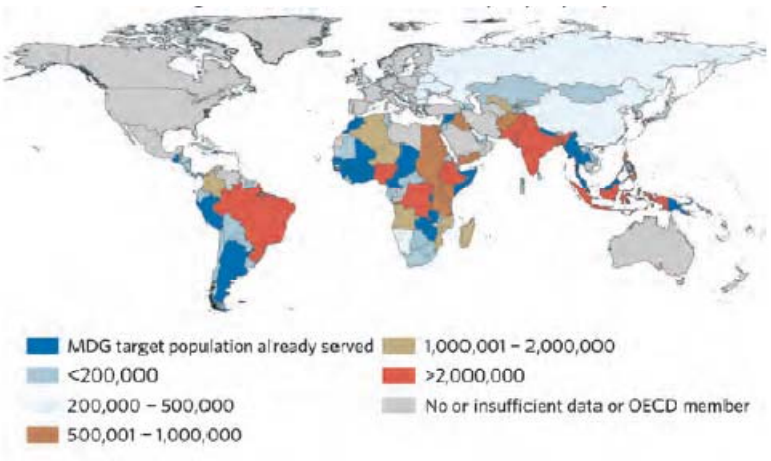

Figure 1.2 - Number of people per year that require access to an improved drinking water source to meet the MDG target, 2006-2015 (rearranged from UN, 2009)

Anyway, reducing poverty and achieving sustained development must be done in conjunction with a healthy planet. The Millennium Goals recognize that environmental sustainability is part of global economic and social well-being. Unfortunately exploitation of natural resources such as forests, land, water, and fisheries-often by the powerful few-have caused alarming changes in our natural world in recent decades, often harming the most vulnerable people in the world who depend on natural resources for their livelihood.
Drinking water, for example, continuously is affected by common problems include exposure to toxic inorganic substances, heavy metals, bacterial and other pathogens, increased nitrogen concentrations and other trace chemicals and micronutrients. The chemical contaminations are often considered a low priority than microbial contamination, because adverse health effects from chemical contaminations are generally associated with long-term exposure, whereas effects from microbial contaminations are usually immediate. The chemicals in water supplies can cause very serious health problems, whether the chemicals are naturally occurring or derived from source of pollution.
Groundwater pollution is usually traced back to four main origins: natural (or environmental), agricultural, industrial and residential (or domestic) pollution.
Natural: some groundwater pollution occurs naturally even if it is unaffected by human activities. The types and concentrations of natural contaminations depend on the nature of the geological material through which the groundwater moves and the quality of the recharge water. Groundwater moving through sedimentary rocks and soils, for example, may pick up a wide range of compounds such as magnesium, calcium, and chlorides. Some aquifers have high natural concentration of dissolved constituents such as arsenic, boron, and fluoride. The effect of these natural sources of contamination on groundwater quality depends on the type of contaminant and its concentrations.

Agricultural: Pesticides, fertilizers, herbicides and animal waste are agricultural sources of groundwater contamination.
Industrial: Manufacturing and service industries have high demands for cooling water, processing water and water for cleaning purposes. Groundwater pollution occurs when used water is returned to the hydrological cycle.
Residential: Residential wastewater systems can be a source of many categories of contaminants, including bacteria, viruses, nitrates from human waste, and organic compounds. Similarly, wastes dumped or buried in the ground can contaminate the soil and leach into the groundwater.

Natural contamination, due to particular geological environments, can be an important factor in limiting available water resources, both in quantitative and qualitative term, particularly in arid and semiarid areas, where the groundwater is the major source of potable water supply. Its availability may be threatened by natural contaminant as fluorine. In fact, although fluorine can prevent tooth decay, and is often added to drinking water in developed countries, when in excess concentration can lead to fluorosis, a serious health pathologies including malformed bones, neurological disease and may exert some stress on the ecological interrelationships among plant and animal populations in natural biological communities. Sources of fluoride on the Earth's surface derived not only from natural sources (rock minerals, air, seawater) but also from anthropogenic activities (Fuge and Andrews, 1988).
In a recent study Swiss researchers (Amini *et al*., 2008) mapped the levels of fluoride and arsenic in groundwater throughout the world (figure 1.3).

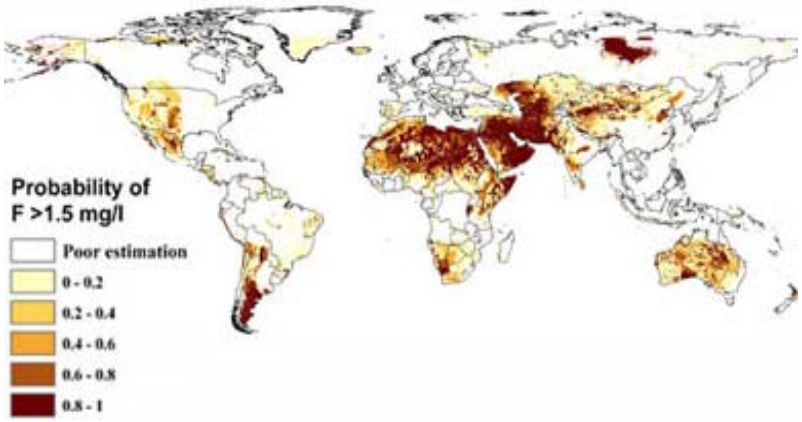

Figure 1.3 - Global probability of geogenic flouride contamination in groundwater

More than 20 developed and developing nations are endemic for fluorosis. These are Argentina, U.S.A., Morocco, Algeria, Libya, Egypt, Jordan, Turkey, Iran, Iraq, Kenya, Tanzania, S. Africa, China, Australia, New Zealand, Japan, Thailand, Canada, Saudi Arabia, Persian Gulf, Sri Lanka, Syria, India, etc.

Degradation of groundwater from fluoride, therefore, is one of the most serious water resources problems in Africa. In Tanzania, for example, fluoride in drinking water exceeds both 1.5 mg/L (the limit suggested by WHO guideline) and, in several cases, the 8.0 mg/L (suggested from the Tanzania government). In some of the groundwater supplies of Manyara, Arusha, Mara, Kilimanjaro, Mwanza, Shinyanga, Mbeya and Singida regions, about 90% of the population are affected by dental fluorosis at varying severity or stages. As such, the Tanzania Food and Drugs Authority categorized dental fluorosis as the 5th most common nutritional disorder in the country.

Considering that the presence of excessive concentrations of F^- in groundwater may persist for years, decades or even centuries (Todd, 1980), in order to mitigate this excess, is essential to determine and monitor the causal factors of enrichment of F^- concentration in groundwater in time and space. This is also one of the main objective of the present thesis's work : study the spatio-temporal variation of fluoride contents in groundwater of two wards (Ngarenanyuki and Oldonyosambu) of Arusha Region in northern Tanzania and its relationship with some influencing factor, like geological, chemical and physical characteristics of the aquifer and the surrounding environment.

Ngarenanyuki and Oldonyosambu areas are involved, from several years, in water distribution and sanitation projects by means of Oikos East Africa (NGO), as limited water resources availability is one of the main problem. In the two wards, the average per capita daily consumption is 8 liters and this value goes down to 3-4 liter per day in the dry period, when most of the population is compelled to concentrate around few water points and cannot resort to temporary ponds or streams. This datum is quite far from the *Millennium Goal* objectives. Moreover, in these rural areas qualitative water problems occurs, due to the abundance of fluoride concentration, that in many cases exceed the 8.0 mg/L limit.

Therefore the results of this study will provide a better understanding about high fluoride concentrations in groundwater, to agree water management plans that aims to:

- find new water resources in a area affected by serious water shortage;
- find safe water as in this area the few available water resources are naturally contaminated by high fluoride contents;
- develop a methodology which trough a multidisciplinary approach will satisfy the previous purposes.

In details the work was devoted to assays the possible groundwater resources of the region trough a general hydrogeological model, by means of geological, geophysical and punctual hydrogeological data. Moreover, trough the analysis of surface and groundwaters, rocks and their weathering products reconstruct the source of fluoride and the factors that control its concentration in the water.

This research was done as part of a project, coordinated by NRD-UNISS (Desertification Research Group- University of Sassari), funded by OIKOS Institute (Italy), Charity and Defence of Nature Fund (private foundation) and Sardinia local Government (Italy) (Regional Law 19/96: cooperation with developing countries).

2. LITERATURE REVIEW

Fluorine is the lightest element of the halogen groups and the most electronegative (Pauling 1960). It is seventeenth in the order of frequency of occurrence of the elements, and represents about 0.06 to 0.09% of the earth's crust (Wedephol, 1974). It is mobile under high-temperature conditions, most reactive of all chemical elements and is therefore, never encountered in nature in the elemental form. As fluoride ions have the same charge and almost the same radius as hydroxide ions, it may replace each other in mineral structures; thus forms mineral complexes with a number of cations and some fairly common mineral species of low solubility contain fluoride (Murray, 1986).

2.1. FLUORIDE CONTAMINATION

The incidence and severity of fluorosis is related to the fluoride content in various components of environment: air, soil and water (figure 2.1).

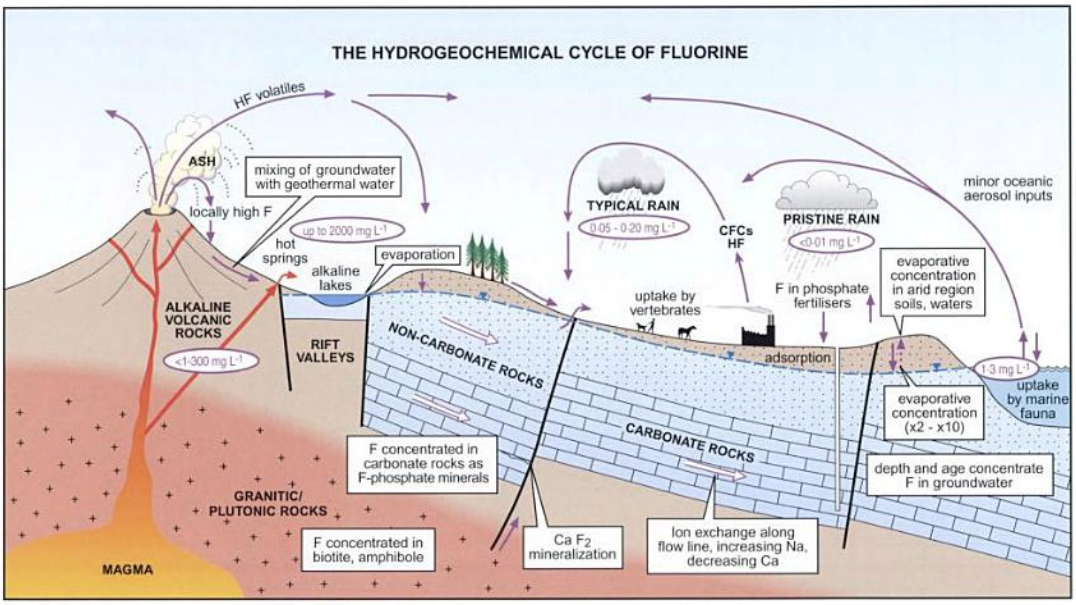

Figure 2.1 - Rearranged from Edmund and Smedley (2005)

In succession the contamination of fluoride in the different environment component is explained.

2.1.1. *Air*

Air is typically responsible for only a small fraction of total fluoride exposure (USNRC, 1993). Due to dust, industrial production of phosphate fertilizers, coal ash from the burning of coal and volcanic activity, fluorides are widely distributed in the atmosphere.

In non-industrial areas, the fluoride concentration in air is typically quite low (0.05–1.90 μg m^{-3} fluoride) (Murray, 1986). In China more than 10 million people suffer from fluorosis, related in part to the burning of high fluoride coal (Gu *et al*., 1990 in Fawell *et al*. 2006).

2.1.2. *Soil*

Common source of fluoride in soil proceed from application of phosphate fertilizers, fumigants, rodenticide, insecticides and herbicides containing fluoride as impurity or constituent, e.g., cryolite (used for the production of aluminium), barium fluorosilicate, sodium silicofluoride, sulfuryl fluoride, trifluralin (Datta *et al*., 1996).
Super-phosphate fertilizers may contain F^- but this is a minor source, since Rao (1997) found that the contribution from fertiliser was 0.34 mg/L in an area with a maximum of 3.4 mg/L. Very common soil minerals, such as biotite, muscovite, and hornblende may contain as much as several percent of fluoride and, therefore, would seem to be the main source of fluoride in soils (Madhavan, 2001).

2.1.3. *Water sea*

The sea water has a relatively high fluoride content (1.0 – 1.4 mg/L) as the fluoride is removed by erosion from the continent and transferred to the sea via stream or rivers (Murray, 1986).

2.1.4. *Surface water*

Generally most groundwater sources have higher fluoride concentrations than surface water, even though, for the later, fluoride levels tend to increase in dry seasons. However closed basins in areas of high evaporation, such as Great Salt Lake, accumulate up to 14 ppm of fluoride, whereas lakes in East Africa formed by leaching of alkali rocks contain 1.000 – 1.600 ppm (Fleischer and Robinson,1963). The primary determinant of surface water fluoride concentration in East Africa, in fact, depends on the weathering processes of fluoride rich rocks (Kilham and Hecky, 1973).

2.1.5. *Groundwater and its hydrogeochemistry*

Fluoride groundwater is introduced mainly through water–rock interaction in the aquifers (Edmunds and Smedley 1996; Nordstrom *et al*., 1989; Gizaw 1996; Saxena and Ahmed 2001; Saxena and Ahmed 2003; Carrillo - Rivera *et al*., 2002), depends on geological, chemical and physical characteristics of the aquifer and the groundwater's age.

Its concentration is a function of many factors such as availability and solubility of fluoride minerals, velocity of flowing water, temperature, pH, concentration of calcium and bicarbonate ions in water (Chandra *et al*., 1981), anion exchange capacity of aquifer materials (OH^- for F^-).

The dissolution of minerals, such as fluorspar, fluorapatite, amphiboles (e.g., hornblende, tremolite) and some micas (Datta *et al*., 1996), offer a considerable contribute to the high content of fluoride. Rocks yielding the highest levels of dissolved fluoride are typically characterized as alkaline igneous rocks, with a high percentage of sodium plagioclase minerals. Such rocks are likely to have formed from magmas enriched in fluorine through progressive differentiation. The predominance of sodium plagioclase is also likely to produce a soft groundwater, which allows higher fluoride concentrations when equilibrium is reached with fluorite. This mineral, controlling aqueous fluoride geochemistry in most environments (Apambire *et al*., 1997), is one of the major sources of fluoride, although its solubility in fresh water and its dissociation rate are very low (Nordstrom and Jenne 1977). Not uncommonly CaF_2 may encounters as a constitution of magmatic rocks (Madhavan, 2001) and often occurs as cement in some sandstones (Rukah and Alsokhny, 2004).

The bulk of the element is found in the constituents of silicate rocks, where the complex fluorophosphate apatite, $Ca_{10}(PO_4)6F_2$, seems to be one of the major fluoride mineral (Rutherford, *et al*., 1995). In silicate minerals, as fluorine is concentrated in the last stages of crystallizing magmas, in the residual solutions and vapours, its concentration increase in highly siliceous igneous rocks, alkali rocks and hydrothermal solutions (Fleischer *et al*., 1963); therefore all these are natural contributors of the fluoride ion to fluids interacting with them, such as groundwater, thermal waters and surface waters. The fluoride in such silicates may even greatly exceed the amount fixed in apatite. Sedimentary horizons also have apatite as accessory minerals (Rukah and Alsokhny, 2004). Next, with regard to fixation of the bulk of fluoride, come some complex hydroxy-silicates and hydroxyalumino- silicates, in which the hydroxyl ions (OH) may be largely replaced by fluoride (Omueti, and Jones, 1977), as is the case in amphiboles and minerals of the mica family (biotite and muscovite). Apatite, amphiboles and micas contain fair amounts of fluorine in their structure, which are ubiquitous in igneous and metamorphic rocks. The fluoride content of amphiboles from metamorphic rocks world-wide varies from 30 to 400 ppm (results of various workers, cited by Wedepohl (1978)).

Mg-hydroxysilicates unstable minerals, such as sepiolite and palygorskite, also may have a control on F^- distribution in groundwater (Wang *et al*., 1993; Jacks *et al*., 2005); sepiolite, in particular has been found to contain a considerable amount of F^- in the OH^- positions.

Villiamite (NaF) too, may contribute considerably on groundwater fluoride distribution when associated with certain peralkaline bodies. Other sources of fluoride, are reported

in literature referred to minerals precipitation both in salt crust like trona, due to chemical weathering of rock minerals (villiaumite or kogarkoite) and high evaporation of the lake waters (Nielsen, 1999), and calcrete (Jacks *et al*., 2005).
The following table 2.1 account the mean values, in ppm of F, for various geological materials, particularly igneous and sedimentary rocks.

Geological Materials	*ppm (average)*
Igneous	
basalts	360
andesites	210
rhyolites	480
phonolites	930
gabbros and diabases	420
granites and granodiorites	810
alkalic rocks	1.000
Sedimentary	
limestones	220
dolomites	260
sandstone and graywackes	180
shales	800
oceanic sediments and soils	730

Table 2.1 - Rearranged from Fleischer and Robinson, 1963

The concentration of fluorine in most basaltic rocks ranges from 0.01 to 0.1 wt% (Allmann and Koritnig, 1974) whereas most granites and rhyolites show a range of 0.01 to 0.2 wt% (Brehler and Fuge, 1974). High fluoride concentrations in groundwater from crystalline basement aquifers, particularly granite, are recognized in several areas of the world: Sri Lanka with up to 10 mg/l, and India, Senegal, Korea, and Wisconsin (US) with up to 7.6 mg/l (Pauwels H. and Ahmed S., 2007). High concentrations of the same halogen, also, can be found whether from groundwater chemical interaction of volcanic rocks and their associates (lahar and ash) or in sedimentary rocks, i.e. in western Senegal (Travi 1993) China, Sudan and Niger, particularly under semi-arid climate conditions. Argentina too, whose groundwater from Quaternary loess of La Pampa recorded up to 29 mg/l of fluoride. Nevertheless, groundwater under more temperate climates of Europe present concentrations above the WHO guideline, but rarely above 4 mg/l: Ledo-Paniselian aquifer in Belgium, Permian carbonates of Lithuania, in the Lutetian limestone and marl aquifer near Paris, as well as in the Bajocian aquifer (Jurassic limestones) in Normandy (western France). Very high concentrations of F^- (Boyle D.R. and Chagnon M., 1995) was found for groundwater associated with Carboniferous sandstone-siltsone-conglomerate sediments which underlie a thick blanket of alluvial-colluvial-glacial overburden in a area of Quebec (Canada).
Most of high fluoride concentration phenomenon in groundwaters, are controlled by pH.

The dissolution of fluoride from apatite, micas, and amphiboles minerals, for example, is most pronounced at low pH values (Apambire *et al*., 1997); on the contrary, Saxena *et al*., (2003), performing an experimental study in laboratory about the dissolution of fluoride in granite aquifers of India, showed like alkaline conditions and moderate specific conductivity, were favourable for fluoride dissolution from fluorite to water. Particularly in semi-arid areas, the pH increase influence the groundwater fluoride increment; in Jacks *et al.,* (2005), for example, the raising of pH contributed both the precipitation of calcite and the formation of Mg-rich calcrete and dolomite rich in fluorine (figure 2.2).

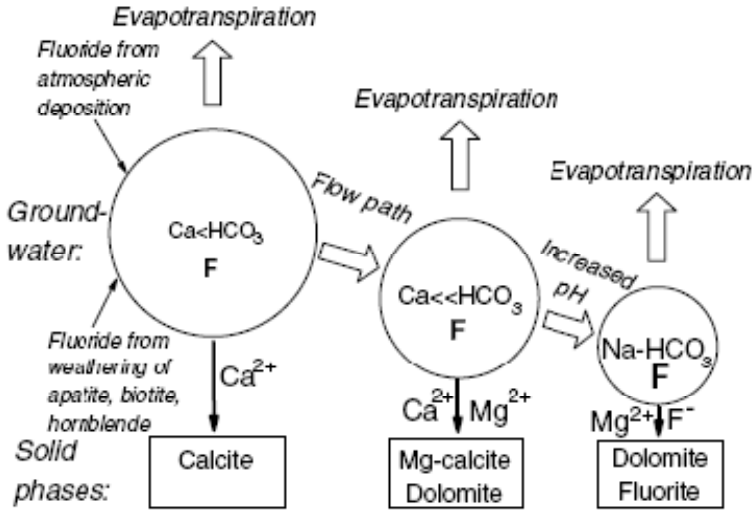

Figure 2.2 - Rearranged from Jacks *et al*. (2005)

In Madhavan and Subramanian (2006), was observed that the solubility of fluoride in soils was highly variable and had the tendency to be higher at pH below 5 and above 6. Conversely, Raju *et al*., (2009) said that in acidic medium, fluoride was adsorbed in clay, whereas in alkaline medium, it was desorbed.

In Jacks *et al*. (2005) was showed a correlation between soil pH and solubility of F^- like probable effect of the content of fluoride in the parent material. Soils having high pH and low levels of amorphous Al species, clay, and organic matter generally sorbs little fluoride (Omueti and Jones, 1977). Thus, it appears that the predominant retention mechanism is that of fluoride exchange with the OH group of amorphous materials, such as Al-hydroxides (Flühler *et al*., 1982; Barrow and Ellis, 1986; Bond *et al*., 1995 and Anderson *et al*., 1991). The pH factor is, therefore, closely relate to ion exchange. In Boyle and Chagnon (1995) the increasing of pH with decreasing of Ca and Mg concentrations, due probably to the involvement of H^+ in the exchange process, turned the water into a strong anion exchange medium for the exchange of OH^- for F^-, favouring the occurrence of high fluoride concentration. The concentration of Ca, Na, hydroxyl ion and certain complexing ions, in fact, can alter the concentration of fluoride in the groundwaters (Raju

et al., 2009). Any processes involving a decrease in calcium concentration, then, favour the occurrence of high fluoride concentration. This decrease can occurs through ion-exchange (substitution of Na by Ca on the mineral surface) during the circulation of groundwater within the aquifer, or through calcite (calcium carbonate) precipitation. Anion exchange is dominant in sedimentary environment but, also, can occur in igneous terrenes (Apambire *et al*., 1997).

Good anion exchange media, from which large amount of fluoride can be generated, are clay minerals like illite, chlorite and smectites (Boyle 1992; Boyle and Chagnon 1995).

Usually, high-fluoride groundwater is typically of the sodium-bicarbonate type with relatively low calcium concentrations (< 20 mg/L) and with neutral to alkaline pH values (around 7-9).

High concentrations of Na, therefore will increase the solubility of fluorite in waters; in fact (Apambire *et al*., 1997) sodium, may exhibit a positive correlation with fluoride in many types of groundwater, especially those having low concentrations of calcium (waters undergoing base exchange). Teotia *et al*., (1981) have reported that water with low hardness, i.e. low Ca and Mg contents, and high alkalinity present the highest risk of fluorosis. Compositional characteristics of the Rift Valley waters, for example, include high alkalinity (pH generally greater than 7) and richness in the components Na, K, HCO_3, CO_3 as well as Cl^- and F^- (Gaciri and Davies, 1993). Again, groundwater interactions with fluoride enriched minerals and residence time have been shown important for controlling the fluoride dissociation process. It is generally accepted that fluoride is enriched in groundwaters by prolonged water–rock interactions (Banks *et al*., 1995; Gizaw, 1996; Nordstrom *et al*., 1989; Frengstad *et al*., 2001; Carrillo-Rivera *et al*., 2002). The chemical composition of lithology, therefore, is regarded as an important factor determining the fluoride concentration of groundwater.

Residence time too, can have an important influence on dissolved fluoride levels (Kim and Jeong, 2005; Saxena and Ahmed, 2003; Conrad *et al*., 1999; Bardsen *et al*., 1996), because the dissolution rates of fluoride minerals are generally slow (Gaus *et al*., 2002).

2.2. FLUORIDE HEALTH PROBLEMS

The fluoride absorbed by the human body circulate in the body and then is retained in the tissues, predominantly the skeleton, or excreted, mainly in the urine. Both uptake in calcified tissues and urinary excretion appear to be rapid processes (Charkes *et al*., 1978). Low doses (<1.5 mg/l) of fluoride prevent decay of teeth, whereas concentrations above 1.5 mg/l in drinking water (the maximum tolerance limit of fluoride prescribed by World Health Organization WHO 1984) cause fluorosis and other related diseases (table 2.2).

F^- Concentration (mg/l)	Corresponding effects on human health
≤ 1	Safe limit
1-3	Dental fluorosis
3-4	Stiff and brittle bones/joints
≥ 4	Deformities in knees; crippling fluorosis; bones finally paralysed resulting in inability to walk or stand straight

Table 2.2 – Level of F- content in groundwater and corresponding effect in human health (rearranged from Chaturvedi *et al*., 1990)

Fluorosis is manifested mainly in three ways: fluorosis in soft tissues, such as muscles and ligaments (Kharb and Susheela, 1994), dental fluorosis and skeletal fluorosis.

As reported by Meenakshi and Maheshwari (2006), fluorine being a highly electronegative element has extraordinary tendency to get attracted by positively charged ions like calcium. Hence, the effect of fluoride on mineralized tissues like bone and teeth leading to developmental alternations, is of clinical significance as they have highest amount of calcium and thus attract the maximum amount of fluoride that gets deposited as calcium–fluorapatite crystals.

Tooth enamel is composed principally of crystalline hydroxyhapatite. Under normal conditions, when fluoride is present in water supply, most of the ingested fluoride ions get incorporated into the apatite crystal lattice of calciferous tissue enamel during its formation. The hydroxylion gets substituted by fluoride ion since fluorapatite is more stable than hydroxylapatite. Thus, a large amount of fluoride gets bound in these tissues and only a small amount is excreted through sweat, urine and stool.

The length of exposure, frequency of ingestion and ingested fluoride dose determine the plasma fluoride steady state, which in turn influences the severity of dental and skeletal fluorosis of an individual.

Skeletal fluorosis may occur when fluoride concentrations in drinking water exceed 4-8 mg/L, which leads to increase in bone density, calcification of ligaments, rheumatic or arthritic pain in joints and muscles along with stiffness and rigidity of the joints, bending of the vertebral column, etc. (Teotia and Teotia, 1988). Grynpas (2008) hypothesize that an increase in bone fluoride affects the mineral-organic interfacial bonding and/or bone matrix proteins, interfering with bone crystal growth and causing inhibition on the crystallite faces as well as bonding between the mineral and the collagen. Attention is also given to the interaction of fluorine with other elements, especially certain metals. Isaacson (2008) reports how fluorides can disrupt semi-independent systems of human nervous system. Of special interest are the anatomical changes induced by fluorides in the brain that resemble alterations found in the brain of Alzheimer's patients. The

hypothesis is offered that the main cause of all dementias is a reduction in the metabolic activity of the entire brain caused by alterations in blood flow and reductions in chemicals essential to aerobic metabolism. Although water is the epidemiologically most important source of fluoride in most areas, considerable exposure risk is also associated with the consumption of fish-bone, canned meat, vegetables, grain and other staples, local salt, drinks (especially tea) and air.

The sources of fluoride that contribute to the total human intake vary geographically between endemic fluorosis areas, but the symptoms are generally similar. In non-endemic areas, skeletal fluorosis has occurred as a result of industrial exposure. This condition, whether of endemic or industrial origin, is normally reversible by reducing fluoride intake. In endemic fluorosis areas, developing teeth exhibit changes ranging from superficial enamel mottling to severe hypoplasia of the enamel and dentine (Gittins, 1985).

Natural contamination of groundwater by fluoride causes, also, irreparable damage to plant and human health. Fluoride is not an essential plant element, but is essential for animals. Uptake of fluoride in plants mainly occurs through the roots from the soil, and through the leaves from the air. High fluoride levels inhibit germination, cause ultrastructrual malformations, reduce photosynthetic capacities, alter membrane permeability, reduce productivity and biomass and inflict other physiological and biochemical disorders in plants.

Considerable differences exist in plant sensitivity to atmospheric fluoride, but little or no injury will occur when the most sensitive species are exposed to about 0.2 $\mu g/m^3$ air, and many species tolerate concentrations many times higher than this. Moreover, the continuous use of water having high fluoride concentration also adversely affects the crop growth. For irrigation purpose fluoride is classified according to criteria given by Leone *et al*., (1948) who proposed a 10 mg L^{-1} limit for all type of plants

Plants, also, are a source of dietary fluoride for animals and human beings. Thus, elevation of plant fluoride many lead to a significant increase in animal exposure. Chronic toxicity has been studied in livestock, which usually develop skeletal and dental fluorosis. Experimentally-induced chronic toxicity in rodents is also associated with nephrotoxicity. Symptoms of acute toxicity are generally non-specific. Fluoride does not appear to induce direct mutagenic effects, but at high concentrations it may alter the response to mutagens. Continuous ingestion by animals of excessive amounts of fluoride can lead to the disorder fluorosis, and suboptimal levels in the diet can have an equally damaging effect. The effects of fluoride in drinking water on animals are analogous to those on human beings.

2.3. FLUORIDE IN THE RIFT VALLEY AND IN TANZANIA

Some of the highest fluoride contents in groundwater ever recorded in the world are in the East African Rift Valley with concentrations of up to 20 mg/L in Ethiopia (Wonji/Shoa area), and even more than 100 mg/L in Tanzania (Nanyaro *et al*., 1984); east Africa (Gaciri and Davies, 1993; Gizaw, 1996), have the most extensive areas of high F^- groundwaters.

The high national standard for drinking water in Tanzania reflect the difficulties with compliance a situation that is worsened by water scarcity. In this country both dental and skeletal fluorosis are recognized health problems.

Fluoride problems are largely found in groundwater from active volcanic zones, where fluorine sources are imputed at the volcanic rocks and geothermal sources (Edmunds and Smedley 2005). Unmodified waters in the Rift Valley were defined by Clarke *et al*., (1990) as waters whose chemical composition is derived from normal water-rock interaction at moderate temperatures. These waters showed high fluoride contents (up to 180 ppm), denoting that chemical leaching (weathering) of the volcanic rocks and their associates (calcareous tufa, lahar and ash) was an important fluoride contributor. The volcanic rocks of the Rift System are predominantly alkaline rocks rich in Na^+ and F^-. Alkali basalts, basanites and tephrites are the main varieties, followed in abundance by phonolites and trachytes (Gaciri and Davies, 1993). Consequently water bodies can accumulate fluoride directly as a result of a weathering of these rocks, as well as from high fluoride geothermal solutions.

High fluoride content of waters in Northern Tanzania was attributed (Nanyaro *et al*., 1984) to the exceptionally low Ca^{2+} and Mg^{2+} concentrations due to the low solubility of Ca^{2+} and Mg^{2+} fluorides. The Na^+-HCO_3^- rich groundwaters too, derived from weathering of the silicate minerals in the lavas and ashes (Jones *et al*., 1977) by silicate hydrolysis reactions, are relatively depleted in Ca^{2+} and Mg^{2+}. Hence high concentrations of fluoride can occur as the solubility of fluorite (CaF_2) is not limiting factor. In fact, only limited incorporation of F^- is permitted in the $CaCO_3$ structure, such that there is always a net balance of F^- in solution. For the computation of thermodynamic equilibrium in groundwaters which are in contact with both calcite and fluorite solid phases, Handa (1975) used a combined mass law equation relating both the solute species as follows:

$$CaCO_3(s) + H^+ + 2F^- \rightleftharpoons CaF_2 + HCO_3^-$$

and

$$K_{cal.-fluor} = \frac{a_{HCO_3}}{a_{H^+} \times \left(a_{F^-}\right)^2} \quad ;$$

If the pH of the groundwater remains reasonably constant, any increase or decrease in bicarbonate concentration/activity will be accompanied by a corresponding increase or decrease in the concentration/activity of fluoride ions, as $k_{cal.\text{-}fluor.}$ is constant.

Villiaumite (NaF) should limit the dissolved concentrations, but because this mineral is very soluble, fluoride can rich very high concentration before this limit is achieved.

High fluoride content for surface water of Tanzania (12-76 mg/L), particularly in the north of the country, was attributed (Kilham and Hecky, 1973) in rivers draining the volcano's slopes. This high concentrations was due to weathering of fluorine-rich alkaline igneous rocks and to contributions from fumaroles and gases as well as to the re-dissolution of fluorine-rich trona (*magadi*), which occurred as a seasonal encrustation in low-lying river valleys and lake margins as a result of extreme evaporation. More recent study, still report the importance of efflorescent crusts *magadi* and scooped *magadi* (formed by capillary evaporation) in the water fluoride enrichment (Nielsen, 1999; Kaseva, 2006; Vuhahulaa *et al*., 2008).

3. DESCRIPTION OF THE STUDY AREA

3.1. LOCATION AND EXTENT

The project involved one portion of the District of Arumeru, that belongs to the Region of Arusha, with an area of approximately 2966 km^2. The District is administratively divided into 6 Divisions, 37 Ward and 133 Villages.

The district of Arumeru is situated in northern Tanzania, between the Mount Kilimanjaro on the east, the Mount Meru on the south, the road that joins Arusha (Tanzania) with Nairobi (Kenya) on the west and the National Park of Amboseli (Kenya) on the north (figure 3.1).

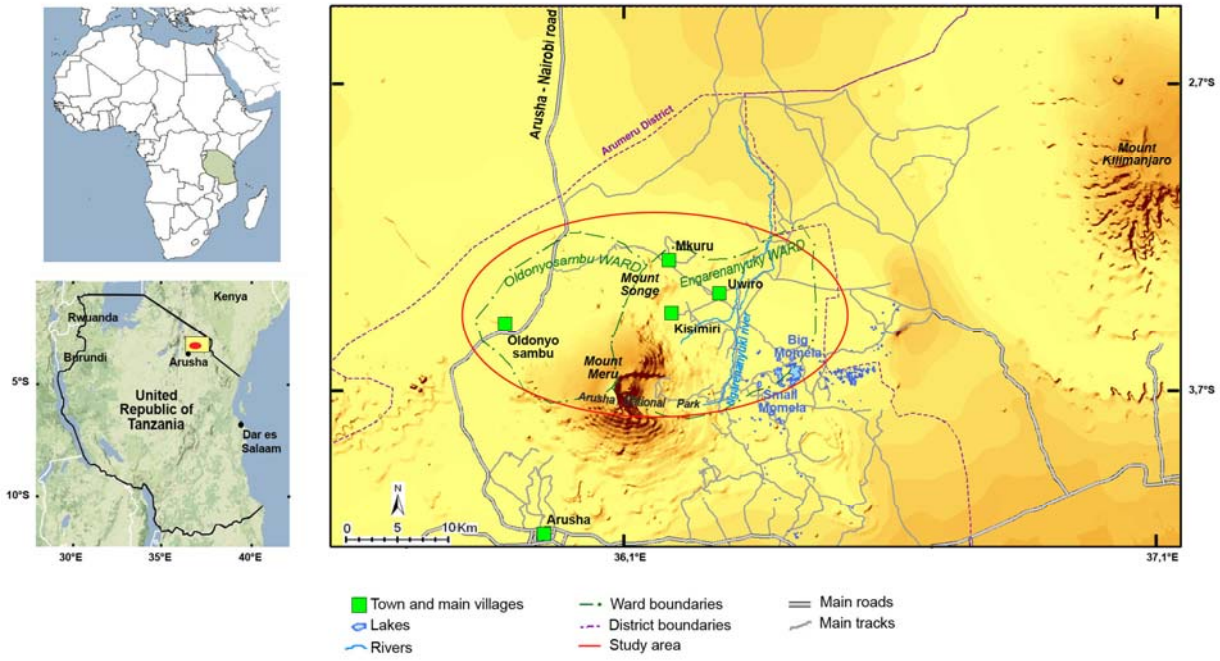

Figure 3.1 – Location of study area

In particular, the working area (approximately 370 km^2) is located in the northern part of the Arumeru district, approximately 50 km from the city of Arusha, is bounded by the Mount Meru (4565 m a.s.l.) and the Arusha National Park, and includes 9 villages belonging to the Oldonyo Sambu and Ngarenanyuki Wards.

This area is one of the most important and interesting fields of the Maasai Steppe, a territory extending for more than 200.000 Km^2 within the Great Rift Valley (figure 3.2), from the Turkana lake, in Kenya, to central Tanzania, which is traditionally inhabited by Maasai nomad shepherds. The natural environment which characterises the Maasai steppe is mainly savannah with wide plains, hills and volcanic mountain crests. Three main ethnic groups are present: the Wameru, which are farmers, Waarusha and Maasai, which are cattlemen.

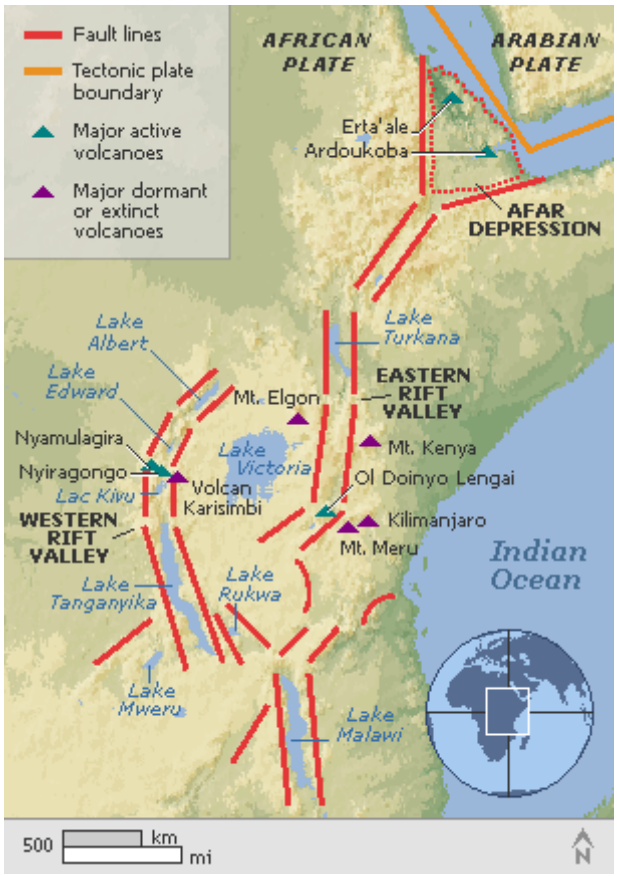

Figure 3.2 – The Rift valley

3.1.1. *The Rift Valley*

A rift can be thought of as a fracture in the earth's surface that widens over time, or more technically, as an elongate basin bounded by opposed steeply dipping normal faults (Wood and Guth, 2009). Geologists are still debating exactly how the East African rift system (EARS), comes about (Chorowicz 2005).

In the EARS the earth's tectonic forces are presently trying to create new plates by splitting apart old ones. The Nubian Plate makes up most of Africa, while the smaller plate that is pulling away has been named the Somalian Plate (figure 3.3).

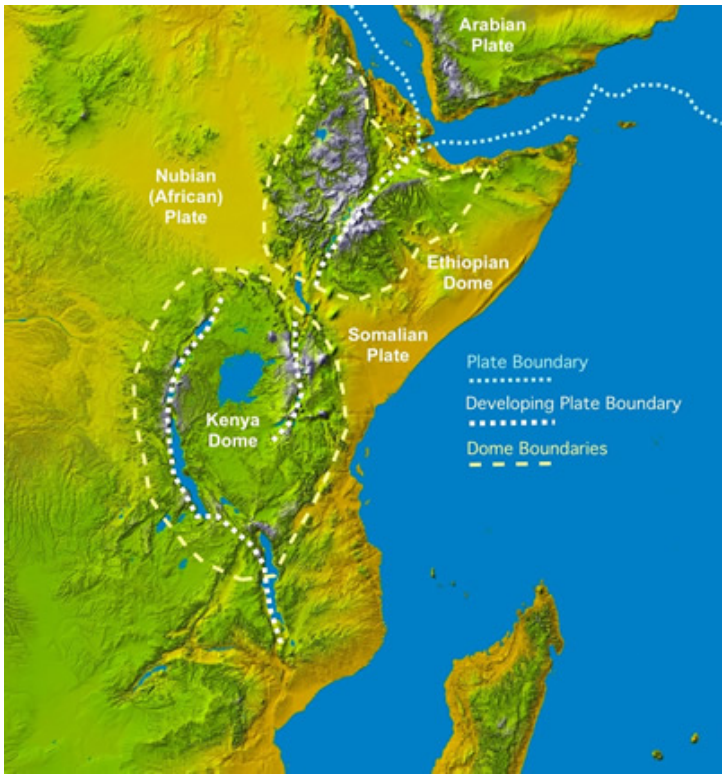

Figure 3.3 – The Nubian and Somalian plate (Wood and Guth, 2009)

The oldest and best defined rift occurs in the Afar region of Ethiopia and this rift is usually referred to as the Ethiopian Rift. Further to the South a series of rifts occur which include a Western branch, the "Lake Albert Rift" or "Albertine Rift" which contains the East African Great Lakes, and an Eastern branch that roughly bisects Kenya north-to-south on a line slightly west of Nairobi (figure 3.4). Another south-eastern branch is in the Mozambique Channel.

The eastern branch runs over a distance of 2200 km, from the Afar triangle in the north, through the main Ethiopian rift, the Omo-Turkana lows, the Kenyan (Gregory) rifts, and ends in the basins of the North-Tanzanian divergence in the south. The western branch runs over a distance of 2100 km from Lake Albert (Mobutu) in the north, to Lake Malawi (Nyasa) in the south. It comprises several segments: the northern segment includes Lake Albert (Mobutu), Lake Edward (Idi Amin) and Lake Kivu basins, turning progressively in trend from NNE to N–S; the central segment trends NW–SE and includes the basins of lakes Tanganyika and Rukwa; the southern segment mainly corresponds to Lake Malawi (Nyasa) and small basins more to the south. The south-eastern branch comprises N-striking undersea basins located west of the Davie ridge. Most of the great lakes of Eastern Africa are located in the rift valleys, except notably Lake Victoria whose waters are maintained in a relative low area between the high mountains belonging to the eastern and western branches.

Figure 3.4 – The Rift's series (Wood and Guth, 2009)

The two branches together have been termed the East African Rift (EAR), while parts of the Eastern branch have been variously termed the Kenya Rift or the Gregory Rift (Wood and Guth, 2009). The two EAR branches are often grouped with the Ethiopian Rift to form the East Africa Rift System (EARS).

It is generally admitted that rift evolution is related to extension. Chorowicz (2005) reports that at more local scale, Bhattacharji and Koide (1987) suggested from theoretical and experimental studies, the development of compressive stress adjacent to and around the active rift zones, due to mantle upwelling and penetrative magmatism. In terms of plate tectonics, block movements in East Africa are divergent, and tension might be considered the major factor (McClusky *et al*., 2003). Deformation of the continental lithosphere, leading to rupture, has been theoretically conceived to occur by two possible ways (Burke and Dewey, 1973; McKenzie, 1978), considering the role played by the asthenosphere.

(1) Active rupture would result from mantle convection (Pavoni, 1993) and plume movements in a dynamic asthenosphere that forcibly intrudes and deforms the overlying lithosphere.

(2) Passive rupture model sees the asthenosphere uplift playing an entirely responsive role in filling the gap produced by lithospheric extension, itself a reaction to stresses generated elsewhere at plate boundaries due to external forces. Models of tectonic rupture range from whole lithosphere simple shear (e.g., Wernicke and Burchfield, 1982;

Lister *et al*., 1986) to combination of upper brittle layer simple shear, lower crustal delamination and lithospheric mantle pure shear (e.g., Lister *et al*., 1986).

Wood and Guth (2009) also assumes that elevated heat flow from the asthenosphere is causing a pair of thermal "bulges" in central Kenya and the Afar region of north-central Ethiopia. As these bulges form, they stretch and fracture the outer brittle crust into a series of normal faults forming the classic horst and graben structure of rift valleys.

These successions of graben basins are generally bordered on the two sides by high relief, comprising almost continuous parallel mountain lines and plateaus, and sometimes volcanic massifs. As shown in figure 3.5, the elevated areas belonging to the EARS are comprised in two ellipses, one is the Ethiopian dome, and the other includes the Kenyan and Tanzanian domes. The longest axes of the two ellipses (Chorowicz, 2005) have a NNE trend: at this scale the main expression of the EARS is uplift, forming on the whole a NNE-trending intra-continental ridge, interrupted by the Omo-Turkana lows. The highest elevations in the EARS region, in addition to volcanoes, are the graben shoulders. Other uplifted areas in the region are due to belts, which may be recent (Atlas, Zagros belts) or ancient (Karroo belt), or to intracontinental hotspots (Hoggar, Tibesti plateaus).

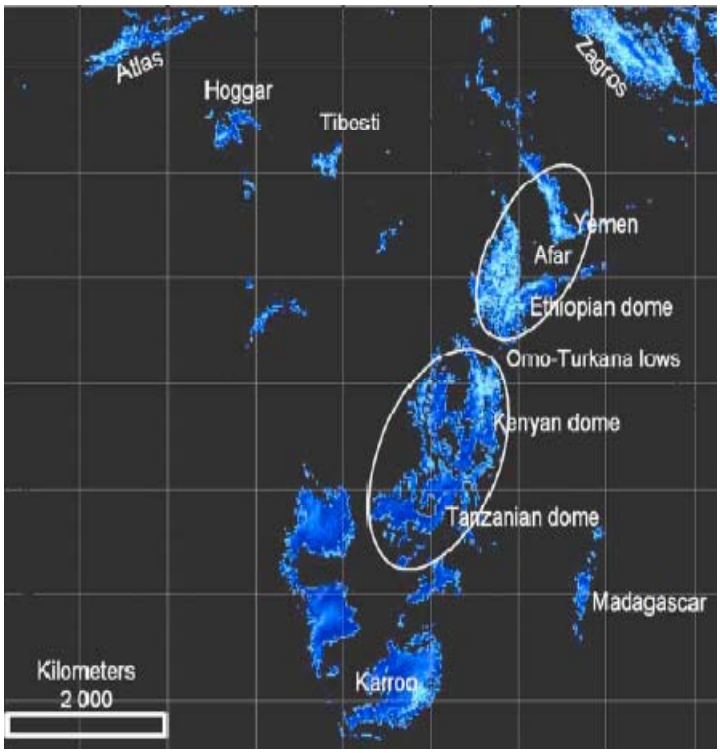

Figure 3.5 – Map of Africa showing in blue levels the elevations higher than 1200 m, evidencing the main Ethiopian and Kenyan–Tanzanian domes (from Chorowicz, 2005)

Ideally the dominant fractures created occur in a pattern consisting of three fractures or fracture zones radiating from a point with an angular separation of 120 degrees (the triple junction) and is well illustrated in the Afar region of Ethiopia (figure 3.6), where

two branches are occupied by the Red Sea and Gulf of Aden, and the third rift branch runs to the south through Ethiopia.

The rifting of East Africa, as mentioned, involves the two branches: one to the west, which hosts the African Great Lakes (where the rift filled with water) and another nearly parallel rift about 600 kilometers to the east which nearly bisects Kenya north-to-south before entering Tanzania where it seems to die out (figure 4). Lake Victoria sits between these two branches. It is thought that these rifts are generally following old sutures between ancient continental masses that collided billions of years ago to form the African craton and that the split around the Lake Victoria region occurred due to the presence of a small core of ancient metamorphic rock, the Tanzania craton, that was too hard for the rift to tear through. Because the rift could not go straight through this area, it instead diverged around it leading to the two branches that can be seen today.

The Neogene tectonics and volcanism in the rift area of northern Tanzania are intimately related. A major phase of late Tertiary faulting, giving rise to a broad tectonic depression, was followed by extrusion of large amounts of basaltic to trachyte magmas from large shield volcanoes. This was separated by a second major phase of faulting at about 1.2 Ma from a Late Pleistocene-Recent phase of small volume, explosive nephelinite-phonolite-carbonatite volcanism that contrasts with the earlier phase in its volume, dominant magma type and eruptive style.

In both its tectonic expression and contemporaneous magmatism, the northern Tanzania province contrasts with the southern Kenya sector of the Rift Valley. The area of tectonic disturbance is considerably broader in Tanzania where ultrabasic-basic magmatism predominates. The major episodes of basaltic magmatism representing major thermal perturbations of the mantle, have moved southwards down the rift since the mid Tertiary (Dawson, 1992).

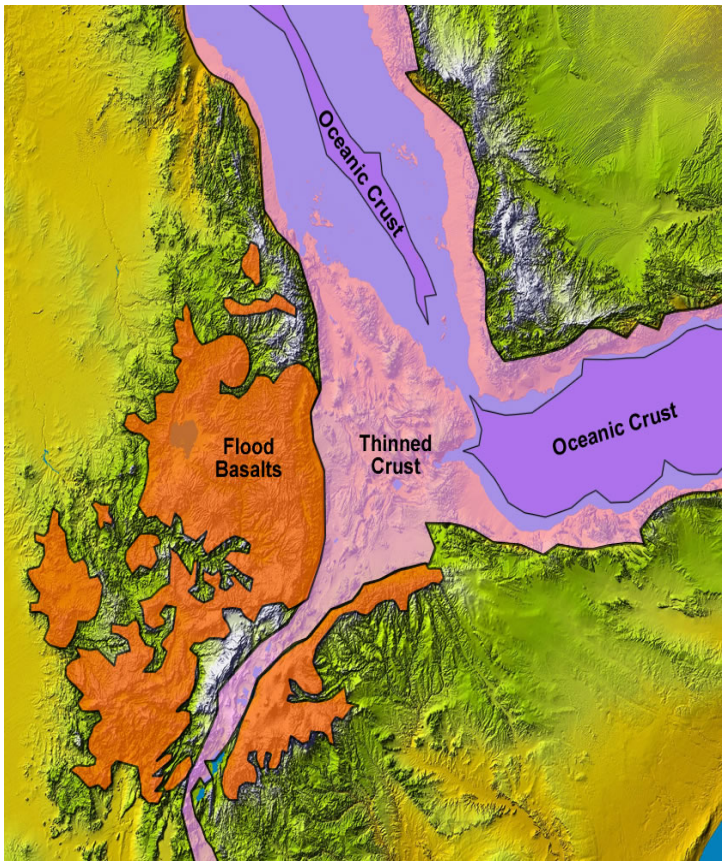

Figure 3.6 – The "triple junction" (Wood and Guth, 2009)

In northern Tanzania, the rift widens from about 50 km, as is typical in southern Kenya, to approximately 200 km wide splitting into three distinctively oriented branches: the Natron–Manyara– Balangida, the Eyasi–Wembere and the Pangani rifts. The change in the rift morphology is thought to be a result of the transition from the rifting of Proterozoic Mozambique Belt lithosphere to the rifting of cratonic Archean lithosphere (Foster *et al*., 1997). Faulting along the East African Rift is considered to have commenced in the Miocene, approximately 13 Ma (Davidson and Rex, 1980; Courtillot *et al*., 1984). Present day faulting along the Gregory Rift in northern Tanzania is thought to have begun by about

1.2 Ma, and is superimposed on an earlier episode of faulting that began at about 3 Ma (Dawson, 1992; Foster *et al*., 1997).

The earliest evidence of volcanic activity along the Gregory Rift in northeastern Tanzania is associated with the Miocene phase of rifting, with the eruption of 8.1 Ma phonolitic lavas at the centrally located Essimingor volcano (Bagdasaryan *et al*., 1973). Volcanic activity appears more widespread in the Plio-Pleistocene, with the eruption of alkali basalt–trachyte-phonolite association lavas. In the vicinity of the Ngorongoro Volcanic Highland situated at the southern end of the Gregory Rift, volcanic activity occurred at Satiman, Lemagurut, Ngorongoro, Olmoti, Embagai, Loolmalasin, Oldeani, and Oldonyo Sambu, Terosero, Kitumbeine, Gelai, Meru and Kilimanjaro (Godwin *et al*., 2008).

Godwin *et al*., (2008) also describe the third phase of volcanic activity occurred after the 1.2 Ma faulting event. Unlike the earlier phase of eruptions, this was smaller in volume and highly explosive. Pyroclastic volcanic cones of Meru, Monduli, Oldonyo Lengai and Kerimasi are thought to be part of this phase of volcanic activity. The magma is ultra-basic to ultra-alkaline in composition and the rocks are mainly phonolites and feldspathoidal syenites.

3.2. HYDROMETEOROLOGY

Average annual precipitation is about 1000 mm, although 50% of the country receives less than 750 mm; in general, rainfall decreases from north to south. Climate is generally semi-arid, with two different seasons: the dry season and the rain season, with rainfall ranging from 400 mm/year in Makami to 1500 mm/year in Ngorongoro. Rains are concentrated between November and December (the so-called small rains or *mvuli* in Swayli language) and March-May (big rains or *masika*). January, Septemebr and October are, normally, the hottest months of the year. Annual temperature ranges from 20 to 28 °C.

Particularly, the study area despite its proximity to the equator, enjoys an Afro-Alpine temperate climate, characterized by two distinct seasonal weather patterns. The main wet season extends from February to mid May and contributes to about 70% of the total annual rainfall. A minor rainy season from September to November contributes the rest of the moisture in the region. The remaining months of the year are more or less dry, at times with occasional, erratic showers. The lowest and the highest annual average temperatures, are 20.6 °C and 28.5°C, respectively, and the mean yearly rainfall is around 400 mm (figure 3.7), as inferred by 30 years of systematic rainfall measurements achieved from WorldClim database, a set of global climate layers (climate grids) with a spatial resolution of a square kilometer (Hijmans *et al*., 2005).

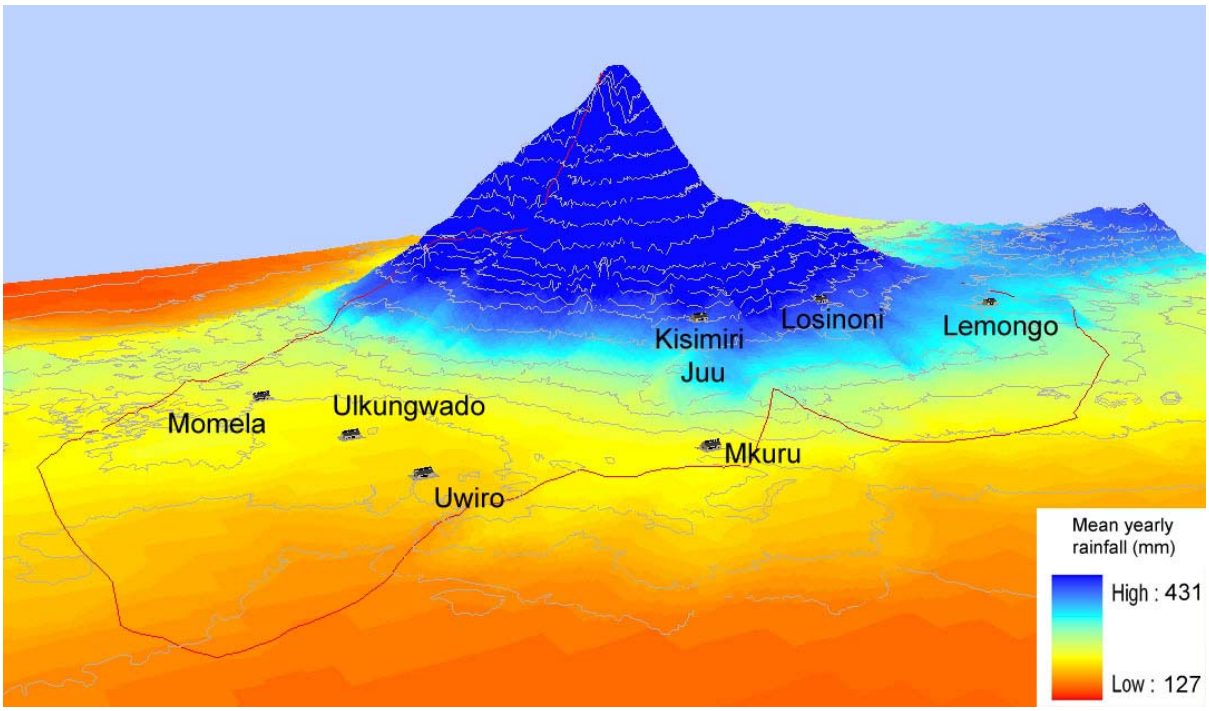

Figure 3.7 - Mean yearly rainfall

3.3. GEOMORPHOLOGY

The topography of the area is dominated by the volcanic cone of the mount Meru (4565 m a.s.l.); its slopes, cover most of the area. Mount Meru is a young volcano of Pleistocene to recent origin, located on a traverse branch of the southern Gregory Rift. The genesis of the mountain can be distingued by a number of a different development stages. The first was as explosive, creating a yellow tuffs. This was followed by an alternation of multiple eruptions that formed the main body of the mountain to a height considerably above the present, with snow and ice on the top. The next stage included a collapse of the summit and upper E side of the mountain. The rock masses lubricated with water, flowed out over the plains between Mt. Meru and Mt. Kilimanjaro, creating the present lahar topography in that area. This area is characterized by a complex of mounds and ridges, the depression between them often being occupied by lakes or swamps. A paleolimnological study of some of these alkaline lakes dates the bottom sediments to only 6000 years, indicating this recent age of the lahar formation and collapse of the mountain (Hecky, 1971). After the collapse a number of lava outflows have occurred, the latest dates back to 1910, when small amounts of black ash were ejected for a few days from the Ash Cone. Likely most of the recent lava activity took place during the half-century prior to the ash eruption in form of lava domes. Up to 1954 significant fumarolic activity was recorded in the Ash Cone area. In 1974 a careful survey showed no fumarolic activity and anomalous soil temperature.

The remaining land is overlain by the alluvial fans, which, with gentle slope, are fed by Mount Meru detritus. Recent small volcanic cones are preserved in the NW part of Meru and small maar-type flat craters occur (i.e. in front of Mt. Songe). Permanent saline water characterise the Big Momela lake and the Small Momela lake, both inside the Arusha National Park, east of Meru. The drainage pattern around the Meru is clearly radial, but downhill the stream courses are modified by tilting and capture. East and north-east of the Mt. Meru, the only perennial is the Engare Nanyuki river, which flows northwards into the inner Amboseli Basin.

3.4. GEOLOGY

The age of the rock sequences of the study area is Cenozoic: in particular, the older ones go back to Miocene-Pliocene; whereas, the most recent are sub-actual. The dominant lithology is represented by volcanic rocks and, subordinately, by recent alluvial deposits. The crystalline basement does not crop in the area; however it has been found at shallow depth, few kilometers north of the study area.

3.4.1. *Litostratigraphy*

The lithologies of the area (figure 3.8) can be summarized as follows:

The Basement

No crystalline Basement rocks are exposed in this area. However, a borehole log west of the Engare Nanyuki river shows pegmatite and gneiss at a depth of about 15m. This evidence, together with the extensive outcropping of Basement only few kilometres to the north, implies that metamorphic rocks underlie the northen part of the study area, very likely at small depths. In addition, at several localities (Matuffa Crater, Olijoro Crater and Meru Caldera), lavas and pyroclastic rocks enclose small pebbles to large blocks of Basement gneiss.

Volcanic rocks

Older and Younger extrusives rocks have been distinguished, based on the relationships with the main phase of rifting and faulting, that should date back to 1.15-1.20 million years. However, the few radiometric ages and field evidences that support this correlation, are still provisional.

Older Extrusives

The Older extrusives include the faulted plateau region of the Flood lava group (Nvz) and the Meru West group (Nvm). The first lavas are quite well exposed in fault-scarps, far from the study area. Lavas belonging to the Meru West group appear as a block-faulted structure emerging from below the Meru. Thick ash fall deposit covers the top and the sides of this volcanic complex, that is exposed only in a few steep scarps where thick sub-horizontal nephelinite lavas and breccias crop. These lavas date back to 1,5 million years BP, and then should be younger than Flood lavas pertaining to Nvz. The associated breccias, however, contain dominant phonolite clasts which have been dated back to 2,0 million years BP, indicating a hidden series of alkaline lavas which must have erupted in concomitance of, or just after, faulting (2,1 million years). The crater-like summit plateau of Meru West is of uncertain origin.

Younger Extrusives

The earliest volcanic activity after the main rift faulting is represented by the phonolites and phonolitic nephelinites of Oldonyo Sambu (Nv); they also crop north of Naigonesoit. Later formations hide the lateral continuity of NV, but it is argued that the formation stretchs further eastwards, since phonolitic nephelinite clasts, in the breccias of Little Meru (Nvp), are coeval (300.000 years BP). Little Meru is a monogenetic volcanic cone rising to more than 3795m a.s.l. from the NE flanks of Meru. The slopes are very symmetrical and, although the basal relations cannot be seen, it probably was completely built and extinct before being partly buried by the later Meru lavas. The rock is a very uniform breccia with clasts of phonolitic nephelinite.

The Meru centre is located to the south where, between about 200,000 and 80,000 years BP, the built up of the actual main cone took place, namely a large and fairly symmetrical cone to an altitude of at least 4877 m a.s.l., perhaps considerably higher in the past. The Main Cone group (Nvm) materials are predominantly volcanic breccias and tuffs of all size-grades, but phonolitic and nephelinitic lavas are intercalated sporadically. The loose nature of much of the original pyroclastic material, resulted in a radial redistribution outwards into fan and fluvio-volcanic sediments. Lahars (Nzd_1) of considerable extension commonly generated, interbedded with alluvial sequences, often over large areas.

Extesive lahars are those of Temi-Burka valley, Tengeru and Engosomit and Lemurge. The latter are characterised by large and abundant boulders and by feldsparphyric phonolite with alkali feldspar phenocrysts up to 5 cm in diameter. This rock probably derives from a concealed portion of the Button Hill tholoid. These lahars are not of a single origin, some being volcanic, some sedimentary. Another feature of the Main Cone group is the common occurrence of viscous domes or tholoids (Nvg), usually of a feldsparphyric phonolite composition. These may occur at all levels, but there is zone of especially large adventitious tholoids on the northern flanks of Meru.

The completion of the main cone was followed by a period of deep gullying and erosion with a recrudescence of activity about 60,000 years BP. The Summit group (Nvn), predominantly of thick phonolitic and nephelinitic lavas, formed a capping of the summit of the main cone, now largely gone, with a few more massive flows persisting further down the flanks, where they now form prominent ridges.

At some undetermined time, subsequent to the Summit group activity, the whole upper part of the Meru cone collapsed, giving rise to huge lahars east of the volcano. These deposits cover about 1500 km^2; they travelled about 50 km to the north and 30 km to the south of the cone and washed up against the lower slopes of Kilimanjaro to the east. The collapse did not occur as a single event and the last phase produced the Momela lahar (Nzd_3), which flowed farther east out of the graben and gives rise to the characteristic mounded topography of the National Park. The episode has been dated at about 7000 years BP by radiocarbon dating of bottom sediments from one of the Momella lakes. It is thought that the mantling ash (Nvf) derives from a plinian eruption associated with the primary collapse and, at its base, there is a concentration of pumice lapilli representing juvenile magma. The ash is thickly deposited over much of the mountain, but especially to the west, even beyond the western margin of the area. In the study area, the tuff is notable for its bright yellow colour, but elsewhere the colour grades to a brown, making difficult a precise correlation. This ash has the unfortunate effect of obscuring much critical geology. There are numerous examples of forms which are manifestly buried volcanic cones, some even retaining the morphology of craters, which display no exposures of underlying structure.

The final phase of activity was prevalently restricted to the collapse caldera. Mainly cinder and ash activity built up the Ash Cone to about 1067 m above the Caldera floor. At a late stage, a lava dome formed between the Ash Cone and the Caldera wall, from which nephelinitic and phonolitic lavas have flowed over the caldera floor and down to the graben. A flank eruption, apparently of the same magma originating SE of Little Meru, flows for some considerable distance.

Other volcanic centres

Parasitic cone are a notable feature of the region; there are a considerable number of cones with ankaramitic or picrite-basaltic affinity. In particular, a group of cones is of phonolitic affinity and is found on the lower flanks of Meru, with which the activity is closely related. The same activity is encountered north of Meru where a block-faulted plateau of laharic debris has been pierced, over a small area, by shallow volcanic craters. Rims are comparatively small breccia and tuff; these maars are clearly the result of mainly gas action, probably phreatomagmatic in origin.

Superficial deposits

Objectively, the interpretation and representation of the geology of this area lies in the lateral gradation of sub-aerial pyroclastic materials of Meru into fluvio-volcanic and lacustrine deposits. Boundaries are often representational and may have been drawn at an appropriate break of slope. The classification "alluvium" has been used for rather diverse deposits which reconnaissance mapping cannot attempt to subdivide. There are present some black soils with distinctive carbonate concretions; soils on volcanic rocks show substantial colour variation from red to brown and even grey. Basaltic cones are commonly fringed by a zone of calcrete (calcareous duricrust).

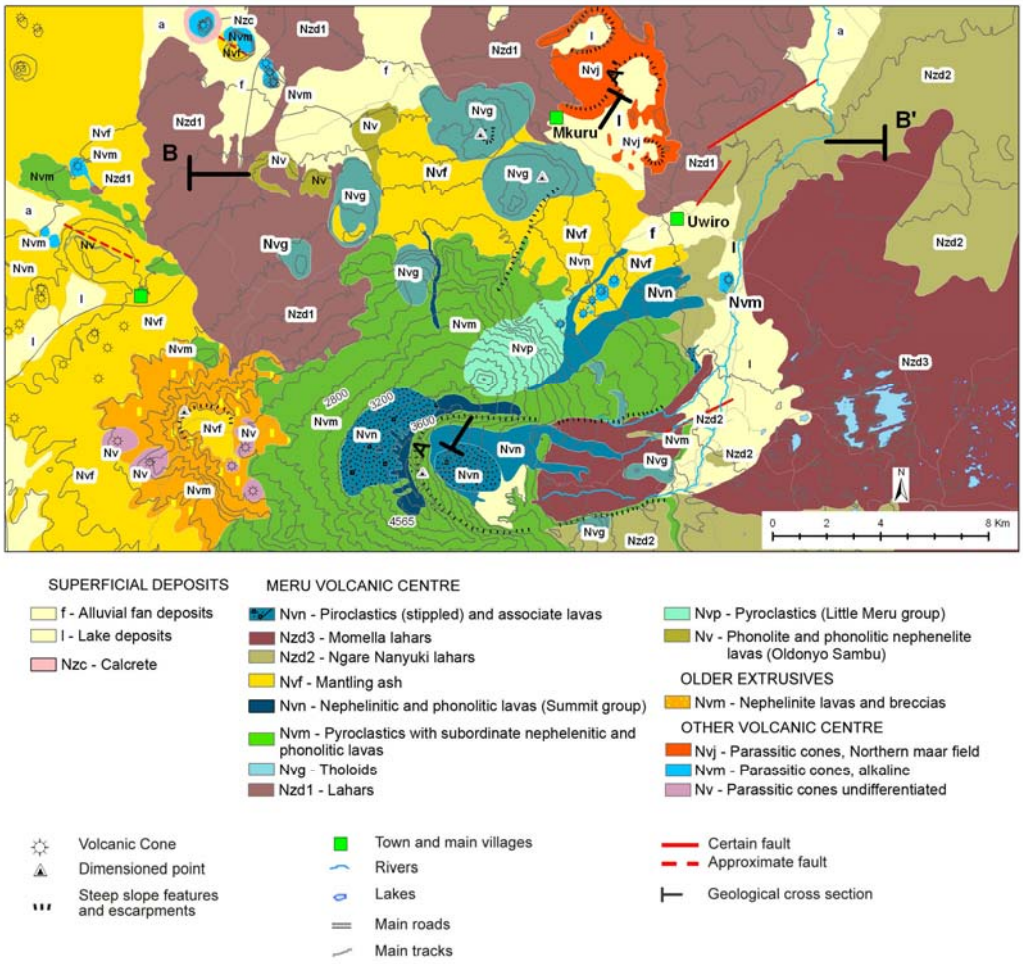

Figure 3.8 – Geological map of the study area

3.4.2. *Geological Structure*

Among the three distinct domains that can be distinguished in the S Kenya–N Tanzania rifted area, the study area fall down in 200×50 km transverse volcanic belt extending at N80°E from the Ngorongoro crater to the Kilimanjaro; includes numerous (<20) volcanic edifices, and their extensively distributed effusive and air-fall material, that were emplaced during the time interval 8 Ma–Present. The NKVB (Ngorongoro–Kilimanjaro transverse volcanic belt) is very little deformed and shows an inhomogeneous distribution

of extensional faulting. In its eastern part the N80°E trend is exclusively expressed by three aligned volcanoes (Monduli, Meru and Kilimanjaro) forming the Meru lineament. Throughout the NKVB, fault structures are inhomogeneously distributed. Monduli and Meru edifices are transected by minor transverse fault structures.
Major rift faults are present in the NW outside part of the area (Matuginigi and Matisiwi Escarpment). Linear features and benches are frequent on the flanks of Meru and it is highly probable that the early volcanic structure has been block-faulted. In the central area, the faulting is N-S to NNE-SSW (Uwiro graben); in the NW area the faulting is NW-SE (parasitic cone in Lassarkartarta). However, thick mantling ash and other younger formations make it difficult to map faults with confidence. The date of this faulting must lie between that of the flood lavas (2.3 million years BP) and that of parasitic cones (1.7 million years BP), some of whose lavas cover the fault scarp. This is consistent with the fault-phase found elsewhere about 2.1 million years BP.

3.5. HYDROGEOLOGY

In the study area, the main aquifer systems are made up of volcanic formations, occurring singularly or superimposed each other. Subordinate perched aquifers are present in sedimentary formations. However, some of these aquifer systems have a local occurrence.
The thickness of the volcanic rocks is known only approximately because of the uncertainties associated with the geologic and geomorphologic events during the Cenozoic. However, it is clear that all these events exerted a strong control on the geometry of the aquifers, on the recharge and discharge areas and on the groundwater quality. Moreover, the scale of the map and the amount of available data does not allow a detailed mapping of all these topics.
From a hydrogeological point of view, the litho-stratigraphic formations, described above, can be grouped in two main hydrogeologic unit:

- volcanic hydrogeologic unit;
- sedimentary hydrogeologic unit.

Volcanic hydrogeologic unit

This unit is divided into four hydrogeologic complexes:

- Meru west Group (Nvm);
- Lahars of various age (Nzd_1), Ngare Nanyuki lahars (Nzd_2), Momella Lahar (Nzd3);
- Main cone group (Nvm), Ash cone group (Nvn);
- Mantling ash (Nvf);

Meru west Group (Nvm) complex

This formation, that belongs to "older extrusive", is exposed in the west side of Meru. The rock are essentially nephelinite lavas and breccias that contain dominant phonolite clasts. The aquifer hosted in this formation has a fractured permeability. Springs, with a good quality water, are fed by this aquifer.

Lahars of various age (Nzd_1,Nzd_2,Nzd_3) complex

From a hydrogelogic point of view, all these lahars can be grouped into a unique complex. Lahars (Nzd_1) of considerable extension were commonly generated interbedded with sedimentary sequences. These lahars are characterised by large and abundant boulders on the surface, of a feldsparphyric phonolite with alkali feldspar phenocrysts and are not of a single origin, some being volcanic, some sedimentary.

North-East and East of the volcano, Nzd_2 and Nzd_3 are exposed. The first, near Ngare Nanyuki and Uwiro graben, the second near the Momella Lakes.

The aquifers hosted in this rocks have double permeability (fractured and porous) and generate springs with high fluoride concentration. Also some hydrothermal springs occur within this complex.

Main cone group (Nvm) complex

The Meru became active in a period ranging about 200,000-80,000 years BP. The volcanic activity built up the main cone to an altitude of at least 4877 m asl, perhaps considerably higher at one time. The Main Cone group (Nvm) materials are predominantly volcanic breccias and tuffs of all size-grades, but phonolitic and nephelinitic lavas are intercalated sporadically. The aquifer hosted in this rocks presents double permeability (fractured and porous). Springs, with low fluoride concentration, are present. In this system there are some important hydrogeological evidences. The first one is the elevations difference between recharge and discharge area that allows the infiltration of rain water, particularly where the permeability is high (intensive fracturing). The second one is the number of springs with important yield and good quality (low fluoride concentration and no human activities are present in the recharge area). Another feature of the Main Cone group is the common occurrence of viscous domes or tholoids (Nvg), usually of a feldsparphyric phonolite composition. These may occur at all levels, but there is a zone of especially large adventitious tholoids on the northern flanks (i.e. M. Songe). The occurrence of domes constitutes a lateral hydrogeological impermeable limit, that controls the groundwater circulation.

Mantling ash (Nvf) complex

Thick ash and tuff deposits lie over large areas in the foothills of Meru, especially to the west of the mount. In the study area, this complex is present especially near Oldonyo Sambu, and Kisimiri (North of Meru) This formation, due to fine granulometry and clay alteration, is practically impermeable, so no springs occur within it. Sometimes this complex underlies or surrounds an aquifer (see ahead).

Sedimentary hydrogeologic unit

This formation contains fine-grained alluvial and lacustrine sediments and hence is characterised by low transmissivity. The main areas of occurrence are near the Engare Nanyuki river. In this formation are hosted some perched aquifer with a low productivity: few springs are present with poor yield.

4. MATERIALS AND METHODS

4.1. FIELD DATA COLLECTION

The water sampling took place in three different time trough a census (February 2007) and a monitoring activity (March-April 2007 and January 2008).

4.1.1. *Census of water points*

Water point were identified in 58 sites (figure 4.1), including 46 springs (30 in the Ngarenanyuki, 16 in the Oldonyosambu ward) and 6 surface waters (rivers and lakes).
The precise locations of these points were determined in the field using a hand-held GPS GARMIN-*Geko*, Global Positioning System (GPS). Some parameters like pH, electrical conductivity (EC), temperature and fluoride also was measured in situ by means of a portable pH-conductivity meter (mod. HI 98130 HANNA Instruments) and a LR Photometer (Hanna Instrument HI 93739). Moreover, the following parameters were collected: elevation, yield (estimated values, since most springs were not active at the time of the sampling campaign), hydrogeological characteristics and spring classification (Annex A). Once the water point census was finished, hydrogeological and hydrochemical information obtained from all the water points was been pre-processed in terms of geographical distribution, using the value of the fluoride content values as an indicator, and the result integrated with the remaining hydrogeological information. This allowed to define the most convenient and efficient monitoring network, which resulted constituted by 25 springs, 6 river points and 2 lake points. One sample of rain, also, was sampled.

Figure 4.1 – Census activities

4.1.2. *Masika and pre-masika monitoring activity*

Masika (big rain) monitoring, was carried out in March-April 2007 whereas in January 2008 vas made the the second sampling activity (figure 4.2). Water samples were filtered (0.45 μm) and collected in 1L capacity polythene bottles. Two samples from each water point were collected. Prior to collection, the bottles were thoroughly washed with distilled water before filling it with sample. The bottle was rinsed to avoid any possible contamination in bottling and every other pre-cautionary measure was been taken. pH, electrical conductivity (EC) and temperature was measured in situ. Collected water samples were carried in a low temperature thermal bag and immediately stored in a refrigerator at the Oikos Mkuru Camp.

Figure 4.2 – Sampling activity

A total of 34 samples were collected during the first phase of monitoring: 25 spring water, 8 surface water (6 from rivers and 2 from lakes) and 1 rain water.
In the second phase was not possible took samples from lakes, rain and two spring water from the *masika* circuit thus, only 31 samples were collected, since two new groundwater samples (1 from spring and 1 from the well), were added.
On 34 samples collected during the *masika* monitoring, 27 (24 groundwater, 3 superficial water, 1 rain water) were analyzed for investigate the isotopic composition.
Six rock samples and eight fluvio-volcano lacustrine sediments, representing the weathered (re-deposited) products of the volcanic rocks, were also collected (figure 4.3 and 4.4).

Figure 4.3 – Rock and sediments sampling

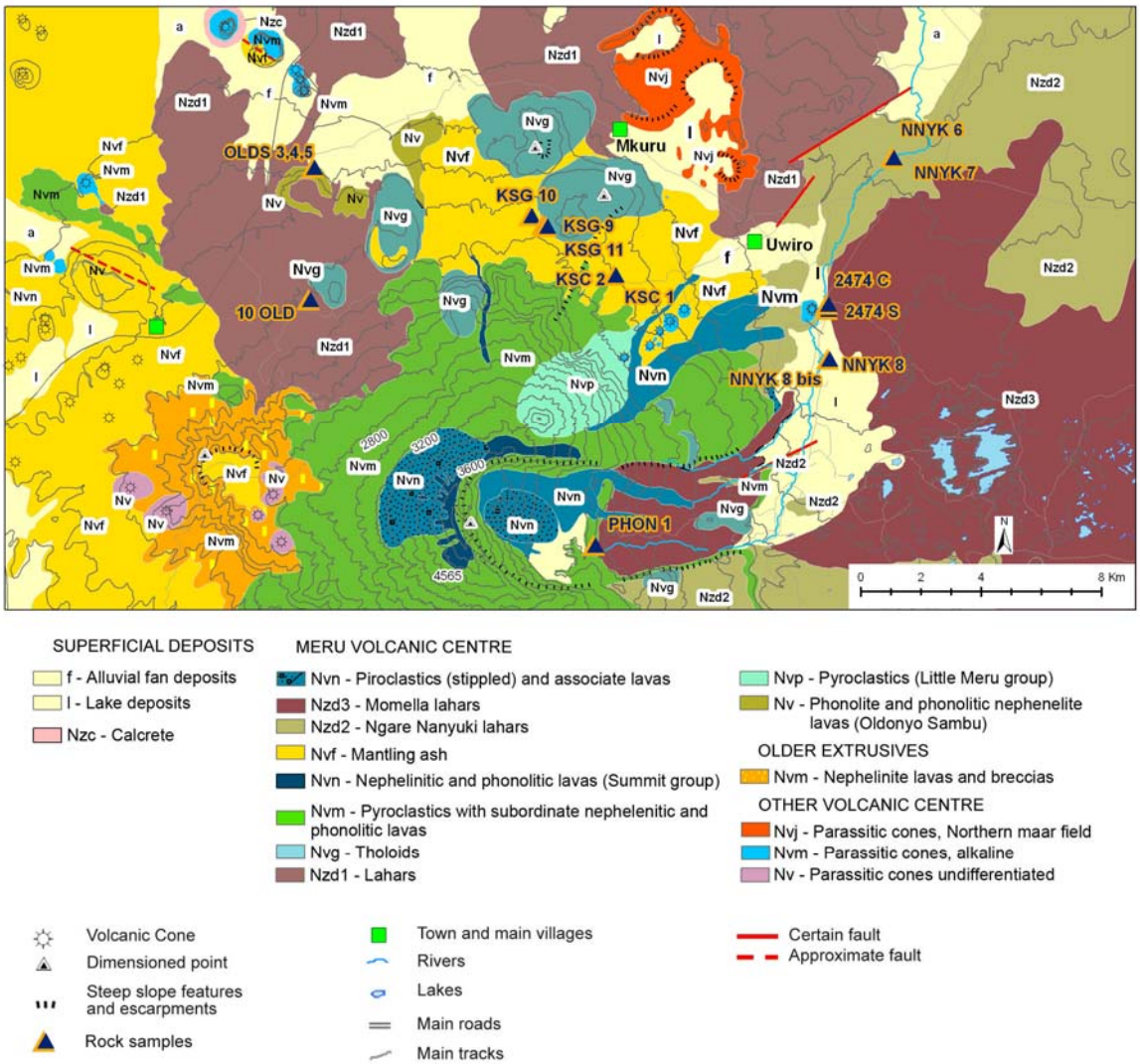

Figure 4.4 – Rock and sediments sample distribution

4.1.3. *Geophysical surveys*

The geophysical surveys coordinated by Prof. R. Balia (Department of Territorial Engineering, University of Cagliari) was been carried out in the two wards of Ngarenanyuki and Oldonyosambu, by means of the VES (Vertical Electrical Sounding) technique with a Schlumberger electrode array, and an ABEM Terrameter SAS 300 as acquisition system. The apparent resistivity curves have been interpreted using a computer software based on the linear digital filtering method (e.g. see Koefoed, 1972; Koefoed, 1979; O'Neill and Merrick, 1984). On the whole, 15 soundings in the Oldonyosambu Ward and 33 in the Ngarenanyuki Ward were acquired. In the Oldonyosambu Ward the results were rather disappointing, since no clear sign of exploitable groundwater was found in the apparent resistivity curves and respective interpretations. Conversely, in the Ngarenanyuki Ward the VES campaign allowed to locate several areas potentially interesting for groundwater, and therefore only soundings pertaining to this ward will be discussed. The VES position map for the Ngarenanyiuki Ward is shown in figure 4.5.

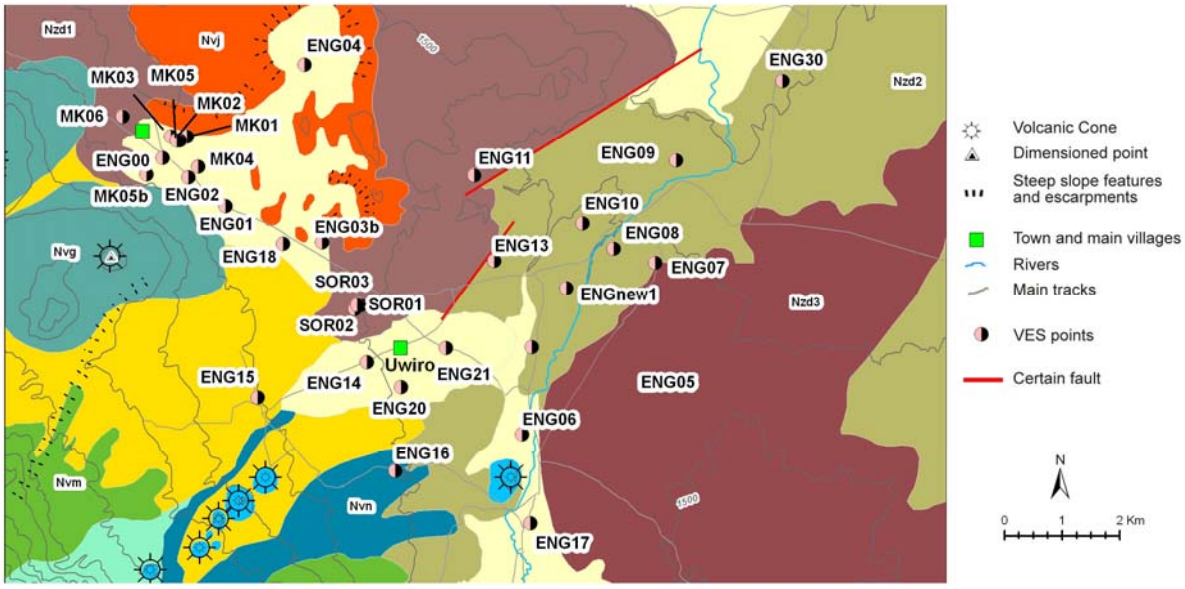

Figure 4.5 – Map of the VES points

4.2. LABORATORY ANALYSIS

As mentioned earlier, 34 water samples during the *masika* monitoring and 31 during *mvuli* time were analysed for major ion chemistry employing the standard methods (APHA, 1992). Water chemical analysis for nitrates, nitrites, ammonia (that must be executed in a very short time after sample collection), and fluoride were carried out at the AUWSA laboratory in Arusha. The remaining chemical analysis were done in Italy, at

the Water an Soil Laboratory of Department of Territorial Engineering, section of Geopedologic and Applied Geology, University of Sassari, following standard methods.
By A.A. spectrometry (Perkin Elmer mod AAnalist 200 UNI 10540 - UNI 10541 - UNI 10542 - UNI 10543 30/11/96), were analyzed cations (Na^+, K^+, Ca^{2+}, Mg^{2+}), whereas anions (F^-, Cl^-, SO_4^{2-}) by ion chromatography (anion column Alltech mod. allsep anion 7 µm, 100 mm). Titration and colorimetry techniques were used, respectively to analyze total alkalinity (CO_3^{2-} + HCO_3^-) and SiO_2.
Analytical precision and accuracy were estimated as better than 5% for both anions and cations on the basis of repeated analysis of samples and standards.
Oxygen (^{18}O), (^{2}H) and Tritium (^{3}H) isotopic analysis was carried out, on samples collected in the *Masika* time and one (Ichnusa Well1) collected in January 2008, at the Laboratory of CNR in Pisa, Italy; the analytical method based on Epstein and Mayeda, (1953) for ^{18}O, Coleman *et al*., (1982) for ^{2}H and U.S. Department of Energy, (1997) for ^{3}H . The isotope content values ($\delta^{18}O$, δD) were expressed permill (‰) relative to Vienna Standard Mean Ocean Water (VSMOW) defined by Craig (1961), tritium concentrations in terms of tritium units (TU).

The rock samples pre-emptively were crushed and powdered. Chemical analysis at ICP, INAA, ICP/MS and XRF technologies to completely characterize the samples, were carried out in Canadian Actalab laboratories. The oxides were analyzed by Fusion ICP with a 0.01% of detection limit (0.001% for TiO_2). Accuracy and precision, based on the analysis of certified international standards, are estimated as better than 3% for Si, Ti, Fe, Ca and K, and 7% for Mg, Al, Mn, Na, and 10% for trace elements at ppm level.
Mineralogical characterization were executed at the laboratory of the Department of Botanical, Ecological and Geological Sciences, University of Sassari. XRD measurements were performed using an X-ray diffractometer SIEMENS D5000 at 40 kV and 30 mA. The instrument uses a copper target tube radiation. Samples were placed on a quartz plate and were scanned from 2° to 70° (2θ) at a rate of 0.020° 2θ min^{-1}.

4.3. INVERSE GEOCHEMICAL MODELING

Inverse geochemical modelling techniques was applied to determine the nature and extent of the geochemical reactions by identifying the reacting minerals and the dissolution or precipitation amount of these minerals. The software PHREEQC 2.15.0 was used. It is an interactive fortran computer program for simulating chemical reactions and transport processes in natural or polluted water. The program is based on equilibrium chemistry of aqueous solutions interacting with minerals, gases, solid solutions, exchangers, and sorption surfaces, but also includes the capability to model kinetic

reactions with rate equations that are completely user-specified in the form of basic statements.

In the present study, this software was run to calculate the dissolution/precipitation amount of the major aquifer minerals and evaluate the effect of major hydrogeochemical processes on the F^- concentration in groundwater.

4.4. CHEMICAL AND MINERALOGICAL DATA

The geochemical analysis of groundwater, surface water, isotopes, rock and sediment of the study area are reported in the follow tables.

Chemical composition of groundwater in the study area in April (Apr) 2007 and January (Jan) 2008; all concentrations are expressed in mg/l except pH, conductivity (μS/cm) and temperature (°C), n.a.= not available. In blue colour are indicated the samples with fluoride content below 8 mg/l (Tanzanian Standard for Rural water), with red colour the samples with fluoride content above 8 mg/l.
* with 0,0 mg/l are represented the values out of instrument sensitivity

ID sample	T		pH		Conductivity		TDS	Ca^{2+}		Mg^{2+}		Na^{+}		K^{+}		HCO_3^{-}		Cl^{-}
	Apr 2007	Jan 2008	Apr 2007	Jan 2008	Apr 2007	Jan 2008	Jan 2008	Apr 2007	Jan 2008	Apr 2007	Jan 2008	Apr 2007	Jan 2008	Apr 2007	Jan 2008	Apr 2007	Jan 2008	Apr 2007
1old	14,6	14,4	8,0	8,4	750	790	603,08	23,00	14,50	3,30	3,15	98,00	110,00	36,00	25,00	374,70	358,10	18,05
2old	23,6	n.a.	6,4	n.a.	210	n.a.	n.a.	8,30	n.a.	1,52	n.a.	24,50	n.a.	18,25	n.a.	98,90	n.a.	5,04
3old	14,4	14,2	6,2	6,5	480	470	355,13	7,00	1,36	0,29	0,25	71,00	74,00	27,75	20,50	197,90	167,90	7,20
4old	14,2	15,9	6,4	7,2	540	540	410,72	11,75	10,50	3,43	3,15	69,00	71,00	33,25	27,75	237,50	197,70	7,49
5old	17,7	17,2	7,4	7,4	610	640	514,34	5,50	2,90	0,52	0,43	100,00	106,00	34,00	29,00	268,00	259,00	8,90
6old	13,1	14,7	6,0	6,0	690	660	587,75	7,25	4,80	2,40	2,30	120,00	120,00	19,50	16,50	383,80	355,60	4,77
8old	10,7	12,3	6,7	7,0	190	190	185,83	1,50	0,80	0,16	0,18	31,00	32,00	9,40	5,50	89,50	77,20	2,31
10old	14,5	14,5	7,2	7,1	480	470	370,05	3,75	2,10	0,31	0,38	73,00	75,00	21,25	18,25	192,90	170,60	5,51
13old	14,1	15,7	7,3	7,1	580	540	442,59	7,80	6,10	2,01	1,63	81,00	74,00	47,50	25,00	304,40	244,20	5,61
16old	11,9	16,0	7,2	7,0	200	170	155,82	4,90	3,50	0,92	0,55	29,00	15,60	18,50	14,00	109,70	74,90	2,56
1eng	18,2	15,4	7,2	7,1	620	600	513,39	13,50	8,25	2,85	4,95	120,00	100,00	23,25	16,25	314,70	300,10	5,10
2eng	15,2	n.a.	5,9	n.a.	490	n.a.	n.a.	15,90	n.a.	5,05	n.a.	58,00	n.a.	23,00	n.a.	227,30	n.a.	7,36
2beng	n.a.	15,5	n.a.	7,1	n.a.	770	632,89	n.a.	25,50	n.a.	7,85	n.a.	100,00	n.a.	34,75	n.a.	365,90	n.a.
3eng	23,6	24,0	7,4	7,3	720	670	577,40	9,75	7,75	1,65	1,43	108,00	120,00	30,00	24,50	380,00	349,30	6,38
5eng	22,1	20,5	7,0	6,7	980	650	502,14	15,00	7,50	3,80	1,95	190,00	90,00	43,00	24,50	503,50	276,80	18.50
8eng	22,7	21,5	7,0	7,0	1220	1340	945,64	19,00	14,75	4,83	3,78	136,00	215,00	49,00	37,00	457,70	526,80	14,35
16eng	17,0	16,5	6,4	6,3	340	340	285,53	2,70	1,70	0,49	0,49	58,00	55,00	10,50	9,10	156,10	140,60	5,52
18eng	18,5	18,1	6,5	6,4	470	450	384,42	4,90	4,00	1,42	1,21	73,00	74,00	14,25	14,10	215,90	185,90	7,35
19eng	16,9	16,2	7,4	7,2	400	390	333,91	4,20	2,90	0,66	0,59	64,00	62,00	17,50	15,00	193,30	169,50	6,50
22eng	12,7	14,0	5,9	6,9	250	230	213,87	11,10	6,20	3,38	1,89	30,00	27,00	16,90	9,60	126,30	94,60	4,56
24eng	18,3	17,7	7,2	7,0	1070	1170	961,22	26,00	41,00	5,98	5,88	180,00	165,00	47,00	37,00	600,00	606,40	2,94
26eng	22,4	22,3	7,7	7,6	5070	4730	3927,60	8,00	13,50	3,25	11,46	1100,00	820,00	235,0	180,00	2143,00	2233,22	189,69
27eng	13,9	12,2	6,8	6,9	330	320	289,63	0,70	0,60	0,03	0,12	47,00	59,00	7,70	5,40	127,00	146,00	2,36
28eng	17,8	17,6	7,6	7,7	1500	1160	896,46	5,50	4,80	1,40	1,17	208,00	195,00	98,00	47,00	581,90	481,20	29,81
29eng	17,3	17,5	7,8	7,7	1390	1870	1537,35	1,60	0,86	0,30	0,55	182,00	345,00	66,00	92,00	486,10	856,68	25,04
30eng	24,8	24,7	8,1	7,9	3740	3500	2808,44	12,00	6,80	3,50	2,93	615,00	700,00	134,0	88,00	1142,24	1360,07	91,86
Ichnusa well 1	n.a.	21,5	n.a.	6,4	n.a.	620	526,46	n.a.	14,50	n.a.	2,75	n.a.	84,00	n.a.	22,25	n.a.	314,30	n.a.

Table 4.1 (continue) - Major ion composition of groundwater (concentration in mg/l)

ID sample	Cl^-	SO_4^{2-}		NO_3^-		NO_2^-		NH_3^+		F^-		SiO_2	RESIDUE 110°C	RESIDUE 180°C	FACIES
	Jan 2008	Apri 2007	Jan 2008	Apri 2007	Jan 2008	Apri 2007	Jan 2008	Aprl 2007	Jan 2008	Apr 2007	Jan 2008	Jan 2008	Jan 2008	Jan 2008	
1old	9,87	13,71	15,05	21	14,20	0,19	0,14	0,02	0,02	4,30	4,80	48,25	460,00	420,00	$Na\text{-}HCO_3$
2old	n.a.	8,55	n.a.	71,5	n.a.	0,72	n.a.	0,04	n.a.	0,90	n.a.	n.a.	n.a.	n.a.	$Na\text{-}HCO_3$
3old	6,55	10,12	11,73	24,3	11,10	0,24	0,11	0,2	0,02	12,30	12,00	49,61	260,00	220,00	$Na\text{-}HCO_3$
4old	7,12	10,66	11,31	30,8	27,20	0,31	0,27	0,03	0,02	2,50	1,90	52,80	340,00	340,00	$Na\text{-}HCO_3$
5old	8,50	13,88	15,08	26,1	18,70	0,27	0,19	0,01	0,02	13,00	19,90	54,62	360,00	340,00	$Na\text{-}HCO_3$
6old	4,62	6,19	6,92	17,4	5,10	0,17	0,06	0,01	0,02	2,50	3,10	68,73	380,00	360,00	$Na\text{-}HCO_3$
8old	2,19	2,23	1,66	22,3	10,10	0,22	0,1	0,12	0,02	4,60	5,10	50,98	80,00	80,00	$Na\text{-}HCO_3$
10old	6,13	11,07	11,18	21,9	12,10	0,22	0,12	0,09	0,02	17,60	20,00	54,17	240,00	220,00	$Na\text{-}HCO_3\text{-}F$
13old	4,90	6,32	6,34	24,6	17,30	0,25	0,18	0,04	0,02	4,00	4,20	58,72	360,00	340,00	$Na\text{-}HCO_3$
16old	1,85	2,85	1,95	34	12,70	0,3	0,13	0,05	0,02	1,60	2,00	29,59	140,00	80,00	$NaK\text{-}HCO_3\text{-}NO_3$
1eng	3,91	9,09	9,26	22,00	16,50	0,25	0,17	0,02	0,02	3,00	3,00	50,98	380,00	380,00	$Na\text{-}HCO_3$
2eng	n.a.	7,35	n.a.	16,50	n.a.	0,17	n.a.	0,01	n.a.	1,30	n.a.	n.a.	n.a.	n.a.	$Na\text{-}HCO_3$
2beng	12,05	n.a.	11,71	n.a.	15,00	n.a.	0,15	n.a.	0,02	n.a.	1,70	58,26	460,00	440,00	$Na\text{-}HCO_3$
3eng	6,63	9,13	6,74	12,60	6,50	0,13	0,07	0,05	0,02	4,90	5,30	49,16	440,00	420,00	$Na\text{-}HCO_3$
5eng	9,49	16,61	16,30	70,00	11,30	0,71	0,11	0,06	0,02	5,40	5,00	59,17	360,00	320,00	$Na\text{-}HCO_3$
8eng	20,54	65,12	52,02	23,30	10,00	0,23	0,10	0,01	0,02	10,00	10,10	55,53	740,00	720,00	$Na\text{-}HCO_3$
16eng	5,38	8,06	8,44	13,40	10,20	0,13	0,10	0,02	0,02	5,30	5,80	48,70	220,00	160,00	$Na\text{-}HCO_3$
18eng	7,44	15,99	15,95	19,80	10,00	0,20	0,10	0,01	0,02	5,20	5,70	66,00	300,00	280,00	$Na\text{-}HCO_3$
19eng	7,51	5,33	6,25	21,60	12,20	0,21	0,13	0,03	0,02	3,50	4,10	53,71	200,00	200,00	$Na\text{-}HCO_3$
22eng	3,84	2,52	1,85	18,24	14,50	0,18	0,15	0,10	0,02	1,40	1,90	54,17	180,00	180,00	$Na\text{-}HCO_3\text{-}NO_3$
24eng	2,95	11,36	13,27	25,42	25,80	0,26	0,26	0,12	0,02	7,10	7,20	56,44	700,00	660,00	$Na\text{-}HCO_3$
26eng	183,48	332,76	366,85	13,00	11,80	0,14	0,12	0,00	0,02	59,00	68,00	39,15	3140,00	3120,00	$Na\text{-}HCO_3$
27eng	3,05	2,81	4,79	17,80	9,90	0,18	0,10	0,00	0,02	3,80	4,60	55,08	220,00	180,00	$Na\text{-}HCO_3$
28eng	27,67	75,70	66,61	16,00	11,00	0,16	0,11	0,00	0,02	28,20	20,00	41,88	720,00	660,00	$Na\text{-}HCO_3$
29eng	46,45	55,12	110,74	34,00	8,90	0,35	0,09	0,04	0,02	17,16	22,80	53,26	1200,00	1120,00	$Na\text{-}HCO_3$
30eng	100,46	512,51	475,61	20,60	9,60	0,22	0,10	0,01	0,02	31,00	29,80	35,05	2380,00	2320,00	$Na\text{-}HCO_3\text{-}SO_4$
Ichnusa well 1	6,44	n.a.	7,33	n.a.	12,90	n.a.	0,13	n.a.	0,04	n.a.	3,10	58,72	420,00	320,00	$Na\text{-}HCO_3$

Table 4.1 - Major ion composition of groundwater (concentration in mg/l)

Chemical composition of surface water in the study area in April (Apr) 2007 and January (Jan) 2008; all concentrations are expressed in mg/l except pH, conductivity (μS/cm) and temperature (°C), n.a.= not available. In blue colour are indicated the samples with fluoride content below 8 mg/l (Tanzanian Standard for Rural water), with red colour the samples with fluoride content above 8 mg/l.
with 0,0 mg/l are represented the values out of instrument sensitivity

ID sample	T		pH		Conductivity		TDS	Ca^{2+}		Mg^{2+}		Na^{+}		K^{+}		HCO_3^{-}	
	Apr 2007	Jan 2008	Apr 2007	Jan 2008	Apr 2007	Jan 2008	Jan 2008	Apr 2007	Jan 2008	Apr 2007	Jan 2008	Apr 2007	Jan 2008	Apr 2007	Jan 2008	Apr 2007	Jan 2008
1 river	24,8	22,1	8,6	8,7	1980	2200	1622,31	8,75	6,00	1,68	1,65	254,00	380,00	114,00	86,00	732,20	882,31
3 river	24,5	22,7	8,0	7,8	1350	1100	884,57	21,40	13,50	6,00	5,00	206,00	160,00	63,00	35,00	658,50	521,30
15 river	13,2	16,6	7,1	7,2	290	420	287,80	5,70	9,40	1,01	1,52	43,00	51,00	17,50	22,50	112,40	125,80
24 river	24,7	24,1	8,6	8,1	1790	2060	1583,80	8,50	5,75	1,55	1,45	296,00	370,00	98,00	80,00	764,10	871,32
28 river	18,5	19,8	8,8	8,6	1500	2250	1524,74	7,50	6,75	1,43	1,88	244,00	350,00	77,00	102,00	591,50	662,64
30 river	13,6	13,0	7,9	8,1	690	590	492,20	8,70	8,50	1,92	1,76	82,00	84,00	24,00	23,00	261,10	282,30

ID sample	Cl^{-}		SO_4^{2-}		NO_3^{-}		NO_2^{-}		NH_3^{*}		F^{-}		SiO_2	RESIDUE 110°C	RESIDUE 180°C
	Apr 2007	Jan 2008	Apr 2007	Jan 2008	Apr 2007	Jan 2008	Apr 2007	Jan 2008	Apr 2007	Jan 2008	Apr 2007	Jan 2008	Jan 2008	Jan 2008	Jan 2008
1 river	39,60	62,44	97,67	136,63	41,15	9,30	0,41	0,09	0,02	0,0	28,00	34,20	23,67	1340,00	1320,00
3 river	11,77	17,10	74,68	51,58	25,00	11,90	0,25	0,12	0,05	0,0	6,20	7,50	61,45	720,00	680,00
15 river	8,50	4,58	10,62	18,20	70,00	21,80	0,65	0,22	0,23	0,0	1,90	0,90	31,86	320,00	220,00
24 river	33,89	60,98	78,95	121,83	43,00	7,70	0,44	0,08	0,04	0,0	26,80	30,08	34,59	1300,00	1280,00
28 river	21,29	101,78	94,50	219,42	18,40	10,30	0,25	0,10	0,03	0,0	28,00	34,80	35,05	1460,00	1380,00
30 river	3,63	4,63	9,05	7,94	29,20	17,50	0,30	0,12	0,03	0,0	3,10	2,80	59,63	380,00	320,00

Table 4.2 - Major ion composition of superficial water (concentration in mg/l)

ID sample	Date	$\delta^{18}O$‰	δD	^{3}H	
		V-SMOW	V-SMOW	(U.T.)	+/- (U.T.)
1old	19/02/2007	-5,29	-27,6	1,2	0,6
2old	21/02/2007	-2,79	-8,3	2,6	0,7
3old	21/02/2007	-6,39	-40,1	1,6	0,6
4old	22/02/2007	-4,76	-24,4	1,7	0,6
5old	22/02/2007	-6.54	-39.07	0.9	0.6
6old	17/04/2007	-6,25	-34,5	0.4	0.3
8old	17/04/2007	-5.47	-28,5	1,1	0,4
10old	17/04/2007	-6.70	-39.5	0.8	0.3
13old	16/04/2007	-5,40	-28,8	1,1	0,4
16old	16/04/2007	-5,19	-27,5	2,2	0,5
1eng	18/02/2007	-4,68	-23,3	1,1	0,6
2eng	18/02/2007	-5,14	16,50	n.a.	
3eng	21/02/2007	-5,78	-35,5	1,1	0,6
5eng	22/04/2007	-5,34	-27,3	1,0	0,4
8eng	17/02/2007	-5,55	-33,9	0,8	0,6
16eng	22/04/2007	-5,88	-31,2	0,7	0,4
18eng	18/04/2007	-5,75	-30,2	0,8	0,3
19eng	18/04/2007	-5,47	-27,8	1,0	0,4
22eng	20/02/2007	-5,03	-26,5	2,4	0,7
26eng	05/04/2007	-6,62	-35,3	1,5	0,5
27eng	05/04/2007	-4,62	-23,9	2,2	0,5
28eng	05/04/2007	-5,15	-24,5	1,7	0,5
29eng	05/04/2007	-4,66	-29,9	2,2	0,5
Ichnusa well 1	18/01/2008	-5,64	-29	1,5	0,6
24 river	23/04/2007	-5,24	-25,4	1,5	0,4
Big Momella Lake	17/02/2007	3,88	19,3	1,8	0,7
Small Momella Lake	17/02/2007	2,65	13,5	2,1	0,7
Rain	22/04/2007	-0,73	5,8	2,8	0,9

Table 4.3 - Isotopic water analysis and composition

Analyte Symbol	SiO_2	Al_2O_3	MnO	MgO	CaO	Na_2O	K_2O	TiO2	P_2O_5	Cl^-	F^-
Unit symbol	%	%	%	%	%	%	%	%	%	%	%
Detection limit	0.01	0.01	0.001	0.01	0.01	0.01	0.01	0.001	0.01	0.01	0.01
ROCK											
KSC1	**51.44**	**17.59**	**0.171**	**1.42**	**5.02**	**6.37**	**3.72**	**1.484**	**0.31**	**0.23**	**0.17**
KSG 10	**54.19**	**18.61**	**0.169**	**1.02**	**3.86**	**7.52**	**4.36**	**1.364**	**0.3**	**0.13**	**0.15**
PHON1	**57.08**	**18.63**	**0.147**	**0.87**	**3.02**	**7.71**	**4.36**	**1.09**	**0.22**	**0.15**	**0.13**
NNYK7	**48.87**	**16.09**	**0.183**	**1.64**	**4.56**	**6.56**	**4.16**	**1.681**	**0.4**	**0.08**	**0.13**
SEDIMENT											
KSC2	**41.9**	**20.42**	**0.125**	**1.03**	**3.01**	**3.01**	**3.35**	**1.17**	**0.29**	**0.04**	**0.2**
OLD 3-4-5	**30.12**	**9.16**	**0.157**	**4.25**	**21.08**	**21.08**	**2.87**	**3.01**	**0.7**	**0.11**	**0.21**
l KSFLO	**47.86**	**16.25**	**0.217**	**3.21**	**7.83**	**7.83**	**6.67**	**2.601**	**0.85**	**0.23**	**0.2**
KSG 9	**20.98**	**9.86**	**0.044**	**1.03**	**32.21**	**32.21**	**1.05**	**0.273**	**0.04**	**0.02**	**0.11**
KSG 11	**46.21**	**18.61**	**0.19**	**1.7**	**4.28**	**4.28**	**3.45**	**1.807**	**0.3**	**0.04**	**0.07**
NNYK6	**51.39**	**14.78**	**0.212**	**1.53**	**3.69**	**3.69**	**3.74**	**2.213**	**0.53**	**0.16**	**0.16**
NNYK8	**44.59**	**15.59**	**0.204**	**2.36**	**6.78**	**6.78**	**9.13**	**2.249**	**0.58**	**0.4**	**0.38**

Table 4.4 - Chemical composition of rocks and sediments

	NNYK6	NNYK7	NNYK8	NNYK8b	2474 C	2474 S	Olds 3-4-5	NNYK7	OLD 10	31 eng	PHON1	KSG9	KSG11
Phillipsite	no	x	x	x	x	x	no	x	x	no	no	no	no
Chabazite	no	x	x	x	x	x	no	x	x	no	no	no	no
Analcime	no	x	x	x	x	x	no	x	no	no	x	no	no
Nepheline	x	x	x	x	x	x	x	x	x	x	x	no	x
Leucite	x	x	x	x		x	no	x	x	x	tr	no	no
Anorthoclase	x	x	x	x	x	x	x	x	x	x	x	x	x
Sanidine	x	x	x	x	no	x	x	x	x	x	x	x	x
Albite/anorthite	no	x	x	x	x	no	no	x	no	no	no	no	x
Riebeckite	x	x	x	no	no	no	no	x	x	x	no	no	x
Augite	no	x	x	x	x	x	x	x	x	x	x	no	x
Miche	no	x	x	x	no	no	x	x	no	no	no	no	no
Illite/smectite	x	no	no	no	no	no	no	no	no	no	no	x	x
Trona	no	no	no	x	x	no	no	no	no	no	no	no	no
Natron	no	no	tr	x	no	no	?	no	no	no	no	no	no
Natrite	x	no	tr	x	no	no	no	no	no	no	x	no	no
Calcite	no	no	no	no	no	no	x	no	no	no/tr	no	x	no
Cancrinite	no	x	x	no	x	no	no	x	x	no	no	no	no
Sylvite	no	no	x	x	no	x	no	no	no	no	no	no	no
Fluorapatite	no	x	x	x	x	x	no	x	x	x	x	no	no

Table 4.5 - XRF analysis results

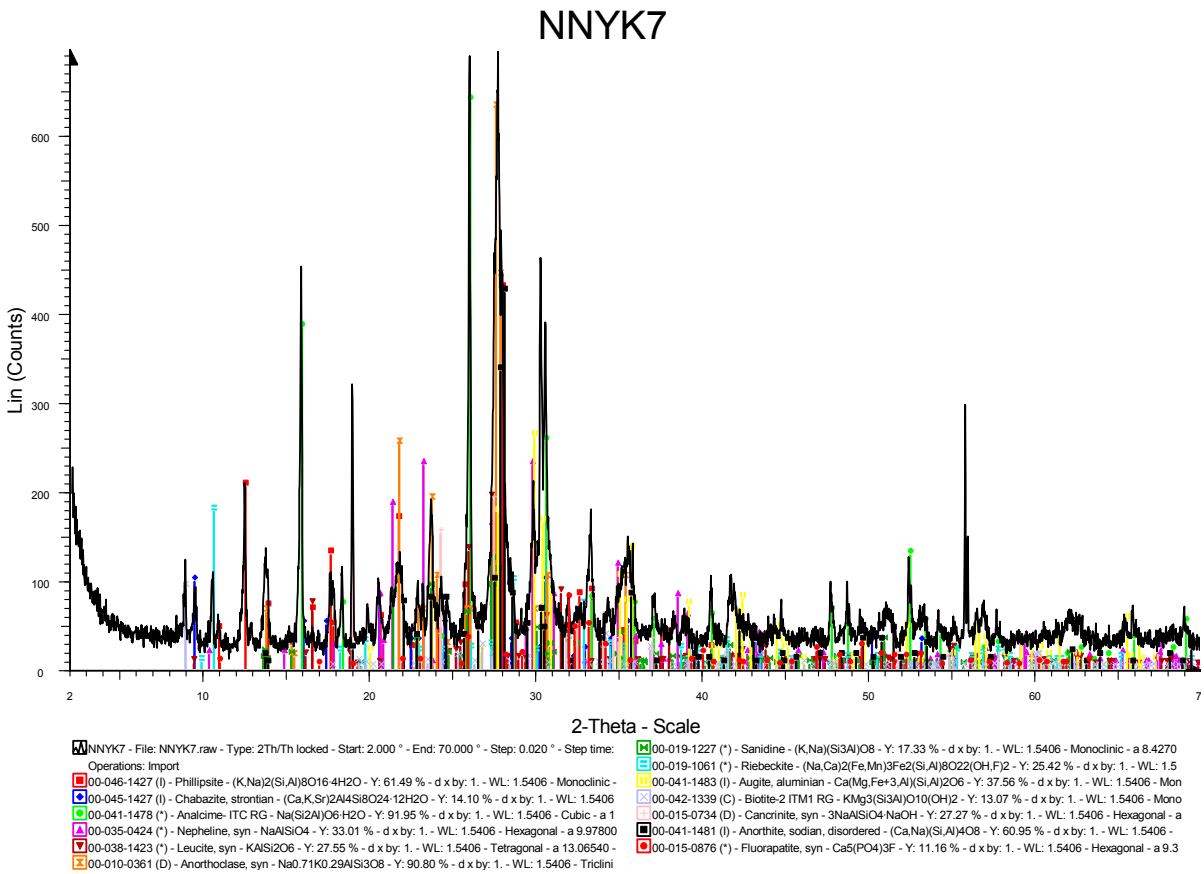
NNYK7
Lin (Counts)
2-Theta - Scale
NNYK7 - File: NNYK7.raw - Type: 2Th/Th locked - Start: 2.000 ° - End: 70.000 ° - Step: 0.020 ° - Step time:
Operations: Import
00-046-1427 (I) - Phillipsite - (K,Na)2(Si,Al)8O16·4H2O - Y: 61.49 % - d x by: 1. - WL: 1.5406 - Monoclinic -
00-045-1427 (I) - Chabazite, strontian - (Ca,K,Sr)2Al4Si8O24·12H2O - Y: 14.10 % - d x by: 1. - WL: 1.5406
00-041-1478 (*) - Analcime- ITC RG - Na(Si2Al)O6·H2O - Y: 91.95 % - d x by: 1. - WL: 1.5406 - Cubic - a 1
00-035-0424 (*) - Nepheline, syn - NaAlSiO4 - Y: 33.01 % - d x by: 1. - WL: 1.5406 - Hexagonal - a 9.97800
00-038-1423 (*) - Leucite, syn - KAlSi2O6 - Y: 27.55 % - d x by: 1. - WL: 1.5406 - Tetragonal - a 13.06540 -
00-010-0361 (D) - Anorthoclase, syn - Na0.71K0.29AlSi3O8 - Y: 90.80 % - d x by: 1. - WL: 1.5406 - Triclini
00-019-1227 (*) - Sanidine - (K,Na)(Si3Al)O8 - Y: 17.33 % - d x by: 1. - WL: 1.5406 - Monoclinic - a 8.4270
00-019-1061 (*) - Riebeckite - (Na,Ca)2(Fe,Mn)3Fe2(Si,Al)8O22(OH,F)2 - Y: 25.42 % - d x by: 1. - WL: 1.5
00-041-1483 (I) - Augite, aluminian - Ca(Mg,Fe+3,Al)(Si,Al)2O6 - Y: 37.56 % - d x by: 1. - WL: 1.5406 - Mon
00-042-1339 (C) - Biotite-2 ITM1 RG - KMg3(Si3Al)O10(OH)2 - Y: 13.07 % - d x by: 1. - WL: 1.5406 - Mono
00-015-0734 (D) - Cancrinite, syn - 3NaAlSiO4·NaOH - Y: 27.27 % - d x by: 1. - WL: 1.5406 - Hexagonal - a
00-041-1481 (I) - Anorthite, sodian, disordered - (Ca,Na)(Si,Al)4O8 - Y: 60.95 % - d x by: 1. - WL: 1.5406 -
00-015-0876 (*) - Fluorapatite, syn - Ca5(PO4)3F - Y: 11.16 % - d x by: 1. - WL: 1.5406 - Hexagonal - a 9.3

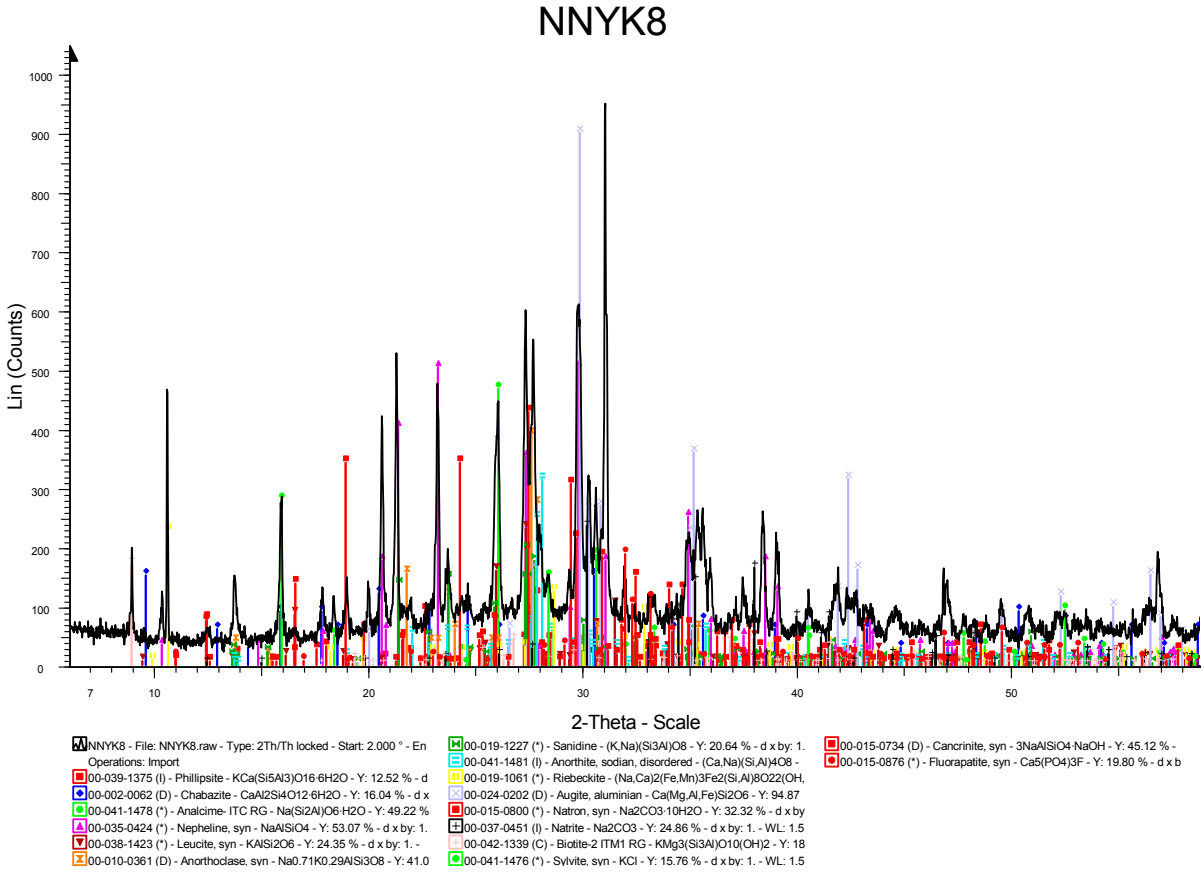
NNYK8
Lin (Counts)
2-Theta - Scale
NNYK8 - File: NNYK8.raw - Type: 2Th/Th locked - Start: 2.000 ° - En
Operations: Import
00-039-1375 (I) - Phillipsite - KCa(Si5Al3)O16·6H2O - Y: 12.52 % - d
00-002-0062 (D) - Chabazite - CaAl2Si4O12·6H2O - Y: 16.04 % - d x
00-041-1478 (*) - Analcime- ITC RG - Na(Si2Al)O6·H2O - Y: 49.22 %
00-035-0424 (*) - Nepheline, syn - NaAlSiO4 - Y: 53.07 % - d x by: 1.
00-038-1423 (*) - Leucite, syn - KAlSi2O6 - Y: 24.35 % - d x by: 1. -
00-010-0361 (D) - Anorthoclase, syn - Na0.71K0.29AlSi3O8 - Y: 41.0
00-019-1227 (*) - Sanidine - (K,Na)(Si3Al)O8 - Y: 20.64 % - d x by: 1.
00-041-1481 (I) - Anorthite, sodian, disordered - (Ca,Na)(Si,Al)4O8 -
00-019-1061 (*) - Riebeckite - (Na,Ca)2(Fe,Mn)3Fe2(Si,Al)8O22(OH,
00-024-0202 (D) - Augite, aluminian - Ca(Mg,Al,Fe)Si2O6 - Y: 94.87
00-015-0800 (*) - Natron, syn - Na2CO3·10H2O - Y: 32.32 % - d x by
00-037-0451 (I) - Natrite - Na2CO3 - Y: 24.86 % - d x by: 1. - WL: 1.5
00-042-1339 (C) - Biotite-2 ITM1 RG - KMg3(Si3Al)O10(OH)2 - Y: 18
00-041-1476 (*) - Sylvite, syn - KCl - Y: 15.76 % - d x by: 1. - WL: 1.5
00-015-0734 (D) - Cancrinite, syn - 3NaAlSiO4·NaOH - Y: 45.12 % -
00-015-0876 (*) - Fluorapatite, syn - Ca5(PO4)3F - Y: 19.80 % - d x b

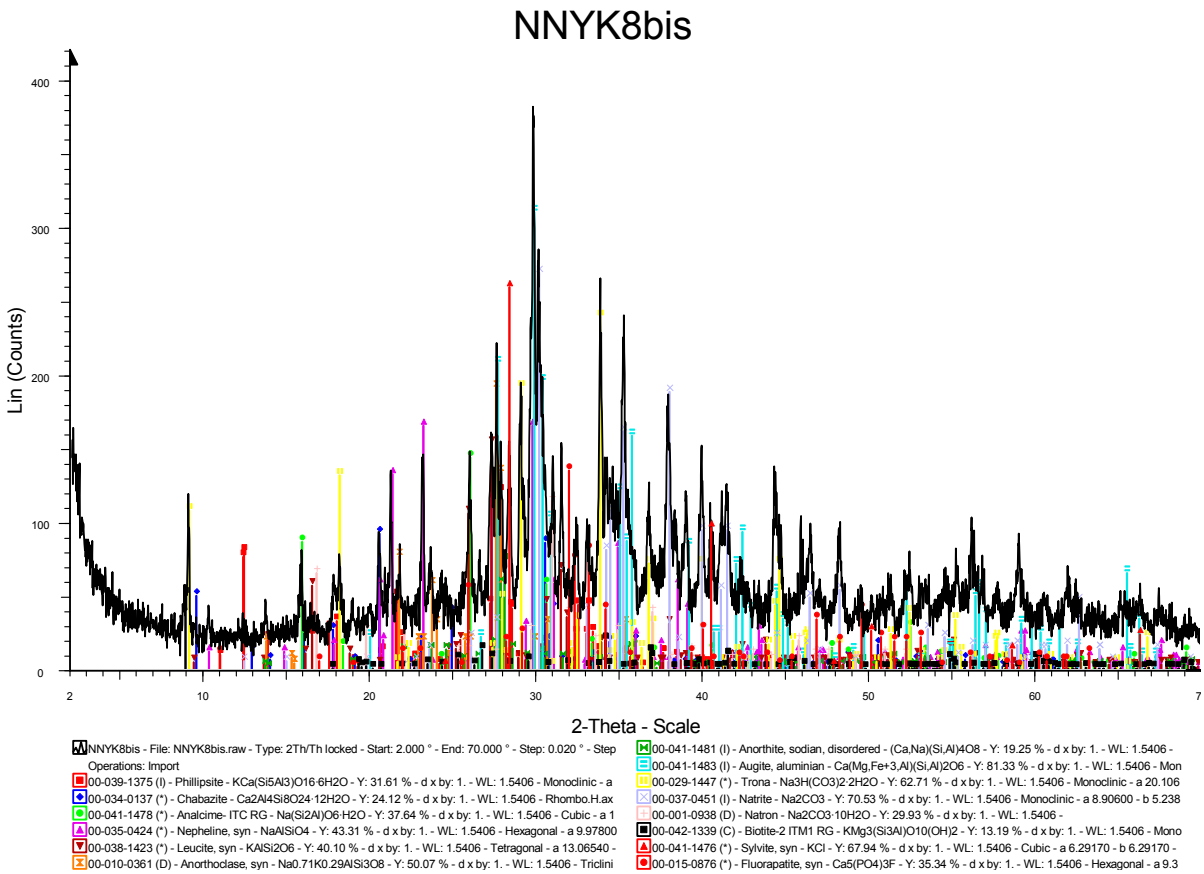
NNYK8bis
Lin (Counts)
2-Theta - Scale
NNYK8bis - File: NNYK8bis.raw - Type: 2Th/Th locked - Start: 2.000 ° - End: 70.000 ° - Step: 0.020 ° - Step
Operations: Import
00-039-1375 (I) - Phillipsite - KCa(Si5Al3)O16·6H2O - Y: 31.61 % - d x by: 1. - WL: 1.5406 - Monoclinic - a
00-034-0137 (*) - Chabazite - Ca2Al4Si8O24·12H2O - Y: 24.12 % - d x by: 1. - WL: 1.5406 - Rhombo.H.ax
00-041-1478 (*) - Analcime- ITC RG - Na(Si2Al)O6·H2O - Y: 37.64 % - d x by: 1. - WL: 1.5406 - Cubic - a 1
00-035-0424 (*) - Nepheline, syn - NaAlSiO4 - Y: 43.31 % - d x by: 1. - WL: 1.5406 - Hexagonal - a 9.97800
00-038-1423 (*) - Leucite, syn - KAlSi2O6 - Y: 40.10 % - d x by: 1. - WL: 1.5406 - Tetragonal - a 13.06540 -
00-010-0361 (D) - Anorthoclase, syn - Na0.71K0.29AlSi3O8 - Y: 50.07 % - d x by: 1. - WL: 1.5406 - Triclini
00-041-1481 (I) - Anorthite, sodian, disordered - (Ca,Na)(Si,Al)4O8 - Y: 19.25 % - d x by: 1. - WL: 1.5406 -
00-041-1483 (I) - Augite, aluminian - Ca(Mg,Fe+3,Al)(Si,Al)2O6 - Y: 81.33 % - d x by: 1. - WL: 1.5406 - Mon
00-029-1447 (*) - Trona - Na3H(CO3)2·2H2O - Y: 62.71 % - d x by: 1. - WL: 1.5406 - Monoclinic - a 20.106
00-037-0451 (I) - Natrite - Na2CO3 - Y: 70.53 % - d x by: 1. - WL: 1.5406 - Monoclinic - a 8.90600 - b 5.238
00-001-0938 (D) - Natron - Na2CO3·10H2O - Y: 29.93 % - d x by: 1. - WL: 1.5406 -
00-042-1339 (C) - Biotite-2 ITM1 RG - KMg3(Si3Al)O10(OH)2 - Y: 13.19 % - d x by: 1. - WL: 1.5406 - Mono
00-041-1476 (*) - Sylvite, syn - KCl - Y: 67.94 % - d x by: 1. - WL: 1.5406 - Cubic - a 6.29170 - b 6.29170 -
00-015-0876 (*) - Fluorapatite, syn - Ca5(PO4)3F - Y: 35.34 % - d x by: 1. - WL: 1.5406 - Hexagonal - a 9.3

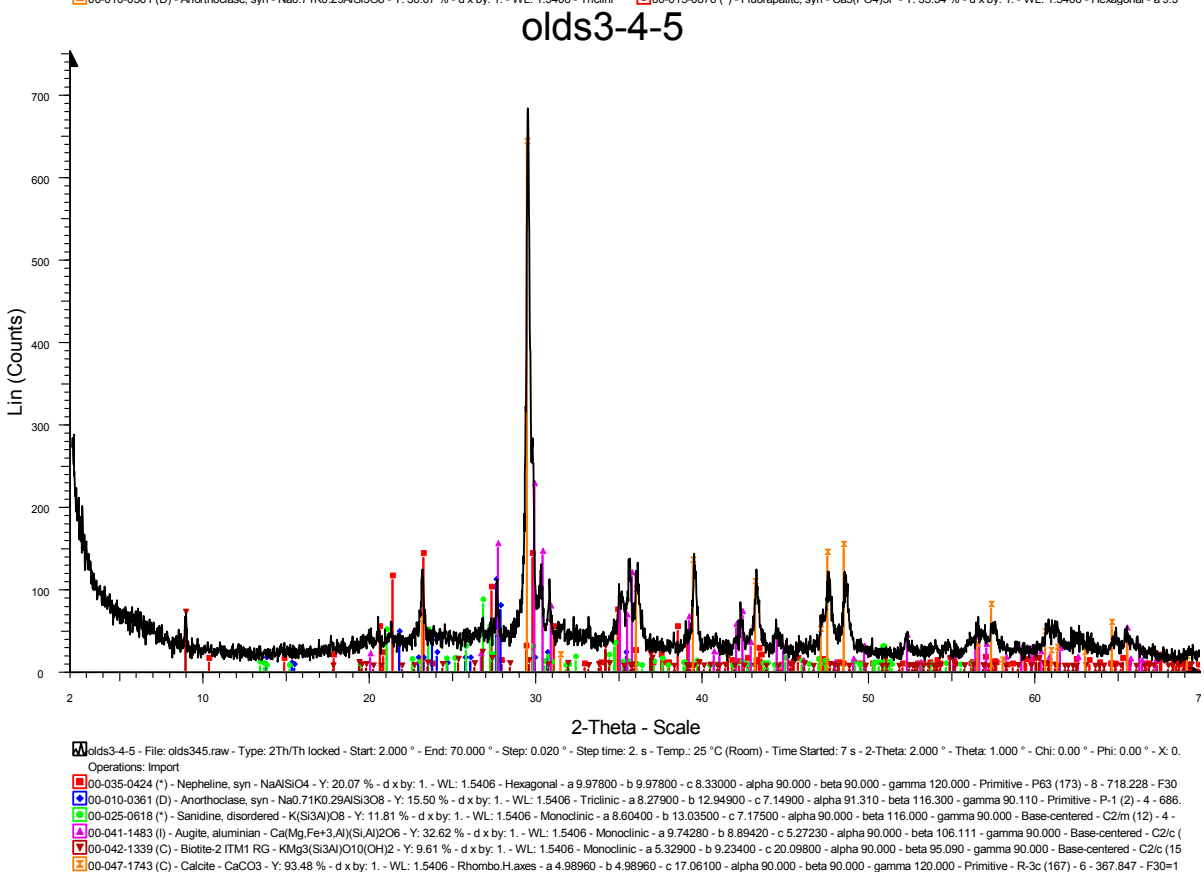
olds3-4-5
Lin (Counts)
2-Theta - Scale
olds3-4-5 - File: olds345.raw - Type: 2Th/Th locked - Start: 2.000 ° - End: 70.000 ° - Step: 0.020 ° - Step time: 2. s - Temp.: 25 °C (Room) - Time Started: 7 s - 2-Theta: 2.000 ° - Theta: 1.000 ° - Chi: 0.00 ° - Phi: 0.00 ° - X: 0.
Operations: Import
00-035-0424 (*) - Nepheline, syn - NaAlSiO4 - Y: 20.07 % - d x by: 1. - WL: 1.5406 - Hexagonal - a 9.97800 - b 9.97800 - c 8.33000 - alpha 90.000 - beta 90.000 - gamma 120.000 - Primitive - P63 (173) - 8 - 718.228 - F30
00-010-0361 (D) - Anorthoclase, syn - Na0.71K0.29AlSi3O8 - Y: 15.50 % - d x by: 1. - WL: 1.5406 - Triclinic - a 8.27900 - b 12.94900 - c 7.14900 - alpha 91.310 - beta 116.300 - gamma 90.110 - Primitive - P-1 (2) - 4 - 686.
00-025-0618 (*) - Sanidine, disordered - K(Si3Al)O8 - Y: 11.81 % - d x by: 1. - WL: 1.5406 - Monoclinic - a 8.60400 - b 13.03500 - c 7.17500 - alpha 90.000 - beta 116.000 - gamma 90.000 - Base-centered - C2/m (12) - 4 -
00-041-1483 (I) - Augite, aluminian - Ca(Mg,Fe+3,Al)(Si,Al)2O6 - Y: 32.62 % - d x by: 1. - WL: 1.5406 - Monoclinic - a 9.74280 - b 8.89420 - c 5.27230 - alpha 90.000 - beta 106.111 - gamma 90.000 - Base-centered - C2/c (
00-042-1339 (C) - Biotite-2 ITM1 RG - KMg3(Si3Al)O10(OH)2 - Y: 9.61 % - d x by: 1. - WL: 1.5406 - Monoclinic - a 5.32900 - b 9.23400 - c 20.09800 - alpha 90.000 - beta 95.090 - gamma 90.000 - Base-centered - C2/c (15
00-047-1743 (C) - Calcite - CaCO3 - Y: 93.48 % - d x by: 1. - WL: 1.5406 - Rhombo.H.axes - a 4.98960 - b 4.98960 - c 17.06100 - alpha 90.000 - beta 90.000 - gamma 120.000 - Primitive - R-3c (167) - 6 - 367.847 - F30=1

KSG9

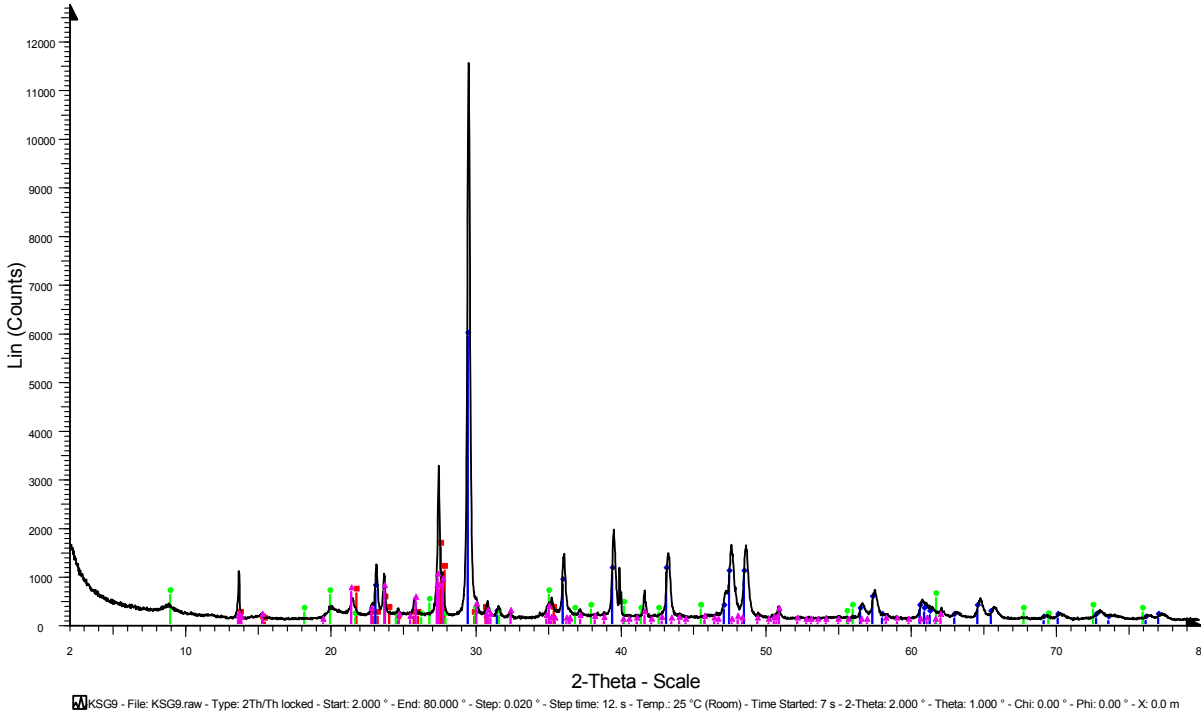
Lin (Counts)
2-Theta - Scale
KSG9 - File: KSG9.raw - Type: 2Th/Th locked - Start: 2.000 ° - End: 80.000 ° - Step: 0.020 ° - Step time: 12. s - Temp.: 25 °C (Room) - Time Started: 7 s - 2-Theta: 2.000 ° - Theta: 1.000 ° - Chi: 0.00 ° - Phi: 0.00 ° - X: 0.0 m
Operations: Import
00-010-0361 (D) - Anorthoclase, syn - Na0.71K0.29AlSi3O8 - Y: 13.63 % - d x by: 1. - WL: 1.5406 - Triclinic - a 8.27900 - b 12.94900 - c 7.14900 - alpha 91.310 - beta 116.300 - gamma 90.110 - Primitive - P-1 (2) - 4 - 686.
00-019-1227 (*) - Sanidine - (K,Na)(Si3Al)O8 - Y: 8.16 % - d x by: 1. - WL: 1.5406 - Monoclinic - a 8.42700 - b 13.00000 - c 7.16800 - alpha 90.000 - beta 116.100 - gamma 90.000 - Base-centered - C2/m (12) - 4 - 705.187
00-005-0586 (*) - Calcite, syn - CaCO3 - Y: 51.23 % - d x by: 1. - WL: 1.5406 - Rhombo.H.axes - a 4.98900 - b 4.98900 - c 17.06200 - alpha 90.000 - beta 90.000 - gamma 120.000 - Primitive - R-3c (167) - 6 - 367.780 - I/Ic
00-002-0050 (D) - Illite - 2K2O·3MgO·Al2O3·24SiO2·12H2O - Y: 5.21 % - d x by: 1. - WL: 1.5406 -

KSG11

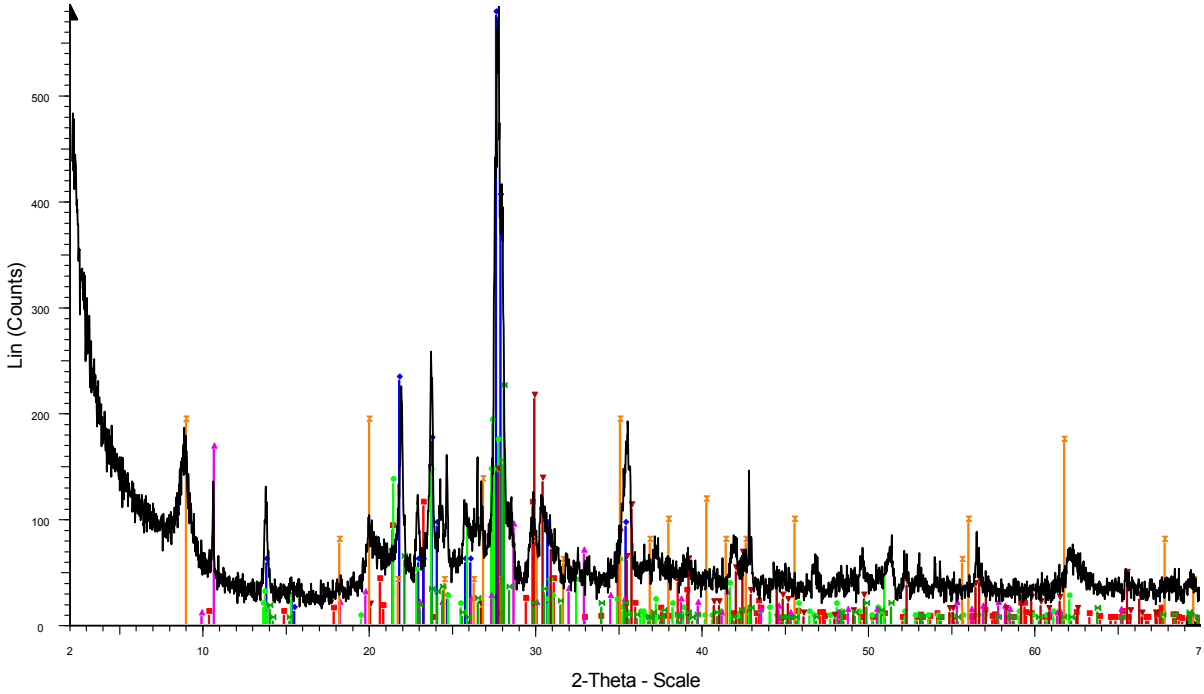
Lin (Counts)
2-Theta - Scale
KSG11 - File: KSG11.raw - Type: 2Th/Th locked - Start: 2.000 ° - End: 70.000 ° - Step: 0.020 ° - Step time:
00-041-1480 (I) - Albite, calcian, ordered - (Na,Ca)Al(Si,Al)3O8 - Y: 38.00 % - d x by: 1. - WL: 1.5406 - Tricli
Operations: Import
00-035-0424 (*) - Nepheline, syn - NaAlSiO4 - Y: 19.01 % - d x by: 1. - WL: 1.5406 - Hexagonal - a 9.97800
00-010-0361 (D) - Anorthoclase, syn - Na0.71K0.29AlSi3O8 - Y: 98.50 % - d x by: 1. - WL: 1.5406 - Triclini
00-019-1227 (*) - Sanidine - (K,Na)(Si3Al)O8 - Y: 32.47 % - d x by: 1. - WL: 1.5406 - Monoclinic - a 8.4270
00-019-1061 (*) - Riebeckite - (Na,Ca)2(Fe,Mn)3Fe2(Si,Al)8O22(OH,F)2 - Y: 28.21 % - d x by: 1. - WL: 1.5
00-041-1483 (I) - Augite, aluminian - Ca(Mg,Fe+3,Al)(Si,Al)2O6 - Y: 36.45 % - d x by: 1. - WL: 1.5406 - Mon
00-002-0050 (D) - Illite - 2K2O·3MgO·Al2O3·24SiO2·12H2O - Y: 32.58 % - d x by: 1. - WL: 1.5406 -

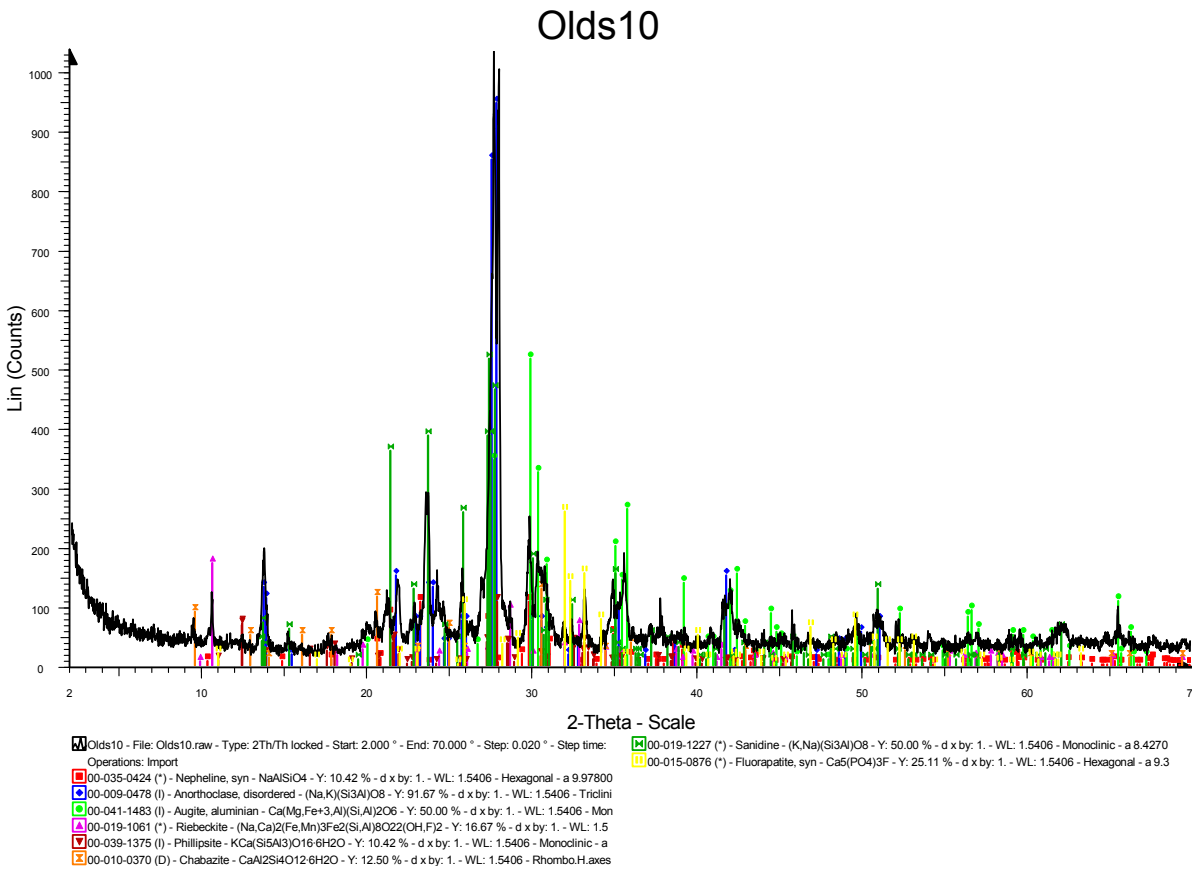
Olds10
Lin (Counts)
2-Theta - Scale
Olds10 - File: Olds10.raw - Type: 2Th/Th locked - Start: 2.000 ° - End: 70.000 ° - Step: 0.020 ° - Step time:
Operations: Import
00-035-0424 (*) - Nepheline, syn - NaAlSiO4 - Y: 10.42 % - d x by: 1. - WL: 1.5406 - Hexagonal - a 9.97800
00-009-0478 (I) - Anorthoclase, disordered - (Na,K)(Si3Al)O8 - Y: 91.67 % - d x by: 1. - WL: 1.5406 - Triclini
00-041-1483 (I) - Augite, aluminian - Ca(Mg,Fe+3,Al)(Si,Al)2O6 - Y: 50.00 % - d x by: 1. - WL: 1.5406 - Mon
00-019-1061 (*) - Riebeckite - (Na,Ca)2(Fe,Mn)3Fe2(Si,Al)8O22(OH,F)2 - Y: 16.67 % - d x by: 1. - WL: 1.5
00-039-1375 (I) - Phillipsite - KCa(Si5Al3)O16·6H2O - Y: 10.42 % - d x by: 1. - WL: 1.5406 - Monoclinic - a
00-010-0370 (D) - Chabazite - CaAl2Si4O12·6H2O - Y: 12.50 % - d x by: 1. - WL: 1.5406 - Rhombo.H.axes
00-019-1227 (*) - Sanidine - (K,Na)(Si3Al)O8 - Y: 50.00 % - d x by: 1. - WL: 1.5406 - Monoclinic - a 8.4270
00-015-0876 (*) - Fluorapatite, syn - Ca5(PO4)3F - Y: 25.11 % - d x by: 1. - WL: 1.5406 - Hexagonal - a 9.3

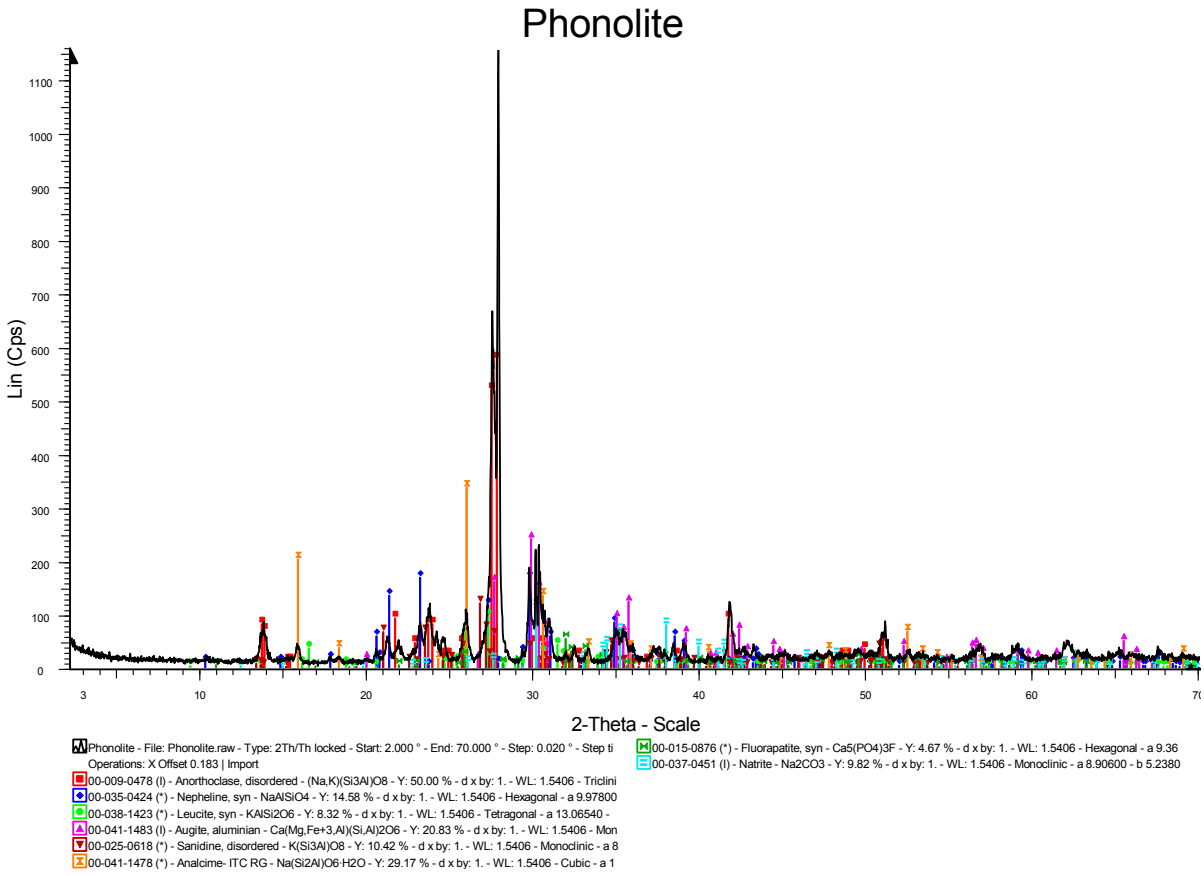
Phonolite
Lin (Cps)
2-Theta - Scale
Phonolite - File: Phonolite.raw - Type: 2Th/Th locked - Start: 2.000 ° - End: 70.000 ° - Step: 0.020 ° - Step ti
Operations: X Offset 0.183 | Import
00-009-0478 (I) - Anorthoclase, disordered - (Na,K)(Si3Al)O8 - Y: 50.00 % - d x by: 1. - WL: 1.5406 - Triclini
00-035-0424 (*) - Nepheline, syn - NaAlSiO4 - Y: 14.58 % - d x by: 1. - WL: 1.5406 - Hexagonal - a 9.97800
00-038-1423 (*) - Leucite, syn - KAlSi2O6 - Y: 8.32 % - d x by: 1. - WL: 1.5406 - Tetragonal - a 13.06540 -
00-041-1483 (I) - Augite, aluminian - Ca(Mg,Fe+3,Al)(Si,Al)2O6 - Y: 20.83 % - d x by: 1. - WL: 1.5406 - Mon
00-025-0618 (*) - Sanidine, disordered - K(Si3Al)O8 - Y: 10.42 % - d x by: 1. - WL: 1.5406 - Monoclinic - a 8
00-041-1478 (*) - Analcime- ITC RG - Na(Si2Al)O6·H2O - Y: 29.17 % - d x by: 1. - WL: 1.5406 - Cubic - a 1
00-015-0876 (*) - Fluorapatite, syn - Ca5(PO4)3F - Y: 4.67 % - d x by: 1. - WL: 1.5406 - Hexagonal - a 9.36
00-037-0451 (I) - Natrite - Na2CO3 - Y: 9.82 % - d x by: 1. - WL: 1.5406 - Monoclinic - a 8.90600 - b 5.2380

2474 C

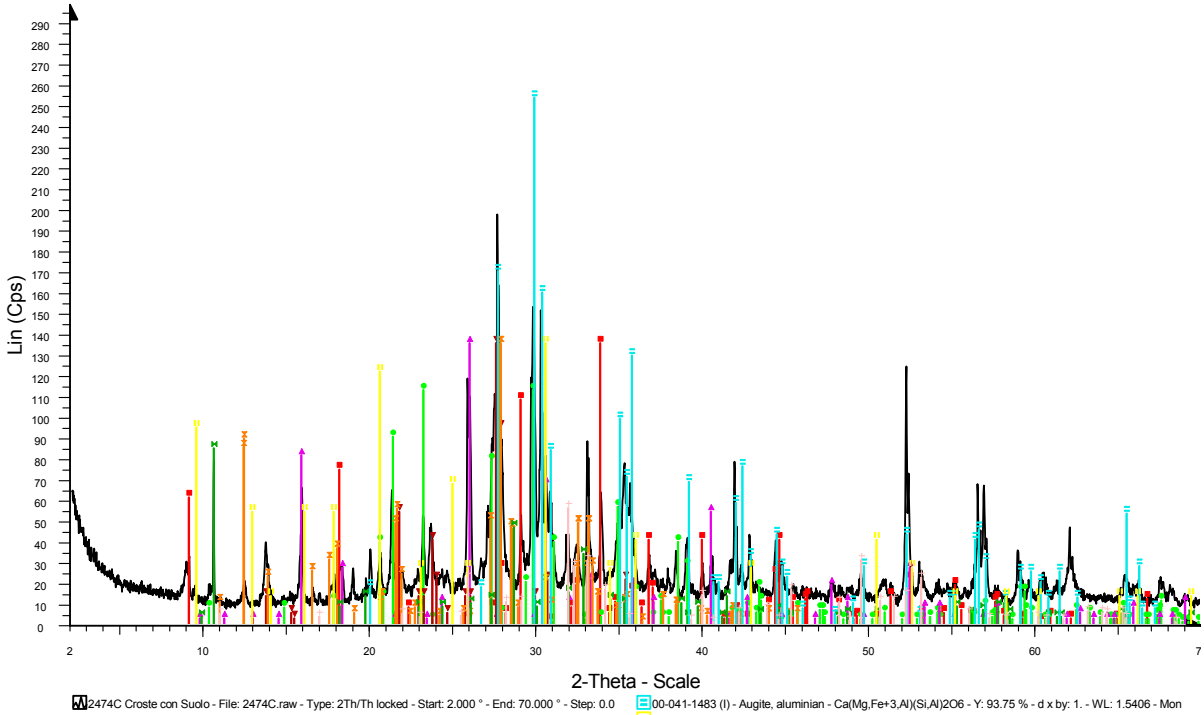

2474C Croste con Suolo - File: 2474C.raw - Type: 2Th/Th locked - Start: 2.000 ° - End: 70.000 ° - Step: 0.0
Operations: Import
00-029-1447 (*) - Trona - Na3H(CO3)2·2H2O - Y: 50.00 % - d x by: 1. - WL: 1.5406 - Monoclinic - a 20.106
00-035-0424 (*) - Nepheline, syn - NaAlSiO4 - Y: 41.67 % - d x by: 1. - WL: 1.5406 - Hexagonal - a 9.97800
00-019-1180 (N) - Analcime- ITO RG - Na(Si2Al)O6·H2O - Y: 50.00 % - d x by: 1. - WL: 1.5406 - Orthorhom
00-010-0361 (D) - Anorthoclase, syn - Na0.71K0.29AlSi3O8 - Y: 50.00 % - d x by: 1. - WL: 1.5406 - Triclini
00-039-1375 (I) - Phillipsite - KCa(Si5Al3)O16·6H2O - Y: 50.00 % - d x by: 1. - WL: 1.5406 - Monoclinic - a
00-019-1061 (*) - Riebeckite - (Na,Ca)2(Fe,Mn)3Fe2(Si,Al)8O22(OH,F)2 - Y: 31.26 % - d x by: 1. - WL: 1.5
00-041-1483 (I) - Augite, aluminian - Ca(Mg,Fe+3,Al)(Si,Al)2O6 - Y: 93.75 % - d x by: 1. - WL: 1.5406 - Mon
00-010-0370 (D) - Chabazite - CaAl2Si4O12·6H2O - Y: 50.00 % - d x by: 1. - WL: 1.5406 - Rhombo.H.axes
00-034-0011 (D) - Fluorapatite, syn - Ca5(PO4)3F - Y: 20.65 % - d x by: 1. - WL: 1.5406 - Hexagonal - a 9.3

2474 S

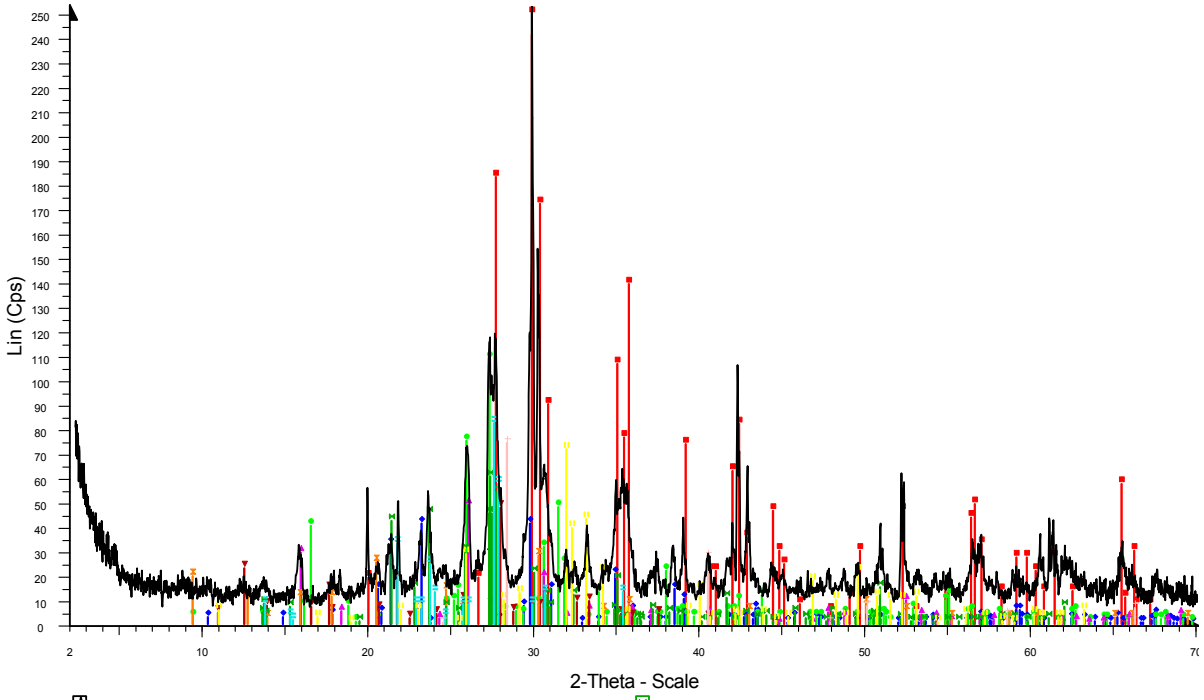

2474S Suolo Sab. Sup. - File: 2474S.raw - Type: 2Th/Th locked - Start: 2.000 ° - End: 70.000 ° - Step: 0.02
Operations: Displacement 0.000 | Displacement -0.250 | X Offset 0.200 | X Offset 0.167 | X Offset 0.200 | Im
00-041-1483 (I) - Augite, aluminian - Ca(Mg,Fe+3,Al)(Si,Al)2O6 - Y: 108.08 % - d x by: 1. - WL: 1.5406 - Mo
00-035-0424 (*) - Nepheline, syn - NaAlSiO4 - Y: 16.33 % - d x by: 1. - WL: 1.5406 - Hexagonal - a 9.97800
00-038-1423 (*) - Leucite, syn - KAlSi2O6 - Y: 43.06 % - d x by: 1. - WL: 1.5406 - Tetragonal - a 13.06540 -
00-041-1478 (*) - Analcime- ITC RG - Na(Si2Al)O6·H2O - Y: 19.35 % - d x by: 1. - WL: 1.5406 - Cubic - a 1
00-046-1427 (I) - Phillipsite - (K,Na)2(Si,Al)8O16·4H2O - Y: 18.87 % - d x by: 1. - WL: 1.5406 - Monoclinic -
00-010-0370 (D) - Chabazite - CaAl2Si4O12·6H2O - Y: 11.14 % - d x by: 1. - WL: 1.5406 - Rhombo.H.axes
00-019-1227 (*) - Sanidine - (K,Na)(Si3Al)O8 - Y: 23.89 % - d x by: 1. - WL: 1.5406 - Monoclinic - a 8.4270
00-010-0361 (D) - Anorthoclase, syn - Na0.71K0.29AlSi3O8 - Y: 32.56 % - d x by: 1. - WL: 1.5406 - Triclini
00-015-0876 (*) - Fluorapatite, syn - Ca5(PO4)3F - Y: 28.36 % - d x by: 1. - WL: 1.5406 - Hexagonal - a 9.3
00-041-1476 (*) - Sylvite, syn - KCl - Y: 29.37 % - d x by: 1. - WL: 1.5406 - Cubic - a 6.29170 - b 6.29170 -

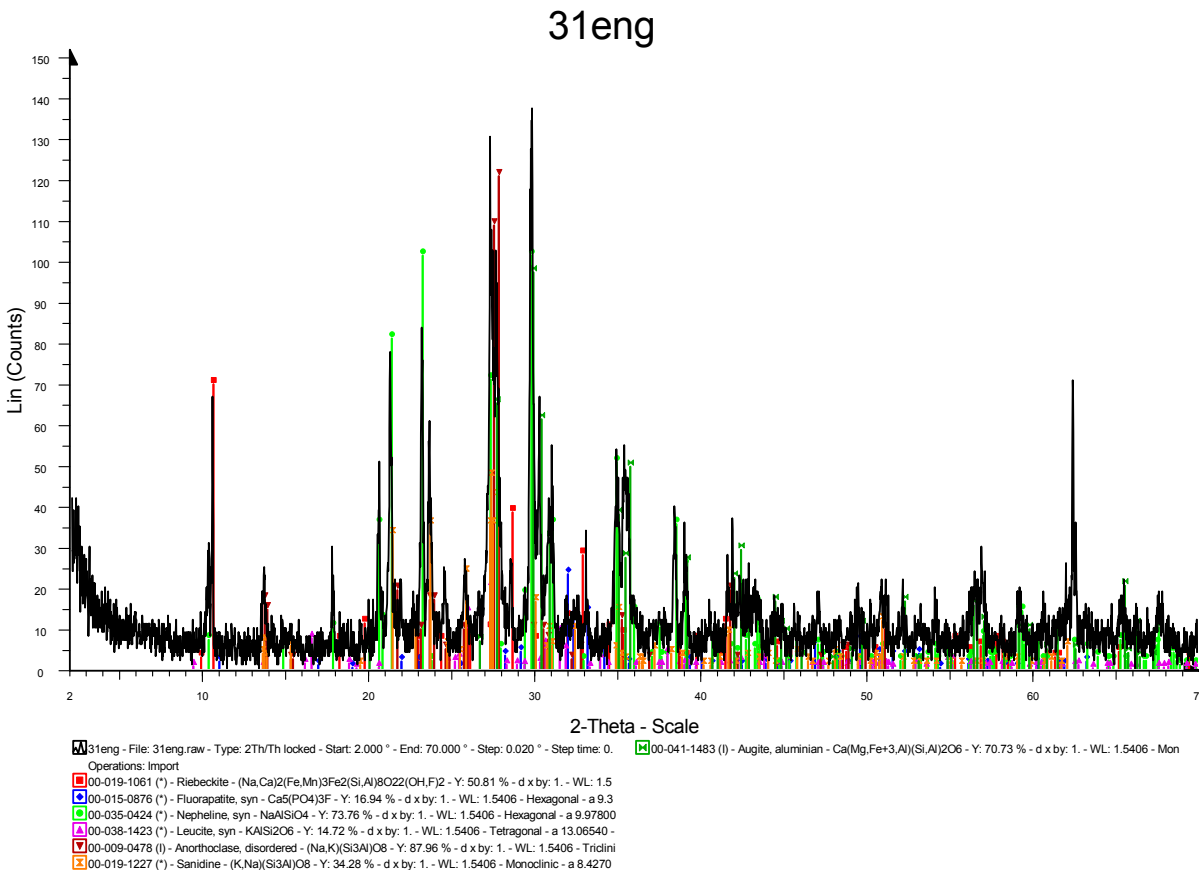
31eng
Lin (Counts)
2-Theta - Scale
31eng - File: 31eng.raw - Type: 2Th/Th locked - Start: 2.000 ° - End: 70.000 ° - Step: 0.020 ° - Step time: 0.
Operations: Import
00-019-1061 (*) - Riebeckite - (Na,Ca)2(Fe,Mn)3Fe2(Si,Al)8O22(OH,F)2 - Y: 50.81 % - d x by: 1. - WL: 1.5
00-015-0876 (*) - Fluorapatite, syn - Ca5(PO4)3F - Y: 16.94 % - d x by: 1. - WL: 1.5406 - Hexagonal - a 9.3
00-035-0424 (*) - Nepheline, syn - NaAlSiO4 - Y: 73.76 % - d x by: 1. - WL: 1.5406 - Hexagonal - a 9.97800
00-038-1423 (*) - Leucite, syn - KAlSi2O6 - Y: 14.72 % - d x by: 1. - WL: 1.5406 - Tetragonal - a 13.06540 -
00-009-0478 (I) - Anorthoclase, disordered - (Na,K)(Si3Al)O8 - Y: 87.96 % - d x by: 1. - WL: 1.5406 - Triclini
00-019-1227 (*) - Sanidine - (K,Na)(Si3Al)O8 - Y: 34.28 % - d x by: 1. - WL: 1.5406 - Monoclinic - a 8.4270
00-041-1483 (I) - Augite, aluminian - Ca(Mg,Fe+3,Al)(Si,Al)2O6 - Y: 70.73 % - d x by: 1. - WL: 1.5406 - Mon

5. INFERENCE FROM THE ANALYTICAL RESULTS

5.1. GEOPHYSICAL DATA

The VES campaign allowed both locate several areas potentially interesting for searching groundwater resources and improve the hydrogeological interpretation of study area. Particularly, the most interesting results comes from the Ngarenanyuki ward. Hereafter, the soundings pertaining to this ward will be discussed. The VES position map for the Ngarenanyiuki ward was shown earlier in figure 3.4.

Most of soundings exhibit a typical feature consisting of a low resistivity layer confined between two relatively high resistivity ones. Figure 5.1a shows four among the most promising apparent resistivity curves acquired in the Ngarenanyuki Ward and the corresponding interpretations. In the figure, the portion of the apparent resistivity curve corresponding to the anomaly, which can be interpreted as a confined or semi-confined aquifer, is evidenced with an ellipse, and the presumed aquifer layer is indicated with an arrow in the respective resistivity column obtained through the inversion process. The consequent deduction is that in the sub-area including the above discussed soundings the occurrence of a layer, associated with a confined or semi-confined aquifer, at a depth of 20-36 m from the ground surface with noticeable thickness is highly plausible.

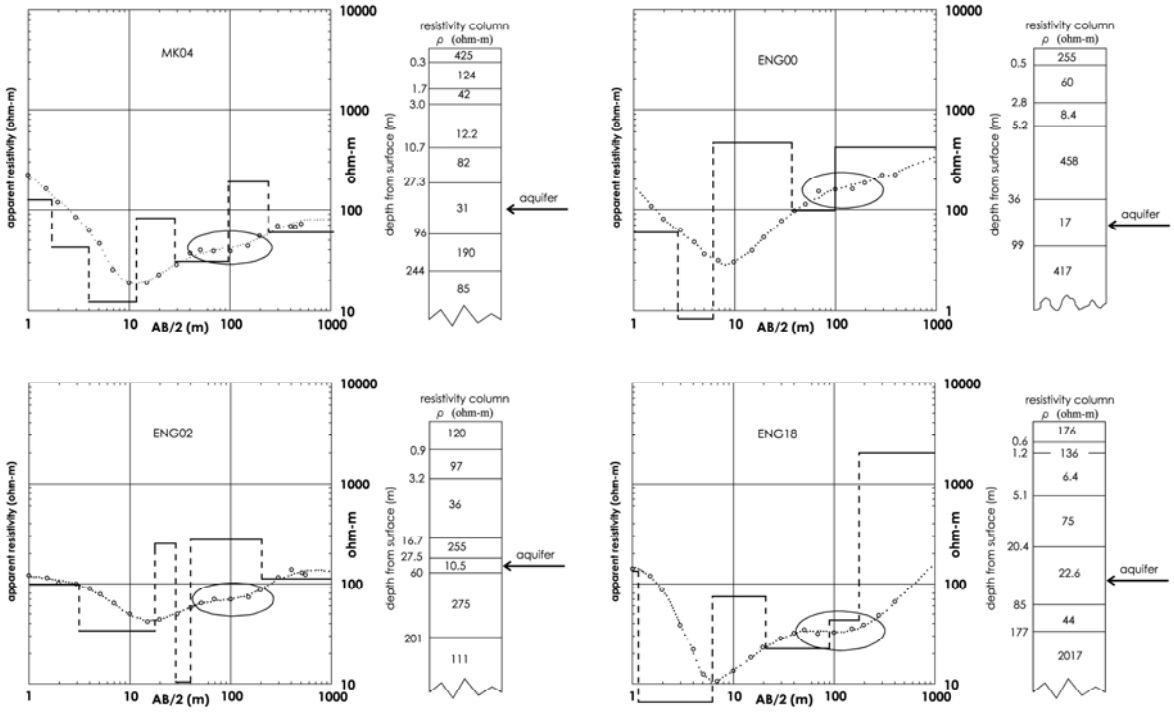

Figure 5.1a - Apparent resistivity curves (left) and interpreted resistivity column (right). In the diagram, the small circles represent the experimental values, and the dotted line the apparent resistivity curve corresponding to the resistivity column on the right

For comparison, the result pertaining to sounding ENG15 is shown in Figure 5.1b: as can be seen, apart the low values associated with the clayey, more or less wet, top soil, the resistivity increases continuously and anomalies that could be associated with a confined aquifer are missing.

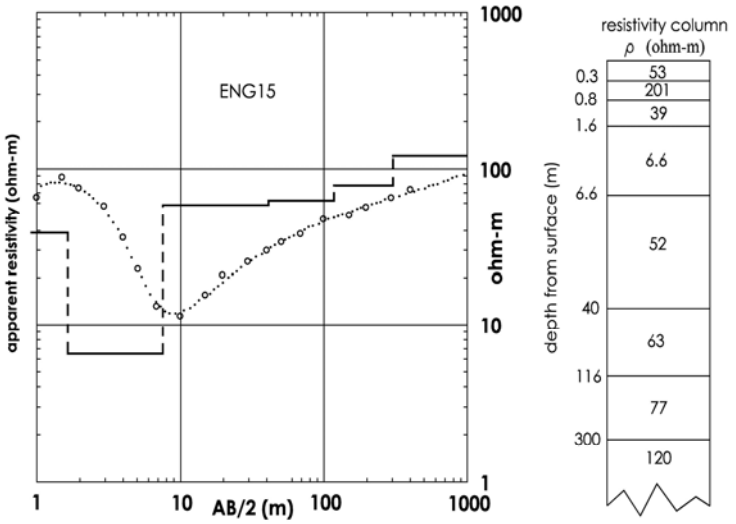

Figure 5.1b - Apparent resistivity curve and interpretation of VES ENG15. The resistivity column doesn't show any sign that could be associated with a confined aquifer

On the basis of the resistivity curves and taking into account the geological and hydrogeological information, several homogeneous sub-areas have been distinguished marked with capital letters in the map of Figure 5.2 and table 5.1.

In detail, sub-area E2 is the most promising for groundwater and includes soundings ENG00, ENG01, ENG02, MK04, ENG18, ENG03b. As seen, these soundings show very similar and rather interesting characteristics: a first conductive layer, extending from few meters to a maximum of 15 meters from surface; a relatively resistive layer, superimposed to a second conductive layer whose top is situated at depths of 36 meters from surface. The latter could be associated to aquifer with thickness ranging from 40 to 150 m.

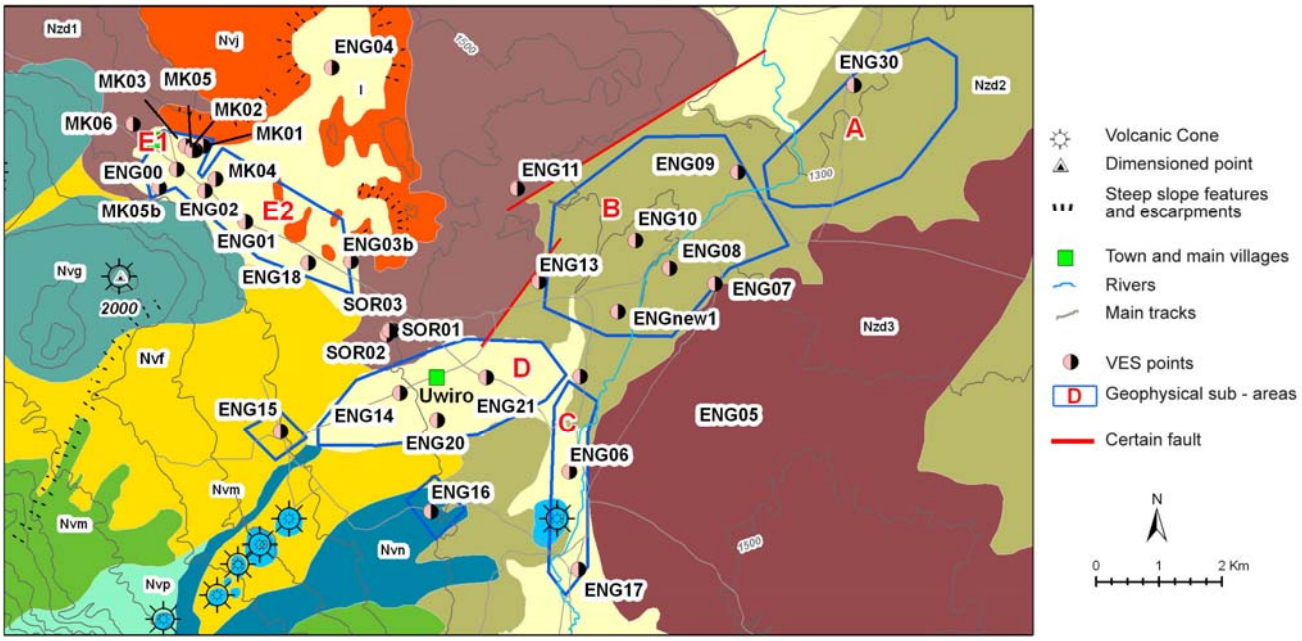

Figure 5.2 - Position map of the electrical soundings in the Ngarenanyuki Ward

Ward	*Sub-area*	*Drilling suitability (0-5)*	*Maximum Drilling depth (m)*
Ngarenanyuki	A	1	40
	B	2	100
	C	1	80
	D	3	80
	E1	2	50
	E2	5	100

Table 5.1 - Operative synthesis of the survey results

5.2. VOLCANIC ROCKS AND DERIVED SEDIMENTS CLASSIFICATION

5.2.1. *Rocks*

The TAS classification (figure 5.3), based upon the relationships between the combined alkali content and silica content, has the prevalent volcanics of the Meru apparatus for phonolite, tephriphonolite and phonotephrite fields. In accordance with the Williams's work (1968), the trend towards phonolites is characterized by a rapid increase in alkalis that corresponds to a steady enrichment in nepheline.

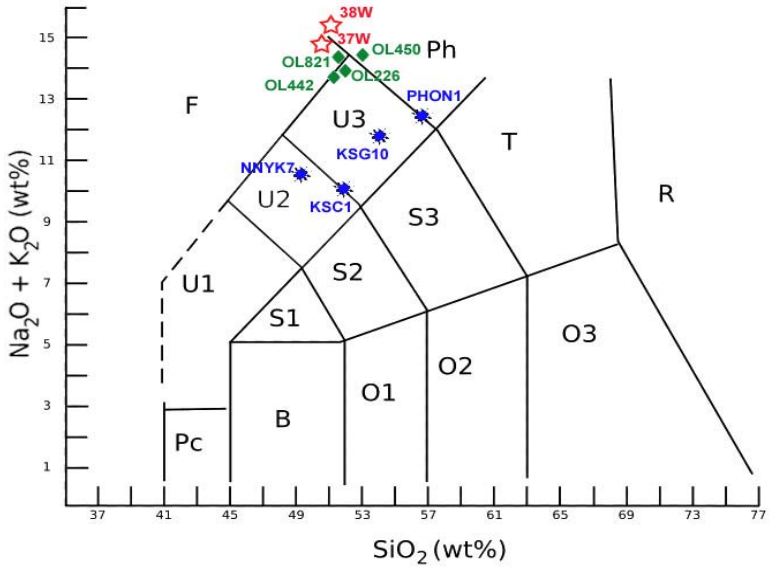

Figure 5.3 – TAS classification: B (Basalt), O1 (Basaltic andesite), O2 (Andesite), O3 (Dacite), R (Rhyolite), T (Trachyte or Trachydacite), Ph (Phonolite), S1 (Trachybasalt), S2 (Basaltic trachyandesite), S3 (Trachyandesite *Sodic and potassic variants are Benmoreite and Latite, Pc (Picrobasalt), U1 (Basanite or Tephrite), U2 (Phonotephrite), U3 (Tephriphonolite), F (Foidite).
37-38 W Phonolite, Kilimanjaro. Williams L. A. J. , 1969.
OL226 OldonyoLengai, Phonolite Upper S-flank; OL442 OldonyoLengai, Phonolite Lower SE-flank; OL 450 OldonyoLengai, Lower SE-flank; OL821 OldonyoLengai, Phonolite Lower E-flank, E-Chasm. Klaudius J. and Keller J., 2006

Particularly, the sample PHON1 from the study area is congruent with other phonolites of East Africa Rift. In fact, in the TAS classification they plot close to the Kilimanjaro and Oldonyo Lengay phonolites (Williams, 1968; Klaudius and Keller, 2006). All the samples collected from the study area, fall in the strongly alkaline nepheline-bearing types (figure 5.4), according to Williams (1969).

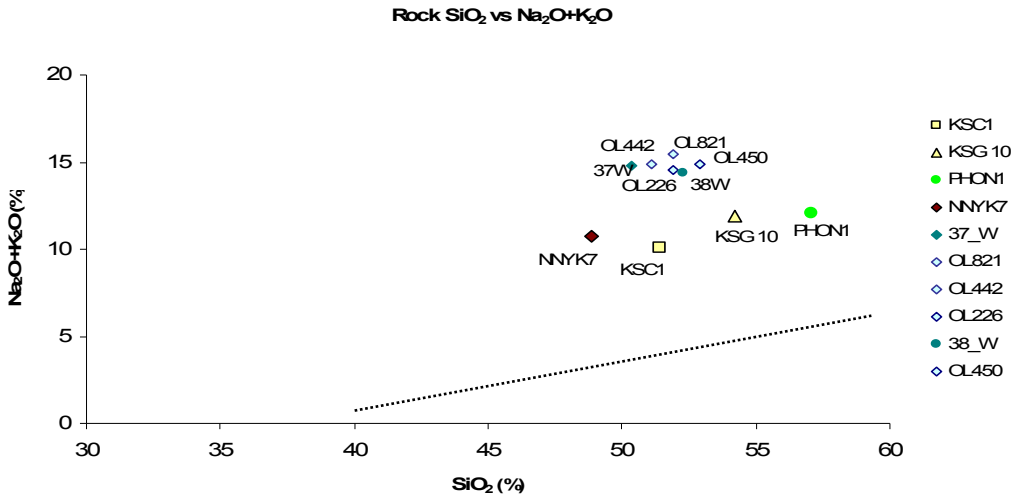

Figure 5.4 - Relations between total alkalis and silica. The dotted line is that used to separate nepheline-bearing from nepheline-free rocks in the petrographic district wich includes Kilimanjaro from Williams (1969).

The nepheline-rich phonolites (38W and 37W) of the Inner Crater Group of the Kilimanjaro Volcan contain higher Na20 and K2O than the Meru samples, but lower SiO_2.

The Meru volcanic phonolites also show the highest content of fluoride within the East Africa area, as reported in the table 5.2 (Kilham and Hecky, 1973).

C	N	R	M	R no.	A	T
Tanzania						
Meru, foot	1	-	0.15	1	Table 1, p. 1125	Nephelirites
Meru, peak	3	0.23-0.37	0.32	1	Table 1, p. 1125	Nephelirites
Meru	2	0.21-0.22	0.215	1	Table 1, p. 1125	Phonolites
Meru mean	6	0.21-0.37	0.268			
Kilimanjaro	1	-	0.13	1	Table 1, p. 1125	Nephelirites
Kilimanjaro	1	-	0.13	1	Table 1, p. 1125	Picrites
Kilimanjaro	3	0.048-0.14	0.082	1	Table 1, p. 1125	Picrite basalts
Kilimanjaro	4	0.078-0.12	0.10	1	Table 1, p. 1126	Olivine basalts
Kilimanjaro	2	0.15 -0.18	0.165	1	Table 1, p. 1126	Rhomben-porphyry
Ngorongoro	1	-	0.076	1	Table 1, p. 1125	Picrites
Ngorongoro	2	0.078-0.091	0.085	1	Table 1, p. 1126	Olivine basalts
Ngorongoro	1	-	0.14	1	Table 1, p. 1126	Trachyandesite
Ngorongoro mean	4	0.076-0.14	0.096			
Kenya						
Naivasha area	4	0.17-0.68	0.387	2	Table 1, p. 14 samples 5-9	Rhyolite & Commendite obsidian
Menengai	4	0.27-0.36	0.307	3	Table 1, p. 511 samples 43/1/S 5.6.6a.11	Glass peralkaline trachytes
Uganda						
Fort Portal Field	4	0.14-0.30	0.25	4	Table 1. p. 1065	Vesicular carbonatitic lava
				5	Table 1, p. 381 sample 1	
				5	Table 11, p. 420 sample 1	Melilite-leucite
Katwe Field mean	7	0.02-0.27	0.11	6	Table 1, p. 53 samples D,E,	Biotite pyroxenite
				6	Table 2, p. 57 samples A,B,J	Biotite, Katungite, Olivine nuachitite
				6	Table 3, p. 59 sample A	Leucite ankaratrite
				7	Table 3, p. 549 sample 19	Leucite ankaratrite
Bunyaruguru mean	7	0.08-0.18	0.12	6	Table 1, p. 53 sample A	Biotite pericotite
				6	Table C, p. 57 samples C,D,E,I	Katungite, Olivine-rich ugandite
				7	Table 3. p. 550 samples 29,30	Mafurite, Leucite mafurite
Birunga mean	13	0.00-0.15	0.06	6	Table 1, p. 53 samples B,F	Biotite pericotite, Biotite pyroxenite
				6	Table 4, p. 60 samples A-G	Kivite, Melilite, Limburgite, Leucite trachybasalt
				7	Table 3, p. 549, 551. samples 12,45,48.50	Nephelinite, Ahsarokite, Banakite, Kentallenite

Table 5.2 - Compilation of fluoride analysis of rocks from volcanic regions of East Africa (Kilham and Hecky, 1973). All analysis in % F. Country and volcanic region (C), number of samples (N), range (R), mean (M), analysis location (A) in referenced papers, and main rock types (T) are given. References (R No.) : l-Gerasimovskiy and Savinova (1969); 2-Bowen (1937); S-MacDonald *et al*., (1970); 4-von Knorring and DuBois (1961) ; S-Holmes and Hnrwood (1932) ; 6-Higaxy (1954) ; 7-Bell and Powell (1969).

The diagrams (figures 5.5 and 5.6) show as the pyroclastic products are depleted in Na_2O and enriched in fluoride with respect to the lava flows. In fact, according to Cronin *et al*., (2003), early phase tephra, deposits within an eruptive sequences may include large fractions of secondary phases from adjacent or underling fluoride rich hydrothermal system. Although few rock samples was available for describing a statistical distribution, some useful informations are inferable.

The lahar sample (NNYK7) is depleted in Na_2O and enriched in K_2O compare to the lavas. This evidence a slight higher mobility of sodium with respect to K^+, in during the epiclastic reworking.

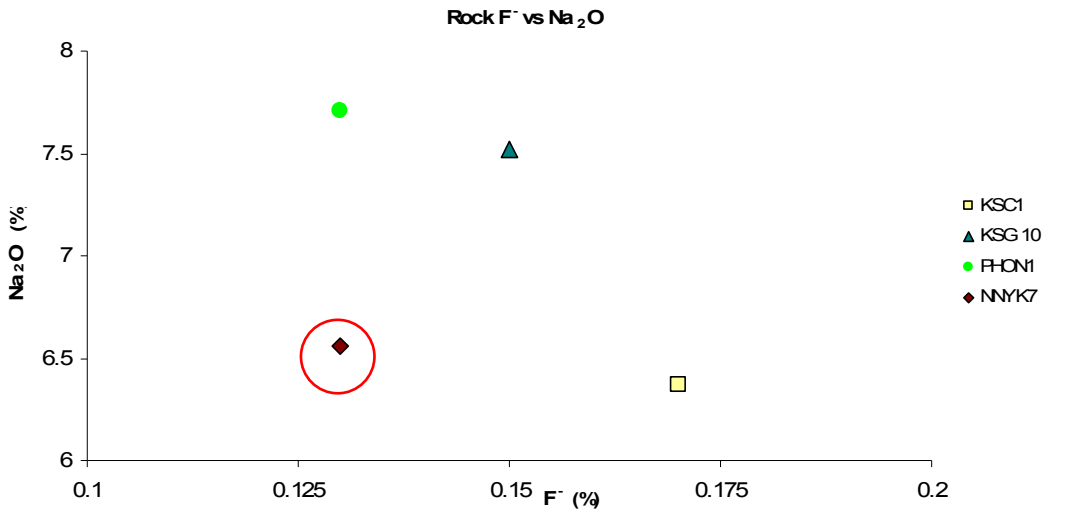

Figure 5.5 - Diagram showing relation between Na_2O and F^- (NNYK7 lahar sample is out of trend)

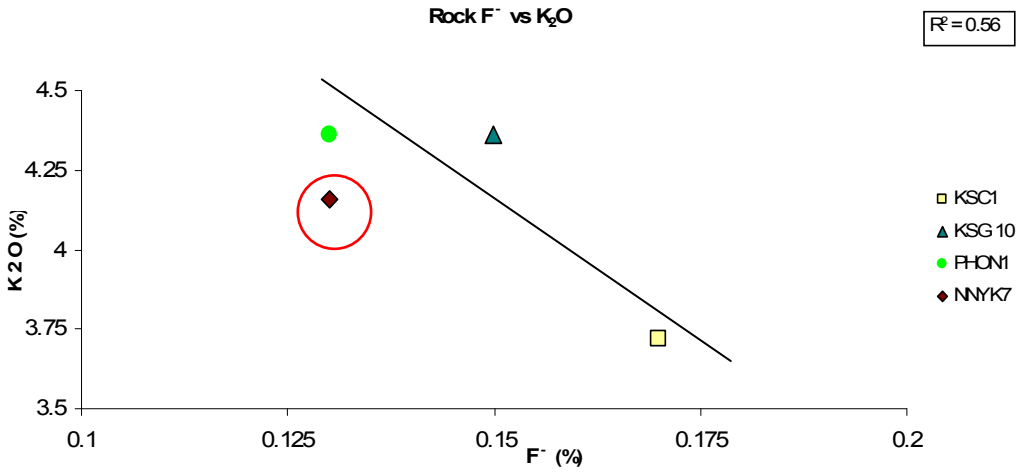

Figure 5.6 - Diagram showing relation between K_2O and F^- (NNYK7 lahar sample is out of trend)

5.2.2. *Sediments*

Na2O shows both depletion and enrichment with respect to the volcanic precursors. Hardpan and calcrete, generally, are depleted in sodium with respect the dominant phonolitic lavas, whereas a slight enrichment was found in soils deriving from lake deposits particularly in the upper part, where white crust of scooped magadi were observed.

Na_2O in lahar as previously stated is generally depleted. As K_2O is concerned, its content in the sediments almost reflects that of the volcanic rocks. In any case both K_2O and Na_2O, show positive correlation with fluoride (figures 5.7 and 5.8). MgO and CaO are not significantly correlated with F^-.

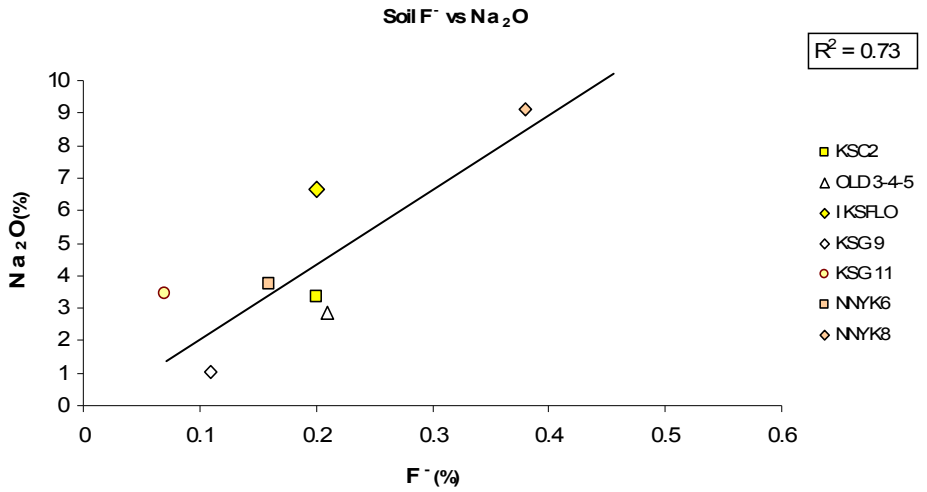

Figure 5.7 - Diagram showing relation between

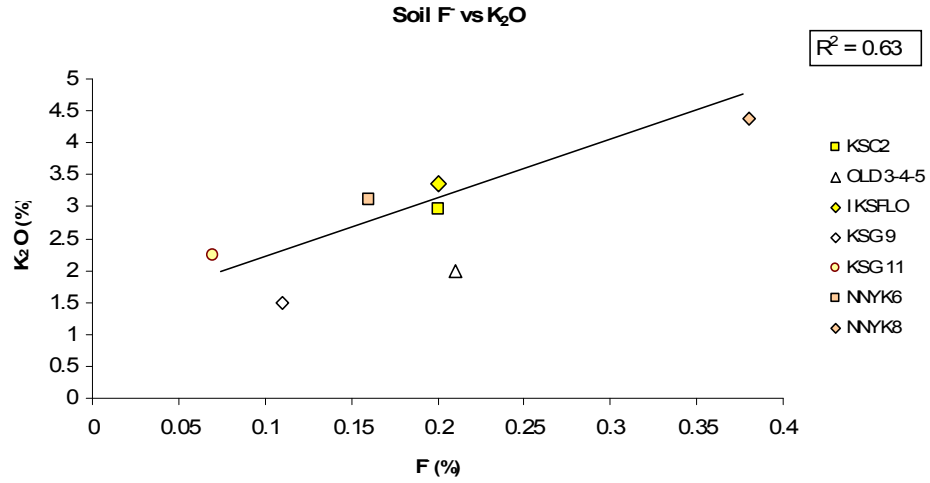

Figure 5.8 - Diagram showing relation between

5.3. ROCK MINERALOGY

Among the difference minerals envolved with water interaction, most are primary i.e. of magmatic origin. XRD and thin sections observation are reported below.

Primary minerals

nepheline, leucite, sanidine, anorthoclase, albite/anorthite, riebeckite/crocidolite, augite, biotite, fluorapatite, olivine particularly within mugearite and basanite e.g. (from the Mkuru aquifer). Cancrinite, which is common in alkaline lavas, was found only in epiclastic sediments.

Authigenic minerals

Among the authigenic minerals, some are clearly derived from the interaction between alkali solutions and volcanic glass; others by direct precipitation from supersatured

solutions. Among the authigenic minerals clay minerals such those of illite/smectite group, were found in paleosoils interbedded within different lahar (figure 3.3), as well in modern soil. Another important group of neoformed mineral basically related to alkaline water- rock interaction, are some zeolite group mineral, such as phillipsite, chabazite, sodalite and analcime. Also cancrinite even if common in alkaline lavas and in pyroclastics, due to its occurrence in lahar and paleosoils, must be considered neoformed phase.

As for minerals deriving from precipitation both in salt crust, hardpan and late clustic sediments, XRD analysis evidences the presence of trona, natron, sylvite and calcite.

This confirm that supersaturation in trona, nitrite, sylvite and calcite, was reached during dry and hot periods. Whereas CaF_2 saturation was never reached, at least in the considered samples.

Trona was found in scooped magadi together with sylvite, whereas chabazite, sodalite, phillipsite were more abundant in dark soils a couple of metres below the encrusted ground level. Cancrinite was found just few millimetres below the magadi crust. The calcrete and hardpan only contain calcite and possibly natron.

5.4. GROUNDWATER AND SURFACE WATER RESULTS

5.4.1. *Masika monitoring*

Physico-chemical properties of analysed groundwater samples for the masika monitoring, were statistically defined by means of the maximum, minimum, mean, median and standard deviation (table 5.3). Some values and concentrations show significant variations.

Masika monitoring					
Parameter	***Minimum***	***Maximum***	***Mean***	***Median***	***SD***
pH	5.90	8.10	6.99	7.20	0.64
T°C	10.70	24.80	17.21	17.00	4.02
EC	190.00	5070.00	932.80	580.00	1120.75
Ca^{2+}	0.70	26.00	9.20	7.80	6.61
Mg^{2+}	0.03	5.98	2.14	1.65	1.72
Na^{+}	24.50	1100.00	154.60	81.00	228.89
K^{+}	7.70	235.00	43.22	27.75	49.17
HCO_3^{-}	89.50	2143.00	396.50	268.00	428.91
Cl^{-}	2.31	189.69	19.39	6.50	39.79
SO_4^{2-}	2.23	512.51	48.60	10.12	117.12
NO_3	12.60	71.50	25.53	21.90	14.7
NO_2	0.13	0.72	0.25	0.22	0.15
F^{-}	0.90	59.00	9.98	4.90	12.97

Table 5.3 - Statistical summary of physico-chemical data for the *masika* monitoring

The groundwater varies from sub-acid to alkaline (pH 5.9–8.1). The Electrical conductivity (EC) varies from 190 to 5070 μS/cm. Sodium and HCO_3^- are the dominant ions ranging, from 24.5 to 1100 mg/L and from 89.5 to 2143 mg/L respectively. The same ions, also, present a high variability as shown by higher SD values and by the difference between mean and median.

The concentration of fluoride in the groundwater varies from 0.90 to 59.00 mg/L. In about 84% of the groundwater samples, F^- is above the WHO limit (1.5 mg/L) whereas the 32% are above the Tanzanian limit for drinking purposes (8mg/L). Groundwater in the river courses have F^- content in the range of 1.90 to 28.00 mg/L. In figure 6.9 the masika monitoring spatial distribution is shown. In red colour are revealed the groundwater and surface water above the Tanzanian government limit of 8 mg/L.

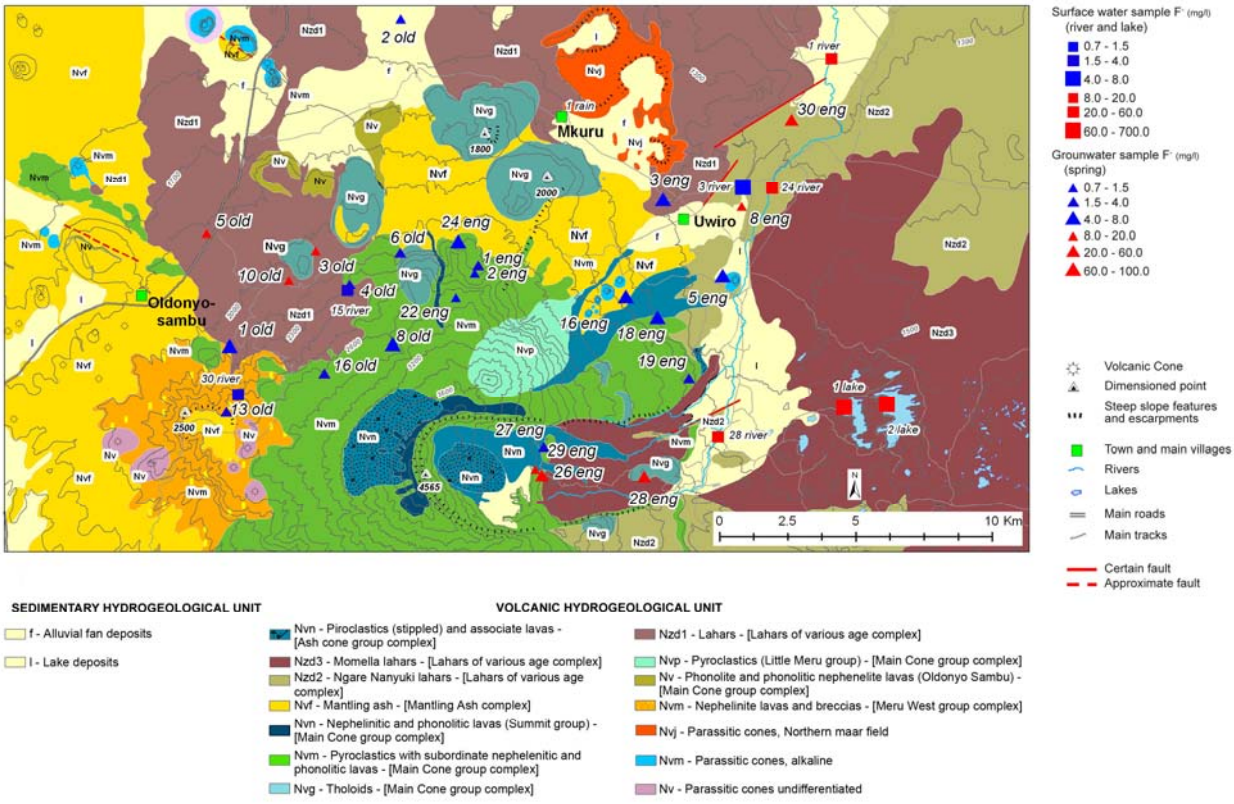

Figure 5.9 - *Masika* monitoring network: data refer to the April 2007 survey

	Masika monitoring												
	pH	T°C	EC	Ca^{2+}	Mg^{2+}	Na^{+}	K^{+}	HCO_3^{-}	Cl^{-}	SO_4^{2-}	NO_3	NO_2	F^{-}
pH	1												
T°C	0.38	1											
EC	0.53	0.55	1										
Ca^{2+}	0.09	0.28	0.13	1									
Mg^{2+}	-0.04	0.32	0.30	0.90	1								
Na^{+}	0.47	0.50	0.98	0.09	0.27	1							
K^{+}	0.54	0.49	0.97	0.10	0.27	0.97	1						
HCO_3^{-}	0.49	0.52	0.98	0.18	0.35	0.99	0.97	1					
Cl^{-}	0.44	0.46	0.96	0.02	0.20	0.99	0.96	0.96	1				
SO_4^{2-}	0.49	0.53	0.90	0.06	0.23	0.85	0.82	0.80	0.83	1			
NO_3	-0.07	-0.28	0.18	0.10	0.05	-0.17	-0.15	-0.17	-0.17	-0.16	1		
NO_2	-0.06	-0.32	0.15	0.11	0.06	-0.14	-0.13	-0.14	-0.14	-0.13	1.00	1	
F^{-}	0.52	0.41	0.91	-0.10	0.04	0.91	0.94	0.90	0.92	0.77	-0.24	-0.21	1

Table 5.4 - Correlation matrix for all the groundwater of *masika* monitoring

In order to examine the relationships of F^- with other geochemical parameters a correlation matrix has been generated (table 5.4). The matrix reveals positive correlation among EC and Na^+, K^+, HCO_3^-, Cl^-, SO_4^-, F^-, since these groundwater contribute to a high TDS from which the EC depends. Fluorine is positively and significantly correlated with EC, Na^+, K^+, HCO_3^-, Cl^-, SO_4^-, whereas a poor negative correlation is found with Ca^{2+}, NO_3^- and NO_2^-. Also the Na^+ and HCO_3^- shows significantly and positive correlation with K^+, Cl^-, SO_4^- and EC; on the other hand the Ca^{2+} only exhibits a good, positive correlation with Mg^{2+}.

The ionic concentration of major cations and anions found are plotted in Piper's trilinear diagram (figure 5.10). Groundwater is basically a bicarbonate-alkaline, being K^+ and Na^+ the prevailing cations and bicarbonate HCO_3^- the prevailing anion. This is typical from volcanic environment, in which feldspar contributes particularly with sodium. Potassium and chloride, as in other Rift countries (Davies, 1996), are less abundant. The amount of the HCO_3^- anion is related to the transformation of CO_2 into hydrogencarbonate: the CO_2 origin can be atmospheric, and/or endogenetic (volcanic).

Also the river water samples fall into the field of bicarbonate-alkaline hydrofacies. The 1, 24 and 28 river are three water point selected along the Ngarenanyuki river, that present higher mineralization and fluoride content than the other river water point sampled (figure 5.11).

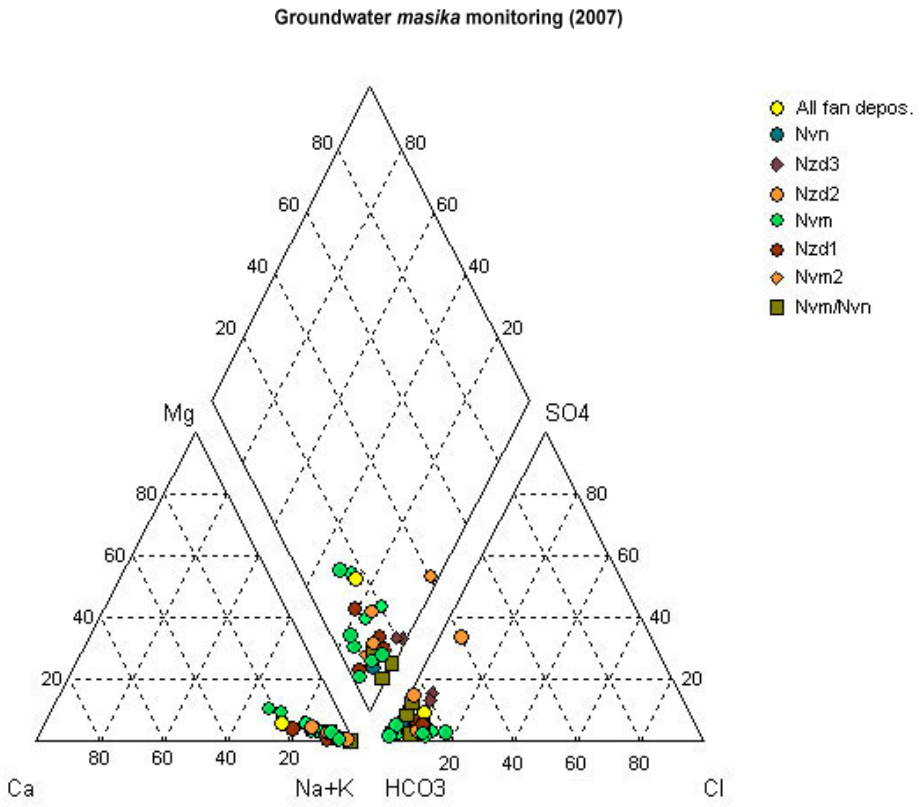

Figure 5.10 - Piper diagram (April 2007): colours represent the spring's aquifer

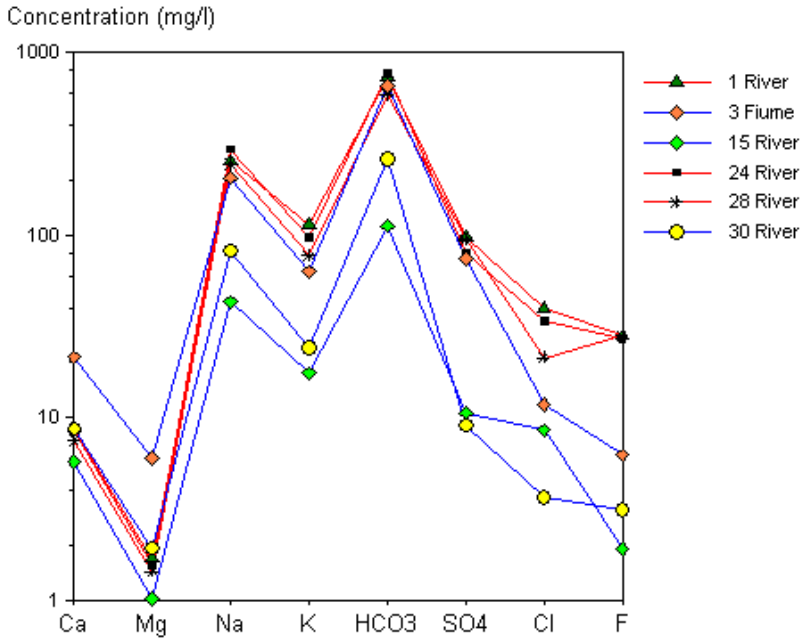

Figure 5.11– Distribution of major ions in rivers

5.4.2. *Pre-Masika monitoring*

The physico-chemical properties of groundwater sampled in the pre-*masika* monitoring, don't show many difference than the first monitoring period (5.5 table). A general raise of temperature and a small increase in fluoride content can be observed for the spring on phonolite hydrogeological unit on the slope front Oldonysambu ward. The concentration of F^- (figure 5.12) for pre-*masika* monitoring (1.70–68.00 with a mean of 10.84 mg/L) appear higher than *masika* period (0.90–59.00 with a mean of 9.98 mg/L). In general, a slight growth can be observed for the fluoride content, except for the 26 eng spring, that pass from 54.0 to 68.0 mg/L. A general reduced concentration of Na^+ is shown, as, for example, for the spring 26 eng that decrease from 1100 mg/L to 820 mg/L.

Pre-Masika monitoring					
Parameter	***Minimum***	***Maximum***	***Mean***	***Median***	***SD***
pH	6.00	8.40	7.08	7.10	0.54
T°C	12.20	24.70	17.20	16.20	3.42
EC	170.00	4730.00	931.20	620.00	1047.72
Ca^{2+}	0.60	41.00	8.26	6.10	9.04
Mg^{2+}	0.12	11.46	2.44	1.63	2.70
Na^+	15.50	820.00	155.50	90.00	195.24
K^+	5.40	180.00	33.51	24.50	37.30
HCO_3^-	74.90	2233.20	412.50	276.80	470.72
Cl^-	1.85	183.48	19.96	6.63	39.79
SO_4^{2-}	1.66	475.61	50.20	11.31	115.34
NO_3	5.10	27.20	12.98	11.80	5.11
NO_2	0.06	0.27	0.13	0.12	0.05
F^-	1.70	68.00	10.84	5.10	14.22
SiO_2	29.59	68.73	52.11	53.71	8.70

Table 5.5 - Statistical summary of physico-chemical data for the pre-*masika* monitoring

The correlation matrix too (table 5.6), reveal similar positive correlation among major ions of the *masika* monitoring, although the Mg^{2+} is more positively correlated with EC, Na^+, K^+, HCO_3^-, Cl^- and in poorly way, also with F^- and SO_4^-, according to a higher mineralization joined to the dry season.

	Pre-Masika monitoring													
	pH	T°C	EC	Ca^{2+}	Mg^{2+}	Na^{+}	K^{+}	HCO_3^{-}	Cl^{-}	SO_4^{2-}	NO_3	NO_2	F^{-}	SiO_2
pH	**1**													
T°C	0.19	**1**												
EC	0.47	0.62	**1**											
Ca^{2+}	0.11	0.23	0.21	**1**										
Mg^{2+}	0.21	0.34	0.64	0.69	**1**									
Na^{+}	0.47	0.62	0.99	0.14	0.58	**1**								
K^{+}	0.48	0.54	0.96	0.18	0.65	0.94	**1**							
HCO_3^{-}	0.44	0.59	0.99	0.25	0.69	0.98	0.97	**1**						
Cl^{-}	0.42	0.53	0.97	0.07	0.62	0.96	0.96	0.97	**1**					
SO_4^{2-}	0.45	0.60	0.93	0.03	0.44	0.96	0.82	0.88	0.90	**1**				
NO_3	0.17	-0.18	-0.11	0.54	0.28	-0.16	-0.06	-0.10	-0.16	-0.18	**1**			
NO_2	0.16	-0.18	-0.11	0.54	0.28	-0.15	-0.06	-0.09	-0.16	-0.17	1.00	**1**		
F^{-}	0.42	0.44	0.89	-0.02	0.49	0.88	0.92	0.90	0.93	0.79	-0.14	-0.14	**1**	
SiO_2	-0.54	-0.24	-0.43	0.13	-0.09	-0.45	-0.40	-0.39	-0.47	-0.53	0.04	0.04	-0.44	**1**

Table 5.6 - Correlation matrix for all the groundwater of pre-*masika* monitoring

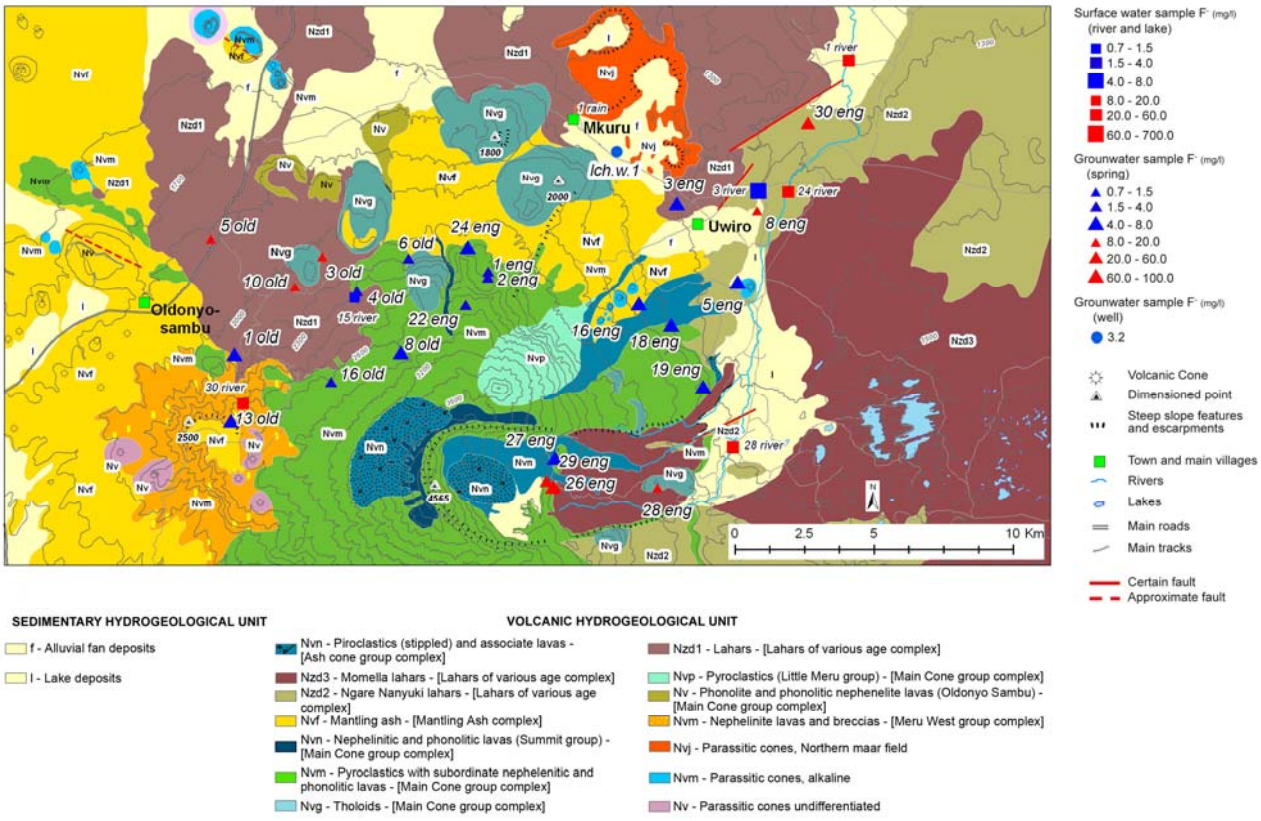

Figure 5.12 - Pre-*masika* monitoring network: data refer to the January 2008 survey

The water hydrochemical composition still maintain a bicarbonate-alkaline facies, as shown in figure 5.13 and 5.14, even if with a shift toward SO_4 field.

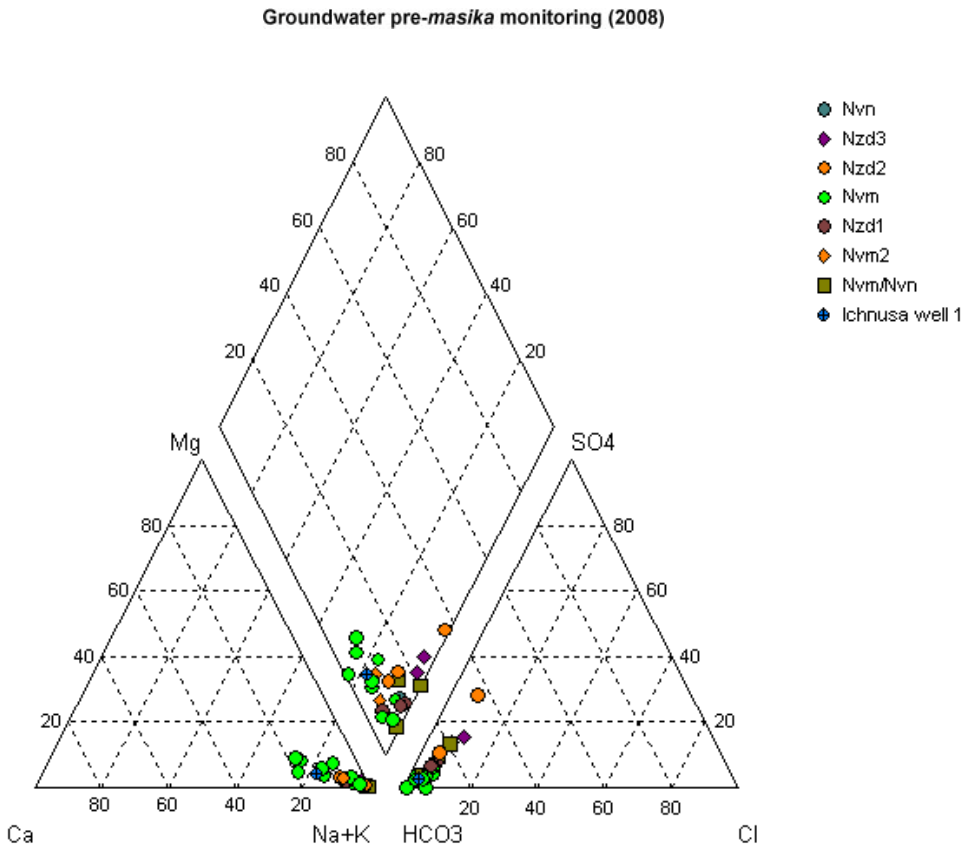

Figure 5.13 - Piper diagram (January 2008): colours represent the spring's aquifer

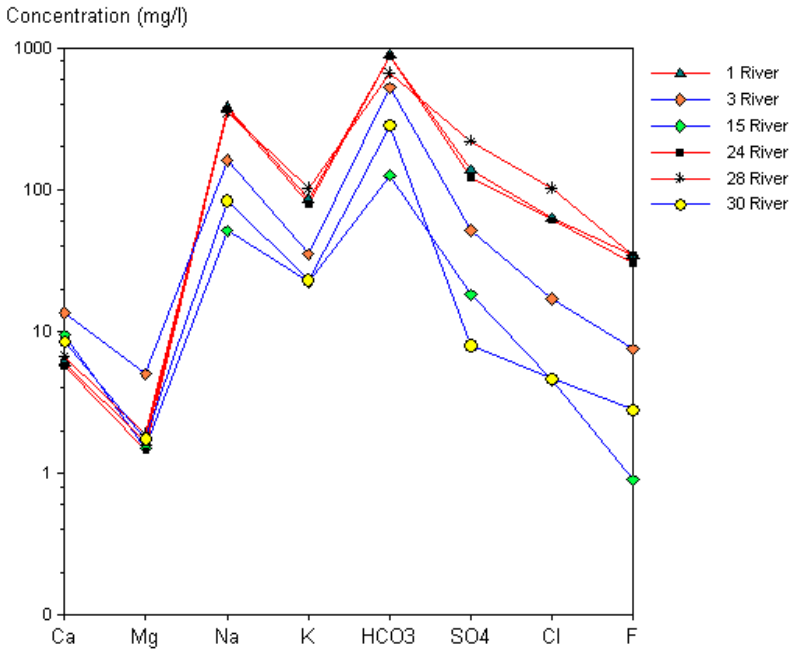

Figure 5.14 - Distribution of major ions in rivers

In order to investigate the source of the fluoride in the sampled water, the abundance of this halogen was compared with a number of chemical and physical parameters, such as pH, temperature, EC and Na^+, K^+, HCO_3^-,Ca^{2+} activities, which in some ways are witness

of the groundwater geochemical evolution, both in time (residence) and space (different aquifers). A straight evidence is the positive correlation between fluoride, pH, Na^+ and K^+ (figure 5.15, 5.16, 5.17); conversely no correlation or weak negative correlation rises from fluoride, Ca^{2+} and Mg^{2+} match (figure 5.18, 5.19).

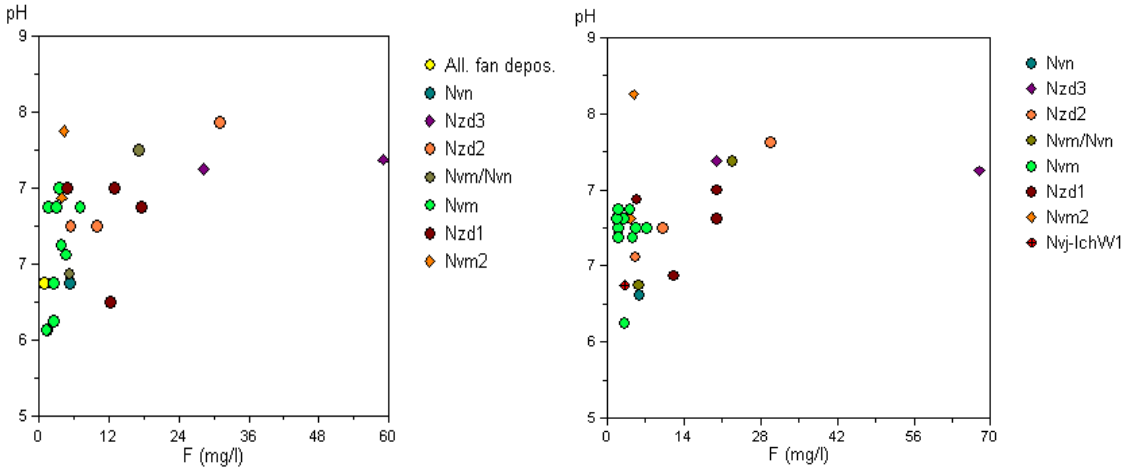

Figure 5.15 – Scatter plot F^- vs pH for *masika* monitoring (sx) and pre-*masika* monitoring (dx)

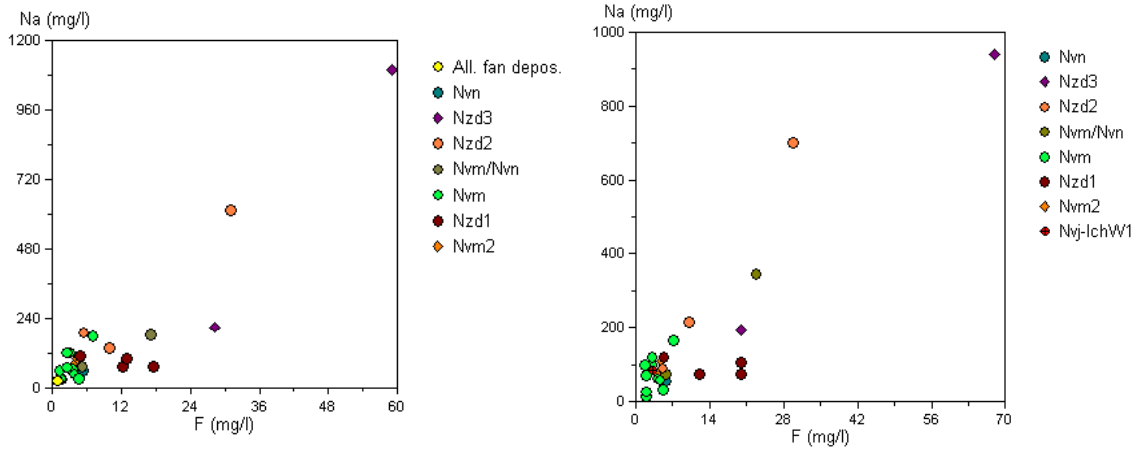

Figure 5.16 – Scatter plot F^- vs Na^+ for *masika* monitoring (sx) and pre-*masika* monitoring (dx)

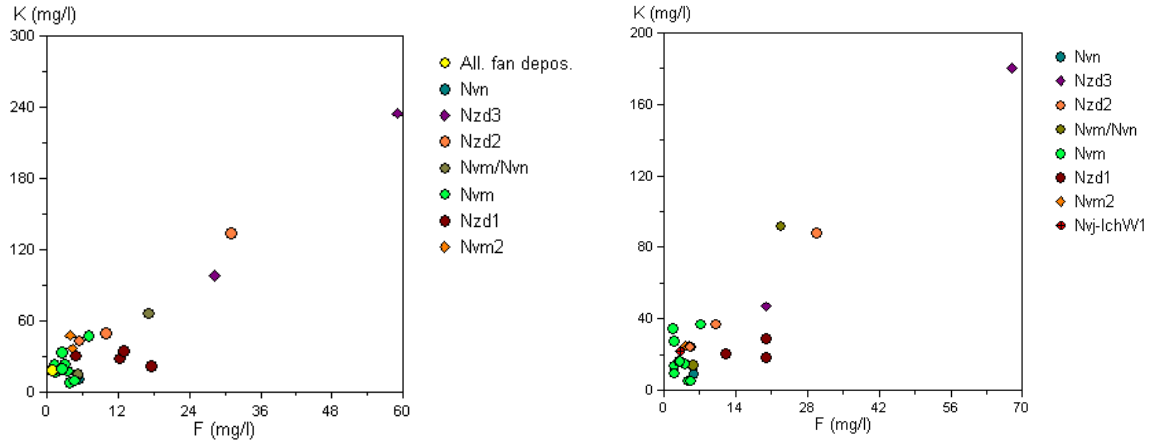

Figure 5.17 – Scatter plot F^- vs K^+ for *masika* monitoring (sx) and pre-*masika* monitoring (dx)

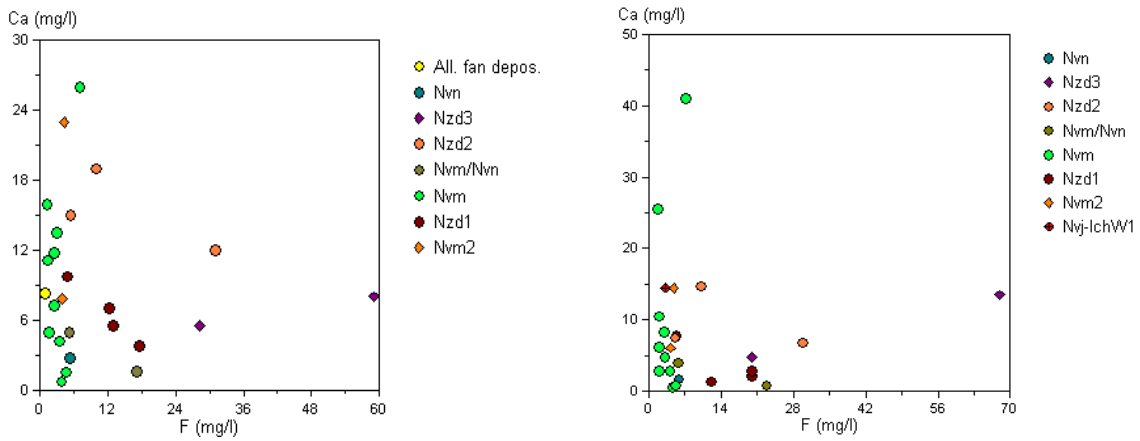

Figure 5.18 – Scatter plot F^- vs Ca^{2+} for *masika* monitoring (sx) and pre-*masika* monitoring (dx)

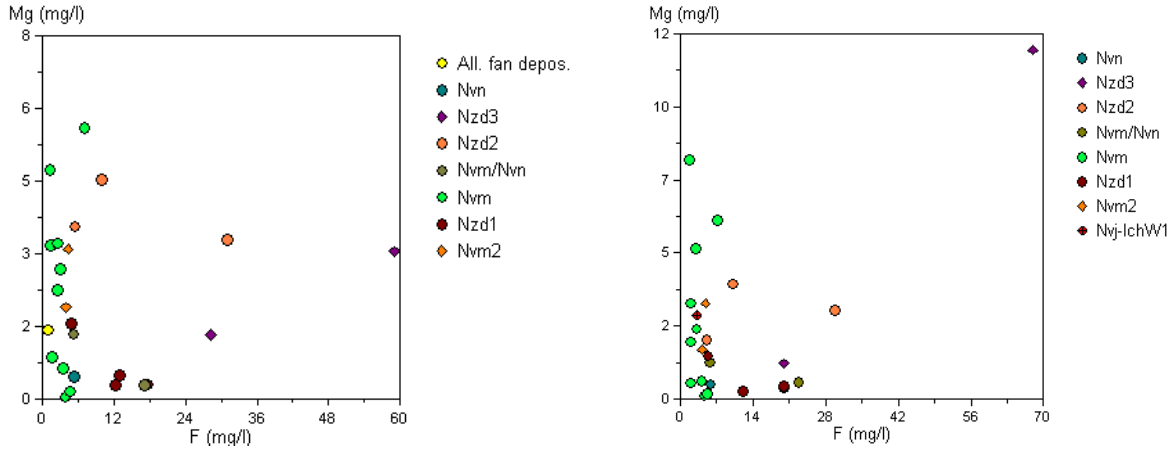

Figure 5.19 – Scatter plot F^- vs Mg^{2+} for *masika* monitoring (sx) and pre-*masika* monitoring (dx)

The correlation between the two former cations and fluoride may reflect the original dissolution of phonolite and tephrite phonolite, both rich in fluoroapatite and Na- K-feldspar and Na-K-feldspatoid. More effective source of fluoride can be represented by secondary mineral associations as scooped *magadi*, clay minerals and other phases (Nielsen, 1999; Vuhahulaa *et al*., 2008) with high cationic exchange capacity (CEC), such as zeolites and other sodium-hydrate silicates typical of evaporative environment (Sebag *et al*., 2001). These minerals are able to concentrate both Na^+, K^+ and F^- and release them according to the different water availability and different temperature (i.e. during the different seasonal cycle).

If the ratio between fluoride and the considered ions is constant and independent from the aquifer, their bulk concentration is strongly related to the previously described hydrological unit. Groundwater outpouring from the phonolite, due to relatively lower reactivity of silicates show low content both in alkaline cations and fluoride. This hydrogeological unit, in fact, is a fractured aquifer with high transmissivity and low

residence time (Ghiglieri *et al.*, 2008). Even lower values were found in a scoriaceous basalt aquifer, also high permeable and relatively poor of alkali-bearing phases (figures 5.20 and 5.21).

The lahars groundwater, generally, show high fluoride content, which can reflect both the rock mineralogy (interbedded paleosoils, zeolite with exchangeable cations) and low permeability (high residence time).

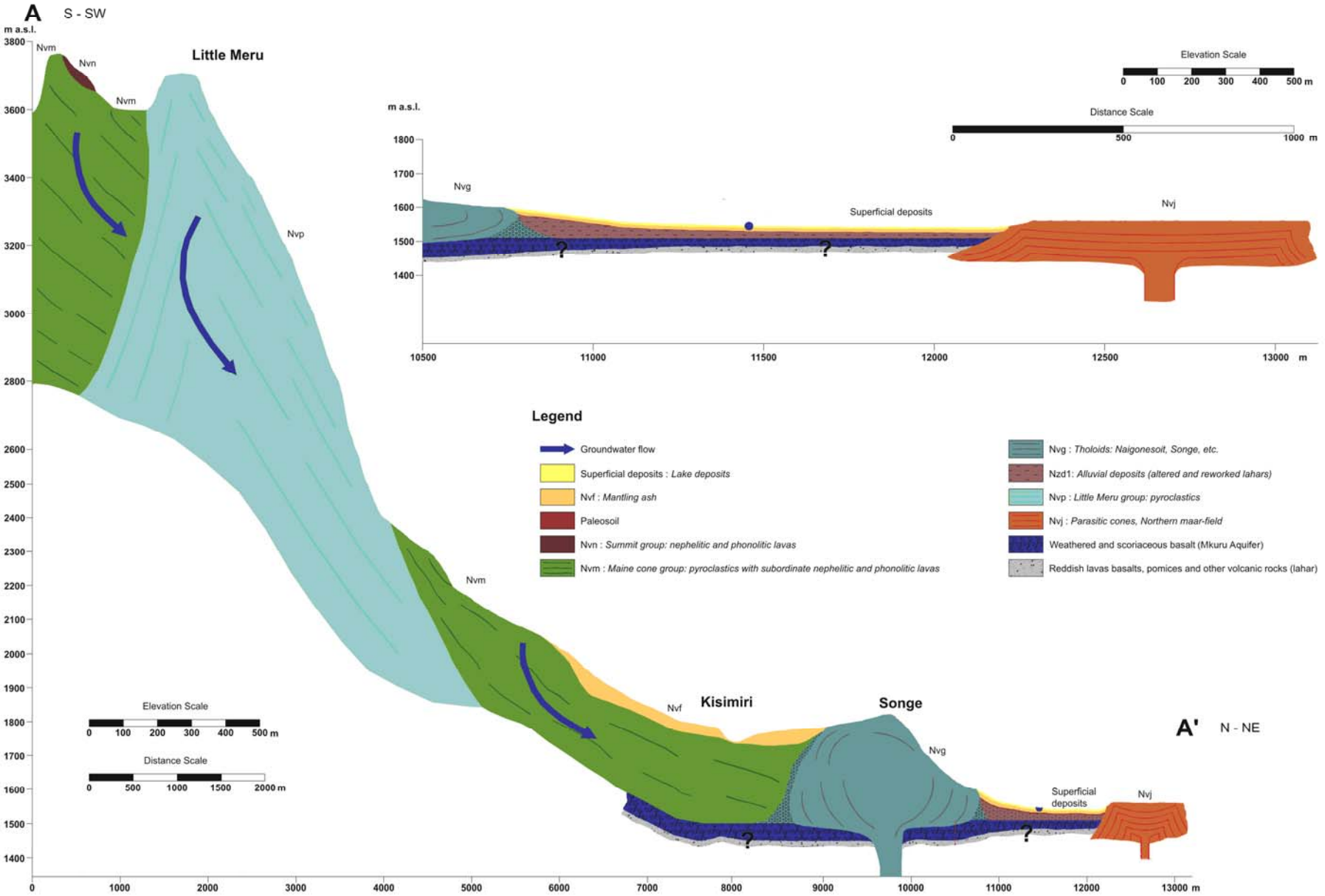

Figure 5.20 – Geolocical-Hydrogeological cross section A-A' (vertical exaggeration about x 4). 2)

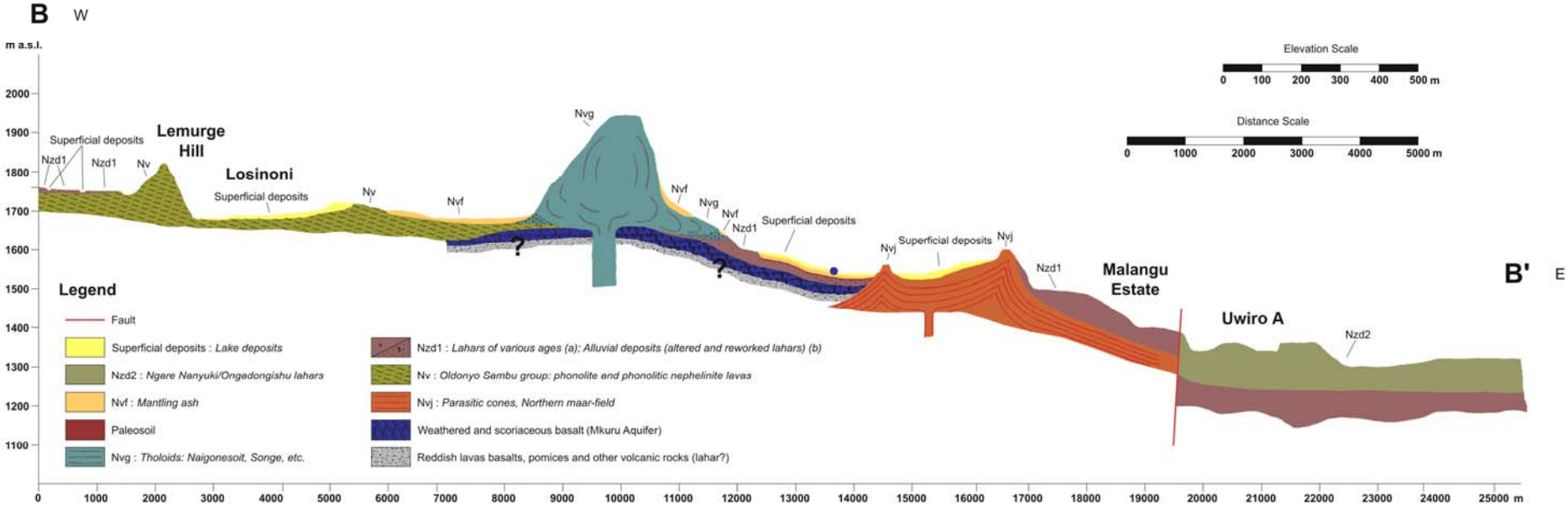

Figure 5.21 - Geological-Hydrogeological cross section B-B (Vertical exaggeration about x7)

The high solubility of the scooped magadi and of the crusts, make these an easy source of alkali and fluoride (up to 3700 ppm) when the runoff leach out them in the perennial and ephemeral rivers.

The distribution of fluoride content shows a zonation from the phonolite slope toward the flat area (figures 5.9 and 5.12). For example, for the NW side of mount Meru, the cross-section of figure 5.22 represents the flow route within the aquifers from the recharge zone of the Mount Meru (phonolite) to the Oldonyo Sambu valley (lahaar), for some springs (16 old, 8old, 4 old, 10 old, 3 old, 5 old).

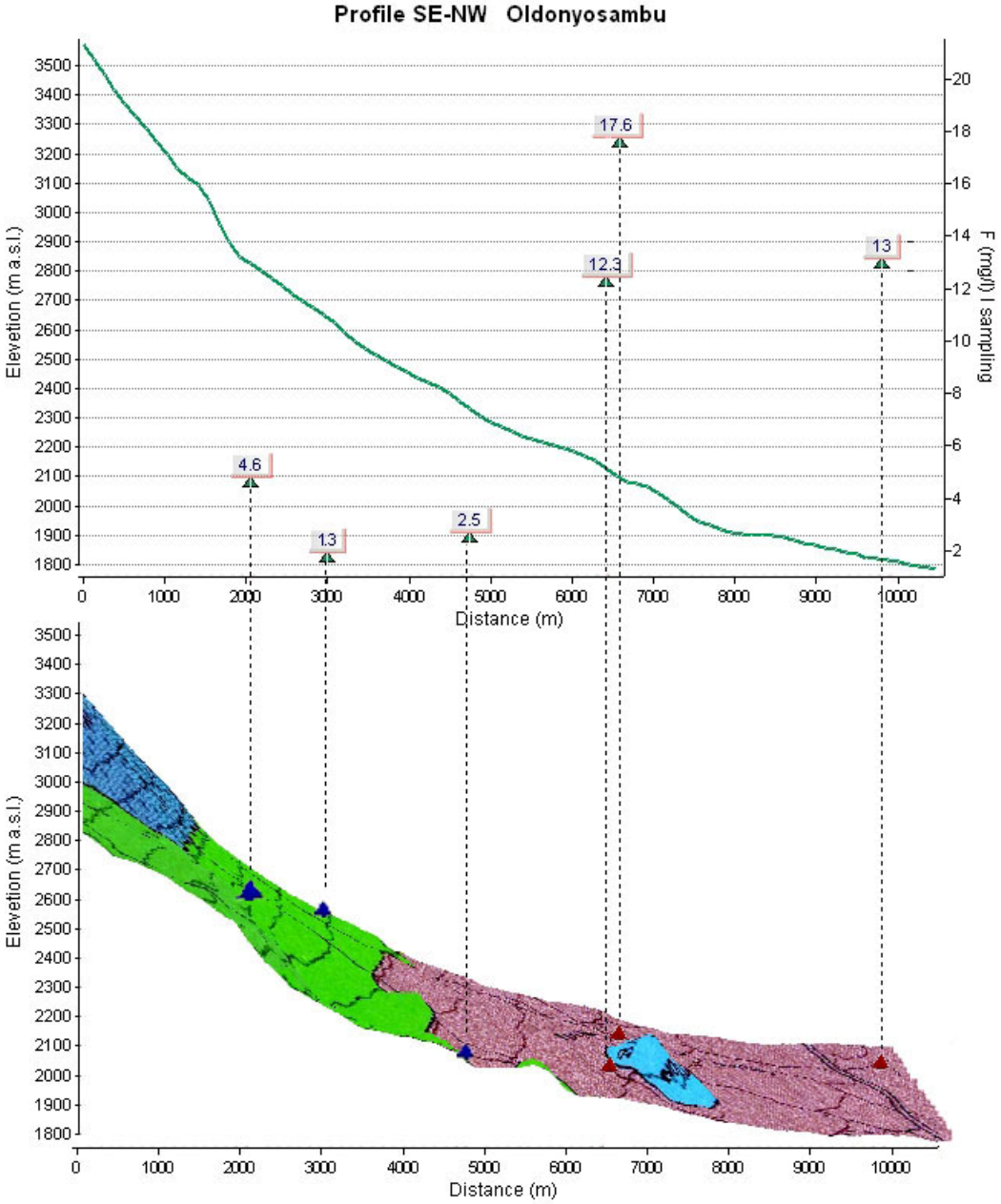

Figure 5.22 – Cross section in the NW side of the mount Meru

In figure 5.23, the hydrogeochimical evolution, relative to major ions, from the spring 8 old to the springs 10 old and 3 old stands out.

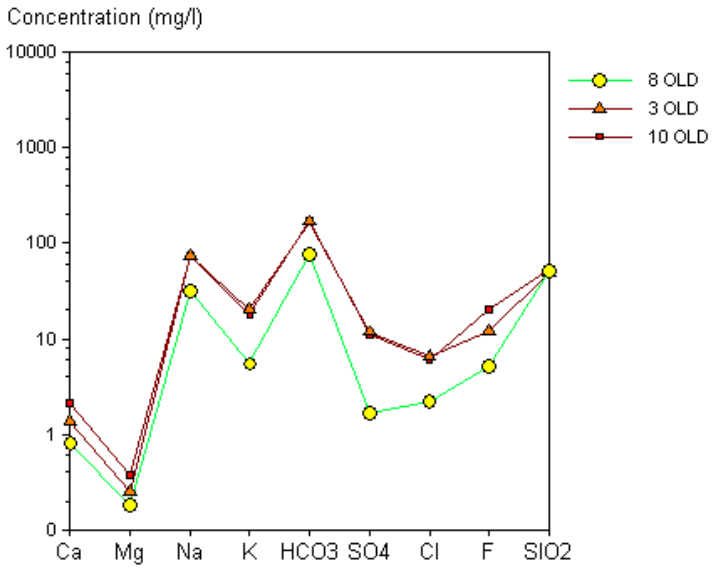

Figure 5.23 - Hydrogeochimical evolution for the spring 8, 3 and 10 OLD

Both from correlation diagrams, particularly those from figure 5.15 to figure 5.19 and from the relation between aquifer (phonolite) and fluoride content, a striking anomaly concerns the springs 26 ENG. The spring, located within the Meru cone (2502 m a.s.l.), show a constant temperature of 22,4 °C and low T.U. (tritium unit) value, that point to an hydrothermal origin, which account for the highest fluoride content as far detected in the Meru area. This spring feeds the Engarenanyuky river with an yeld of 6L/s.

This water can be considered a pollutant for the river and, consequently, for the aquifers in hydraulic communication with it. Particularly the area of structural low within the Uwiro graben were some epiclastite-hosted aquifers can be fed by the river.

It can not be excluded that within this structural low the feeding from this spring to the Ngarenanyuki river, joined to that deriving from the lacustrine deposits (scooped magadi), might contribute to the increasing of fluoride content within the lahar aquifer.

5.5. ISOTOPIC DATA

Data of stable isotopes are reported in figure 5.24, where the Local Meteoric Water Line (LMWL) for the area of Lake Tanganyka (Dettman *et al*., 2005), the closest one to the study area, along with the Global Meteoric Water Line (GMWL) are also reported for comparison. Nkotagu and Mwambo (2000) indicates that the rainfall in this region has a wide range of $\delta^{18}O$ values, with an average $\delta^{18}O$ of -2.9 ‰, and ranged from -14.1 to + 3.0 ‰.

5.5.1. *River and Lake water samples*

The relatively consistent isotopic composition of the Ngarenanyuki river water reflects an important contribution of groundwater to the flow.

There is enrichment in the heavier isotopes because the lakes are finite reservoirs and then water resides for a long time under evaporative conditions. The dynamics of the evaporation process causes the isotopic composition of the lake to follow an "evaporation line", with a lightly slope depending on the local rates of evaporation.

5.5.2. *Groundwater samples*

The $\delta^{18}O$ and δD values of samples vary in the range of -6,39 ÷ -2,79 and -40,1 ÷ 8,3 respectively.

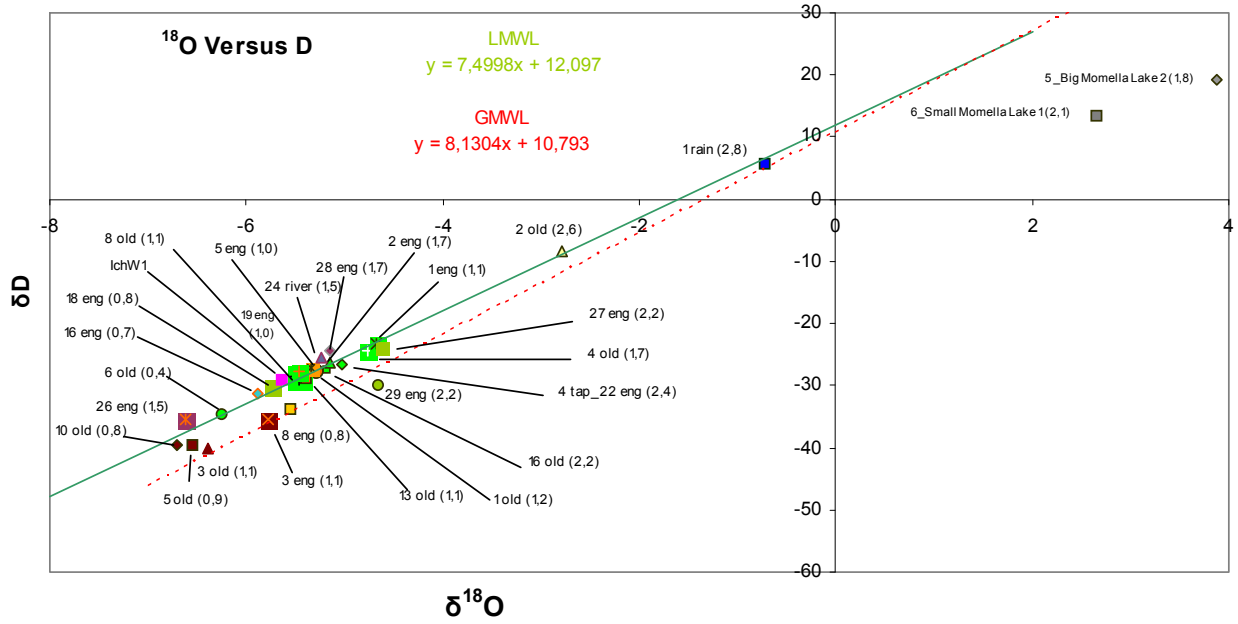

Figure 5.24 - Stable isotope: $\delta^{18}O$ and δD relationship of water sample. Tritium values are enclosed between brackets.

The clustering of stable isotopes of some groundwaters near the LMWL (1, 2, 4, 6, 8, 13, 16 OLD, 1, 2, 5, 16, 18, 19, 22, 27 ENG and IchW1) indicates that the recharge derives from local precipitation. Another noteworthy information is the absence of the evaporation effect on the isotopic composition, which means that the recharge of the reservoir is quite rapid and the recharging meteoric water does not occupy the soil zone of the recharge area for a long time. For this case, it is assumed that no processes to change the isotopic composition of the precipitation are operating once it recharges the groundwater. In figure 5.25, the spatial distribution of ^{18}O values is shown.

The 8 and 29 ENG springs show a shift from the LMWL, which could represent the effect of evaporation on infiltrating waters or isotopic exchange between minerals and

groundwater in geothermal system. The 3, 5 and 10 OLD samples are relatively depleted in $\delta^{18}O$ and δD. At the same time, these springs presents very low values of ^{3}H, thus represent a relatively high elevation recharge area and a long travel time. This is congruent with the hydrochemical interpretation said earlier.

The tritium values gave rise to meaningful information of the time of recharge, the relative ages and aquifer nature. An interesting trend about the residence time was obtained by the relation between ^{3}H and fluoride (figure 5.26). Groundwater circulating in phonolitic acquifers, generally, are enriched in fluoride cation when tritium concentration is depleted. Chemically, the 22 ENG and 6 OLD can be identified like end-members waters of the phonolite hydrogeological unit. The former with low TDS, sodium, bicarbonate contents as well as fluoride (1.4 mg/L), accordingly a high ^{3}H content (2.4 U.T.) is observed. Conversely, the spring 6 OLD have much higher concentration of the same elements and correspondent low ^{3}H content (0.4 T.U. which is the lowest among the sampled springs). The high residence time of the 6OLD spring, is also confirmed by the anomalously high SiO_2 content in relation to the sub-acidic pH value. Such an anomaly points to a possible hydrothermal contribute.

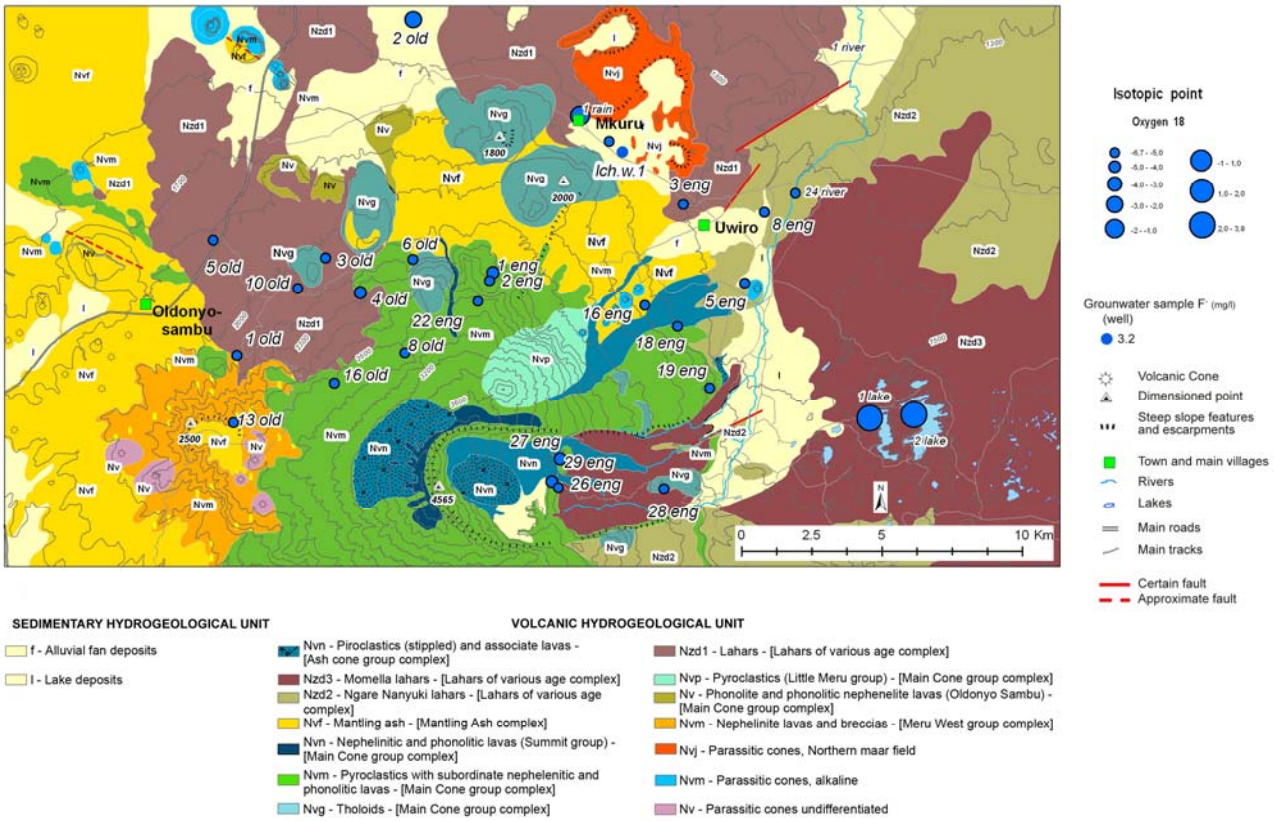

Figure 5.25 - Water samples classified according to ^{18}O values

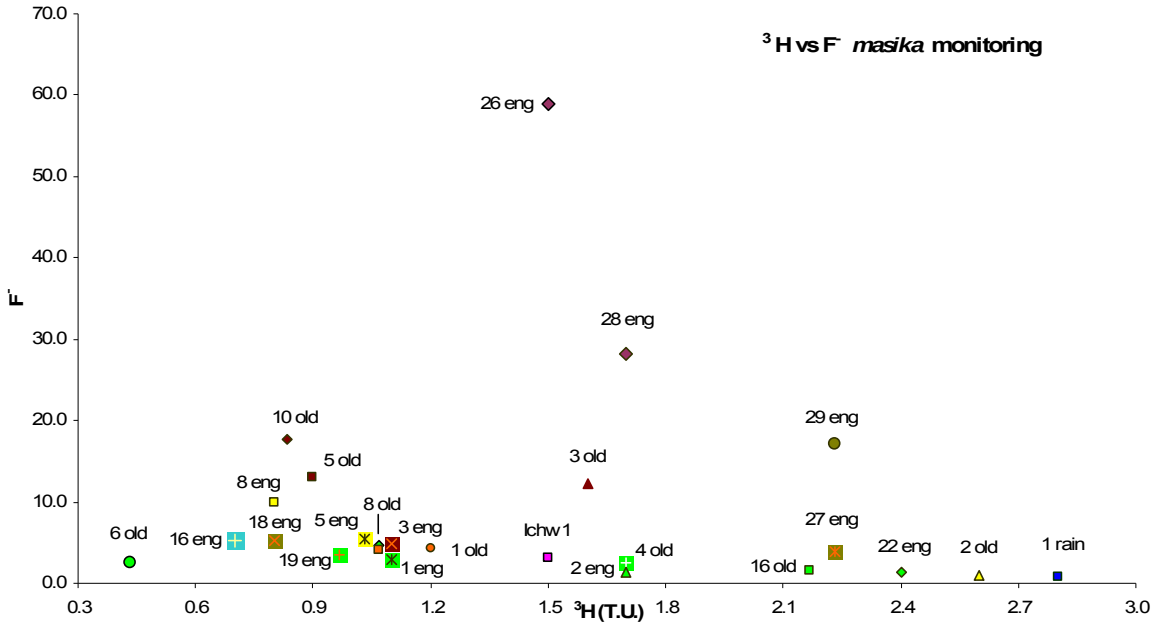

Figure 5.26- Scatter plot ^{3}H vs F$^-$

5.6. INVERSE GEOCHEMICAL MODELING

According to geochemical modelling, also fluorite (CaF_2), villiumite (NaF) and calcite ($CaCO_3$) can potentially affect the fluoride groundwater content. By means of the computer code PHREEQC, the speciation of groundwater was calculated. The results of the saturation index (SI) calculated, therefore was plotted in scatter plots. Some differences have been found, plotting the values concerning the two monitoring periods (figures 5.27 and 5.28). As shown in figure 5.27, the groundwater referred to springs 26, 28 and 30 ENG appear supersatured with respect to fluorite and, besides the 26 and the 30 ENG, also with respect to calcite. The springs 3,5 and 10 OLD and the springs 8 and 24 ENG show an intermediary sub-saturation for fluorite with SI approaching to the equilibrium, anyway suggesting dissolution. The 1 OLD spring precipitate respect to calcite phase but result subsatured referred to fluorite phase.

In general phonolite's groundwater result subsatured respect both fluorite and calcite, for the two monitoring periods. Therefore these mineral phases can have an important role in fluoride groundwater dissolution of the study area. In fact a positive growth has been observed between groundwater fluoride content and CaF_2 saturation index (figures 5.29 and 5.30).

On the contrary, the spring 26 ENG, showing a strong super-saturation for fluorite, precipitate respect to that phase and for calcite since that has and an intermediary SI value for both the monitoring periods. For this reason other sources of fluoride has been investigated.

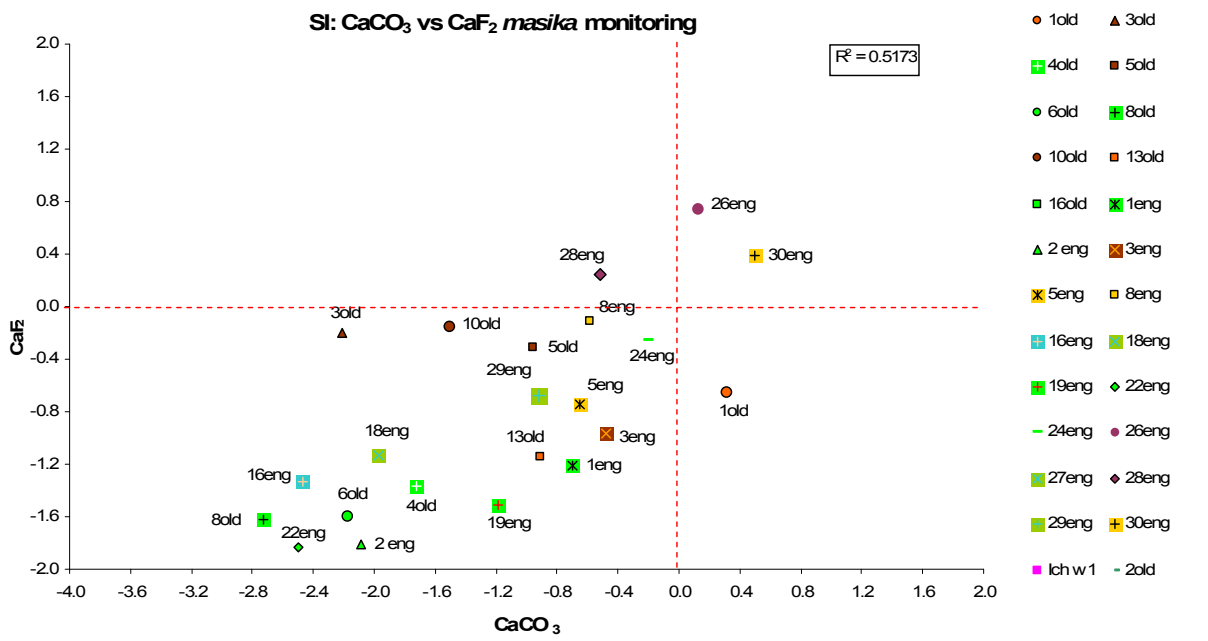

Figure 5.27 – Scatter plot CaF_2 vs $CaCO_3$ referred to *masika* monitoring

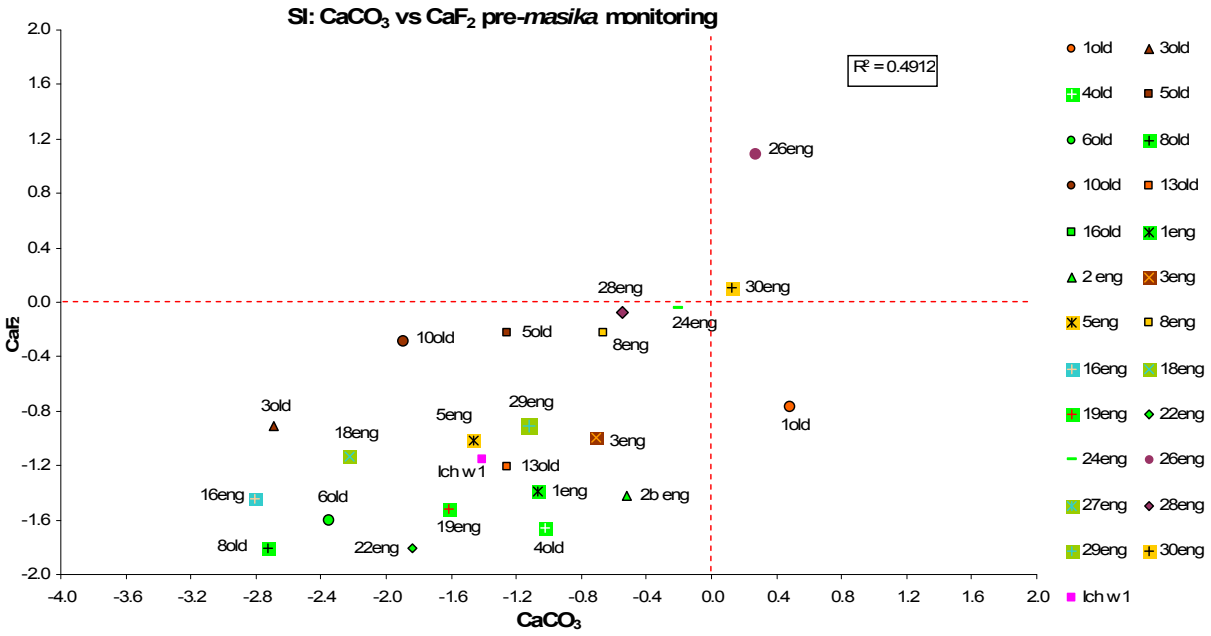

Figure 5.28 – Scatter plot CaF_2 vs $CaCO_3$ referred to pre-*masika* monitoring

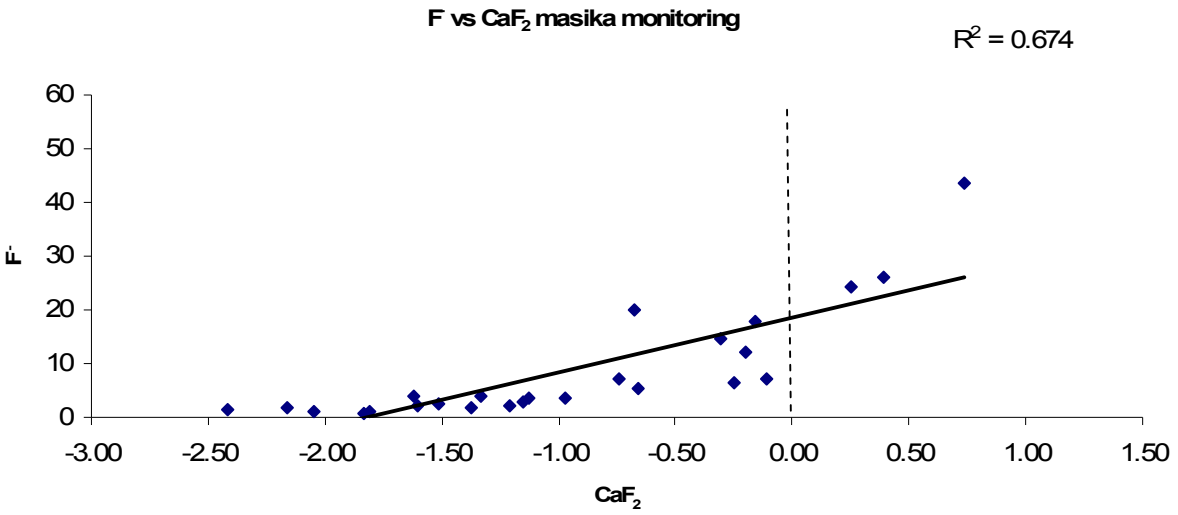

Figure 5.29 – Scatter plot CaF_2 vs F^- referred to pre-*masika* monitoring

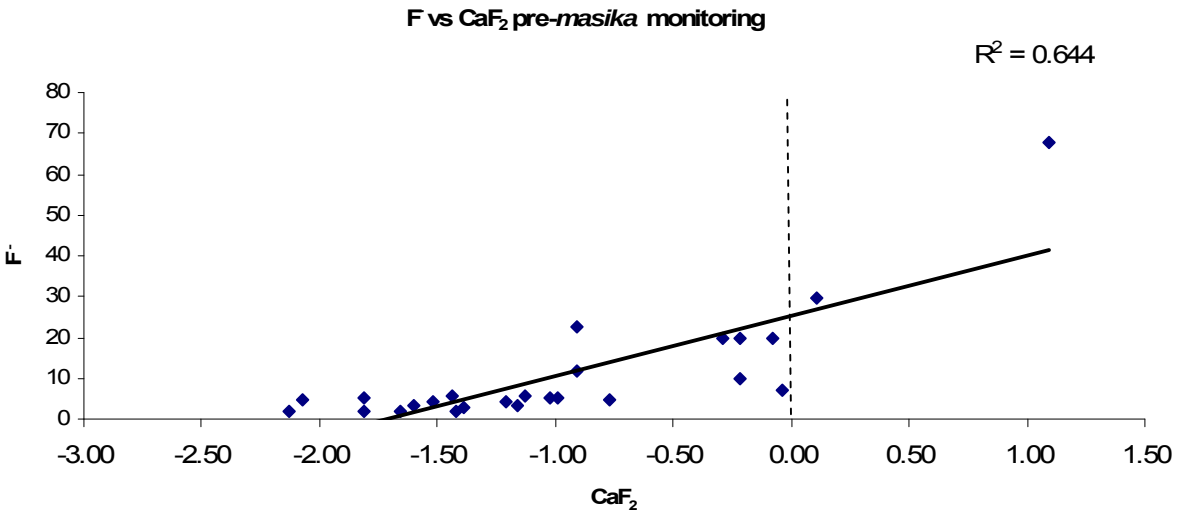

Figure 5.30 – Scatter plot CaF_2 vs F^- referred to pre-*masika* monitoring

In the figure 5.31, the 26 ENG saturation index variations for different minerals respect to the temperature increasing are shown. The CaF_2 phase, for the 26 ENG chemical composition, is not the fluoride rise since the saturation values only could be reach for temperature over 150°C. At the rise spring temperature (22°C), this phase is abundantly precipitated. The fluorapatite, instead, could be one of the sources of fluoride content; in fact whereas CaF_2 phase is thermodynamically stable and hence weakly soluble at low temperatures, the $Ca_5(PO_4)_3F$ (fluorapatite) is somewhat more soluble (Rutherford, *et al.*, 1995).

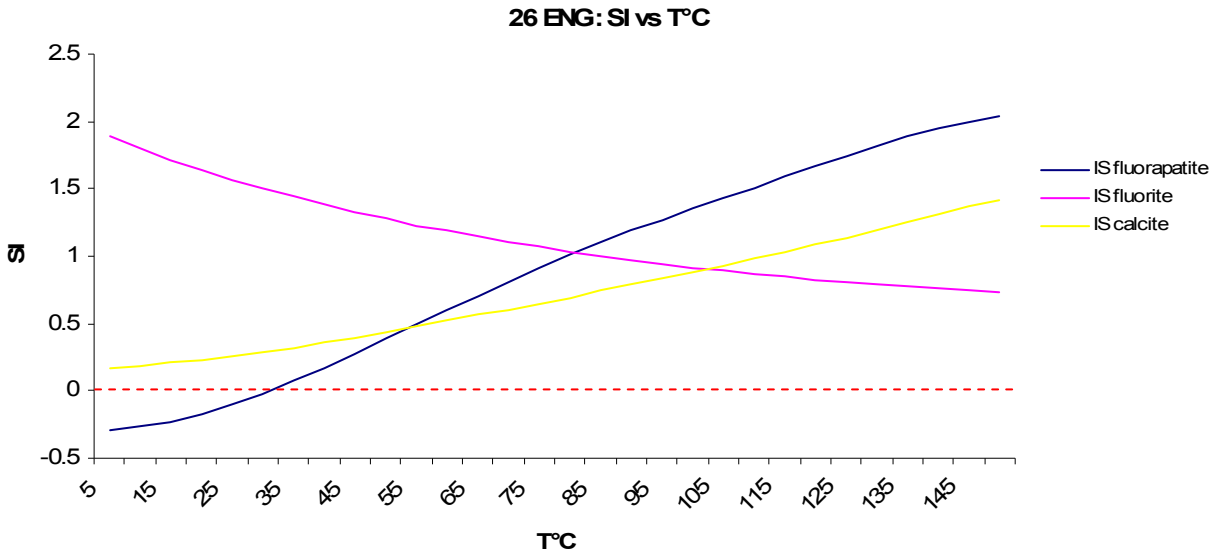

Figure 5.31 – SI mineral phases vs T°C relation for the spring 26 ENG

The groundwater sampled in the study area, show a strong sub-saturation refer to Villiaumite. According to the diagrams of figure 5.32 and 5.33, the positive correlation verified show that a common dissolution between NaF and CaF_2 can happen. The very high solubility of NaF phase is significantly correlated with fluoride content for both monitoring periods(figures 5.34 and 5.35).

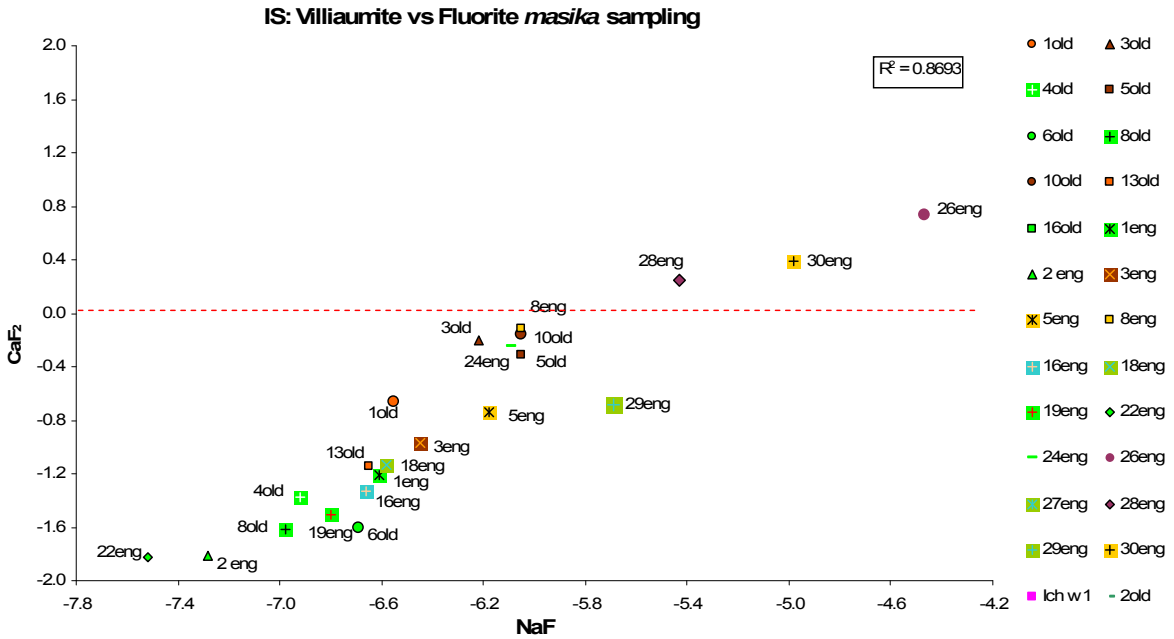

Figure 5.32 – Scatter plot CaF_2 vs NaF referred to *masika* monitoring

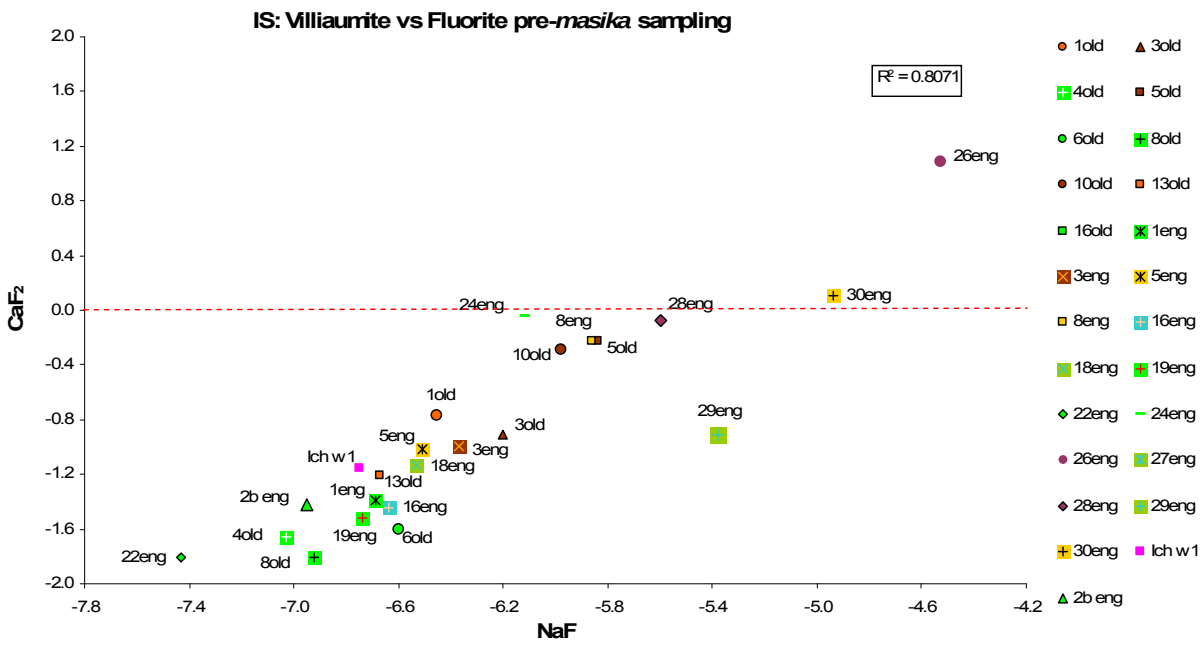

Figure 5.33 – Scatter plot CaF_2 vs $CaCO_3$ referred to pre-*masika* monitoring

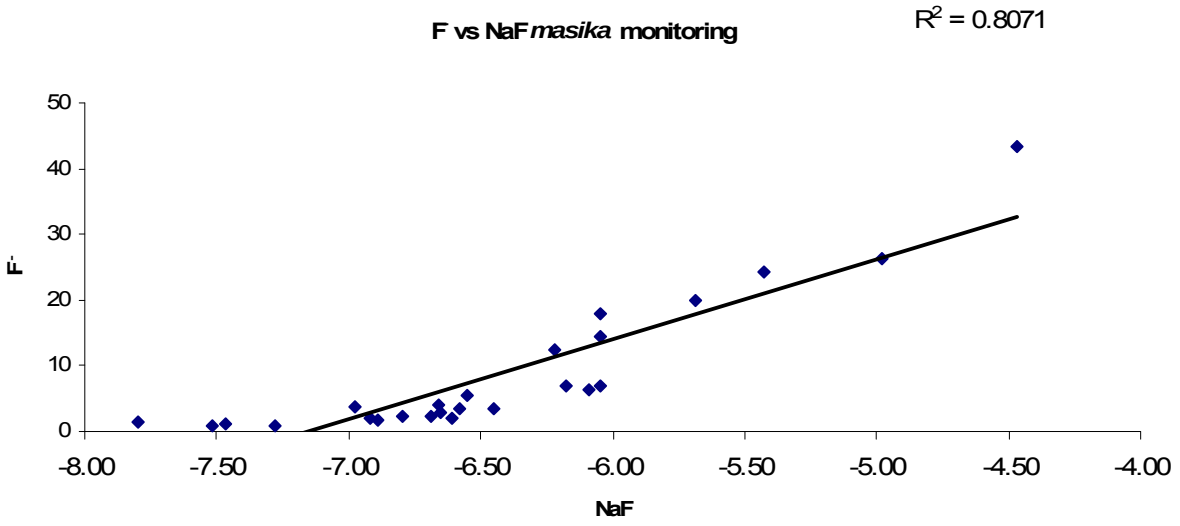

Figure 5.34 – Scatter plot NaF vs F^- referred to *masika* monitoring

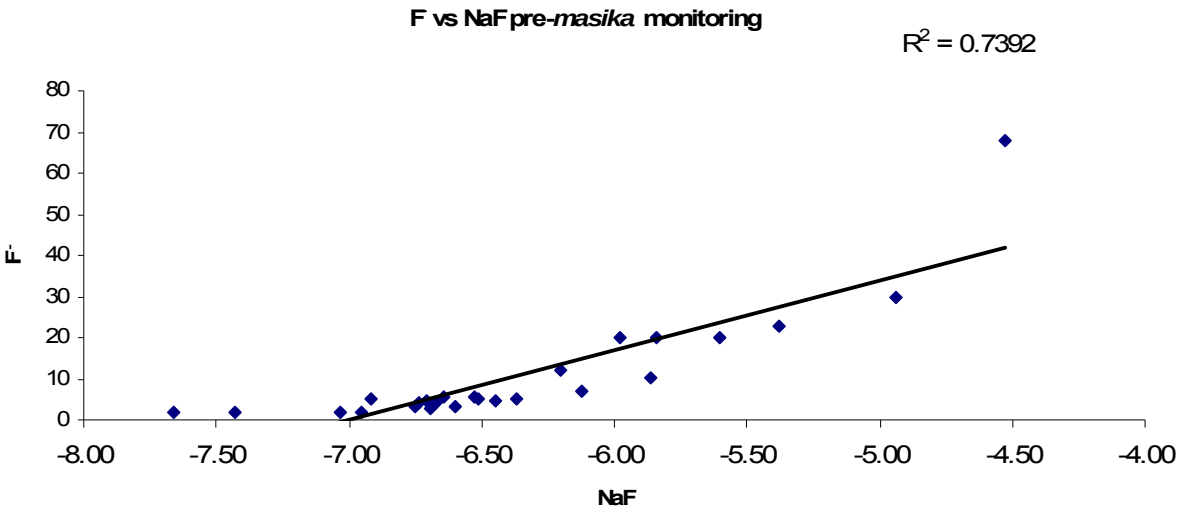

Figure 5.35 – Scatter plot NaF vs F^- referred to pre-*masika* monitoring

6. DISCUSSION

The hydrogeological issues, including the monitoring of springs and the relative fluoride content, evidenced as water pouring out from unaltered volcanic rocks such as phonolite, basalt, piroclastites, generally located at relatively high elevation on the mount Meru slope, are those affected by low content of fluoride. Two reasons can account for this feature:

- the short residence time of the groundwater responsible for the relative low water-rock interaction;
- the absence of alteration products such as paleosoils, which conversely are widesprads within the lahars. Moreover no calcrete and lacustrine salty deposits with salty soils and scooped magadi (Nielsen 1999) occur in the area. All these easy leachable products, instead occur in the Uwiro Graben and elsewhere in the distal and flat part of the volcanic building.

The weathering processes in the phonolite rocks, although limited by short residence time, enhance the leaching and the released of dissolved ionic species like HCO_3^-, SiO_2, F^-, Ca^{2+}, Na^+.
The F^- ion increase, especially in groundwater with high HCO_3^- following, fluorite dissolution reactions :

$$CaF_2 + 2HCO_3^- = CaCO_3 + 2F^- + H_2O + CO_2 \ ;$$

Moreover, as groundwaters with high HCO_3^- and Na^+ content are usually alkaline the relative high OH^- content can replace the exchangeable F^- of fluoride-bearing minerals, increasing the F^- content in groundwater. For example the reaction of biotite, that is basically:

$$KMg_3[AlSi_3O_{10}]F_2 + 2OH^- = KMg[AlSi_3O_{10}][OH]_2 + 2F^-$$

Weathering reactions also take place in silicate rocks percolated by groundwater with highest concentration in silica that are found in volcanic rocks which (Apello and Postma, 1994) contain more reactive material than rock types like mica schists or granite.
The increase of temperature enhances the dissolution rate of silicate (activation energy near 60 KJ mol^{-1}). Higher F^-, Ca^{2+} and SiO_2 concentration are reached in deep groundwater, where higher temperature of the circulating water, probably enhances the leaching of the volcanic rocks. This is also evidenced by the Na/K ratio. Relatively low

Na/K ratios tend to occur in high temperature waters (Nicholson, 1993) that have reached the surface rapidly (4 and 13 OLD).
Research developed in the North of Tanzania (Klaudius J. and Keller J., 2006; Stollhofen H. *et al*., 2008) suggests, within phonolite, the presence of phenocrysts of nepheline, augite, accumulation of sanidine and K-feldspar. From these minerals, verified also trough mineral analysis (section 5.3) the dissolution and released of the major ionic species presents in the groundwater of the study area, take place. For example, the nepheline dissolution:

$$NaAlSiO_4+2CO_2+2H_2O\rightarrow Na^+ + Al(OH)_2^+ + SiO_{2(aq)} + 2HCO_3^-\ ,$$

contribute to the release of dissolved ions like SiO_2 and HCO_3^-.
These ions too can arranges as:

$$SiO_{2(chalcedony)} \rightarrow SiO_{2(aq)}$$

$$2HCO_3^- + Ca^{2+} \rightarrow CaCO_{3(calcite)} + H_2O + CO2$$

As in the section 5.6 shown, the main fluoride source for the spring 26 ENG was attributed, especially, to the fluorapatite, according to the reaction:

$$Ca_5(PO_4)_3F+6CO_2+6H_2O\rightarrow 5\ Ca^{2+}+3H_2PO_4\text{-}+F^-+6HCO_3^-\ ;$$

as the F^- return in the groundwater, also can be available for Ca^{2+} bond:

$$2F^-+Ca^{2+}\rightarrow CaF^{2+}$$

In the lahar hidrogeological unit the composition of primary minerals and paleosoils widespread within it, strongly contribute to F^- rising. In fact, groundwater containing CO_2 can reacts with alkaline-metals silicate (albite, for example) during its seepage, thus Na^+ ion is obtained and react with water as follows:

$$2NaAlSi_3O_8 + 2H_2O\rightarrow H_2Al_2Si_2O_8\text{-}H_2O + Na_2CO_3 + 4SiO_2;$$

$$Na_2CO_3 + H_20\rightarrow 2Na^+ + HCO_3^- + OH^-$$

The above-mentioned hydrogeochemical characteristics of dominant Na ion, provide favourable conditions for migration of fluorine from rocks and concentration into water (figure 6.1 and 6.2). When Na ion in water increases, its solubility will increase correspondingly and divert more fluorine into water (Ayenew, 2008). Gao *et al*., (2007), by means a PREEQC model, evaluated as in a solution with increased Na^+/Ca^{2+} ratio (due to sodium content increase and calcium content kept invariable), the chemical conditions was advantageous to the complexation of F^- with Na^+. In fact, since the solubility of NaF is very high (42 g/L), this is favorable to the release of more fluorine into the solution.
This NaF increase was accompanied by a decrease of the HF, HF_2^- and CaF^+ concentration. The reduction of CaF^+, particularly, may induce a more undersaturated state with respect to CaF_2, and consequently an increase in fluoride content of the water.

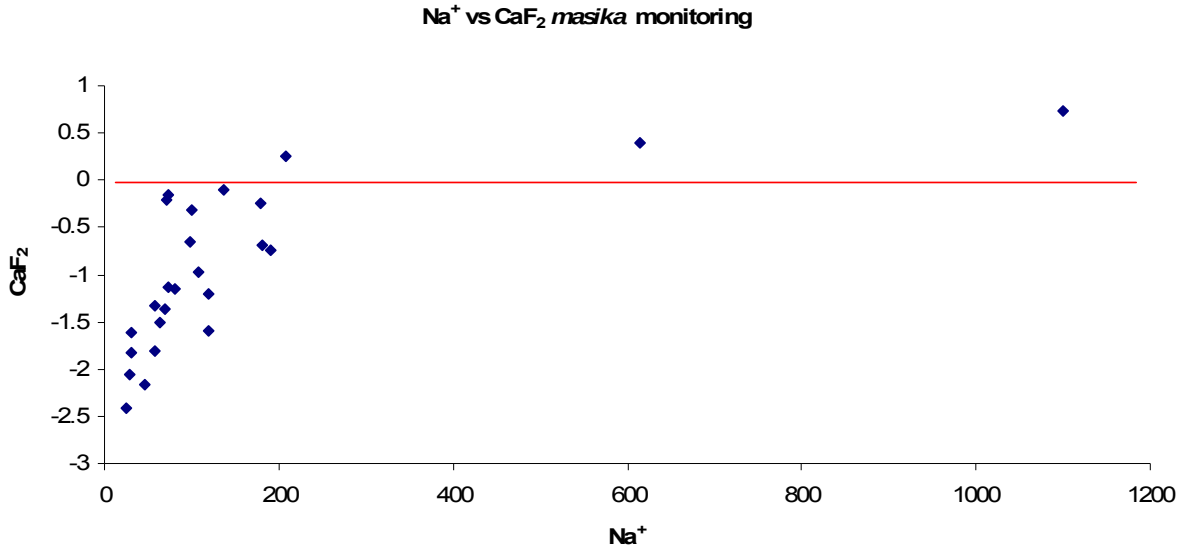

Figure 6.1 – Na^+ vs CaF_2 in *masika* monitoring

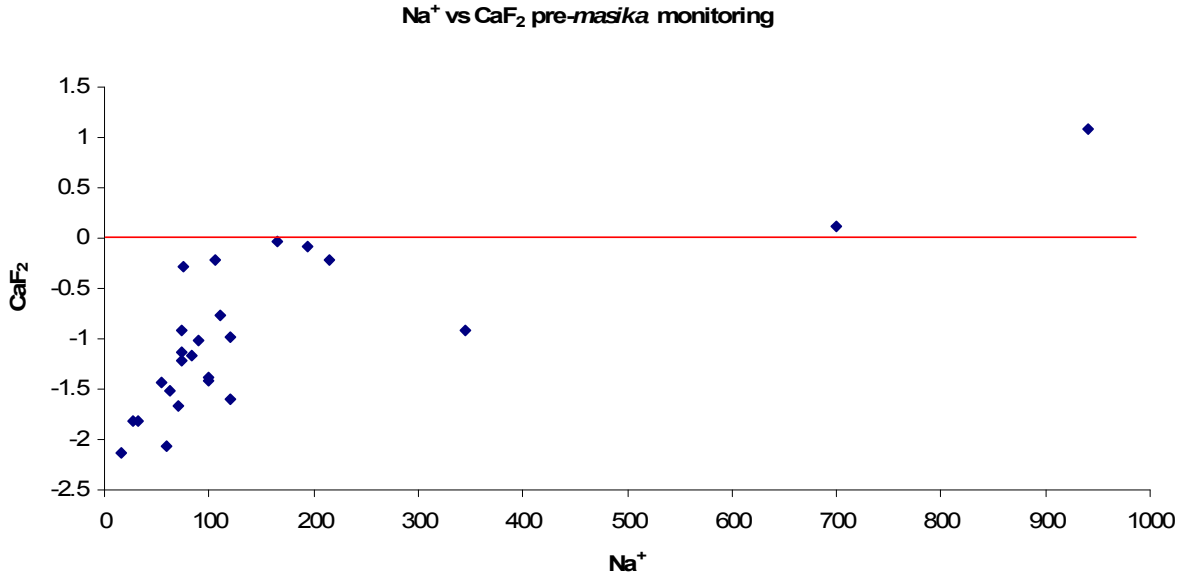

Figure 6.2 – Na^+ vs CaF_2 in pre-*masika* monitoring

7. CONCLUSION

On the basis of acquired data, shallow and deep circulating groundwater will be distinguished. Shallow groundwater that are present in perched aquifers hosted in unconsolidated or semi-unconsolidated sediments, is scarce. These aquifers are referred to as local systems because of their limited occurrence: in fact, shallow groundwater occurs only within sandy river beds. Intermediate and deep groundwater circulation systems are present in areas where the permeability of the aquifers and the elevation difference between recharge and discharge areas allows relatively deep infiltration. Another situation that can favour deeper infiltration takes place where fracturing and faulting affect brittle rocks over wide areas. In such cases a large recharge area joined with substantial rainfall can also result in good yielding wells and springs (e.g. Main cone group complex Nvm). The groundwater regional flow system has been found as generally controlled by the morphology, and involving a multidirectional flow with the dominant pattern from the higher elevation area in the south, towards the lower area in the north. Recharge occurs by direct infiltration (rainfall), by infiltration following runoff, and through lateral systems where some groundwater can flow laterally between different hydrogeologic unit. In particular, the second feature occurs in volcanic uplands, especially in correspondence of slope changes (decrease in drainage density); the third case occurs in Mkuru area where an aquifer hosted in the weathered and scoriaceous basalts, at a depth of about 40-60 m, is fed by the groundwater infiltrated at high elevation in the main cone group and Tholoid phonolites. Fractured or autobrecciated lava-flows are aquifers with low release of fluoride either for their high trasmissivity, which reduce the residence time of groundwater, and for the absence of weathering-derived products or salty deposits that, conversely, come in contact shallow groundwater mainly hosted within lahars. Geo-structural and hydrogeological data (geometry and hydraulic properties of the aquifer systems, boundary conditions, spring flow, streamflow, etc.) of the whole investigated area are not enough to allow the definition of a correct water balance, that should be necessary for computing runoff, actual infiltration and groundwater recharge.

In any case, the hydrogeochemical and hydrogeological data and the contamination fluoride model derived from the thesis work was sufficient to localized and highly suitable area for low F groundwater in the structural high within the basalt (Nvj-Northern Maar field) in correspondence of MK04 SEV. In correspondence of this favourable location a borehole was drilled (figure 7.1).

This borehole, the Ichnusa Well1, has provided a detail stratigraphy (both lithologies and thicknesses) of the Mkuru area. In particular the presence of a buried formation, which does not outcrops in the area, was observed. It was crossed from 38 m to 59 m below

g.l.; it consists of scoriaceous, autobrecciated basalt, that host a confined aquifer with high permeability, that we have named Mkuru aquifer. After drilling, one pumping test at a constant rate (drawdown log-time test) was carried out (January 2008) in order to estimate the hydraulic parameters (transmissivity and storativity) of the Mkuru aquifer. In detail, due to the limited pumping rate (3,8 L/s) allowed by the available submersible pump (lowered down the borehole at 60 m below g.l.), it was not possible to estimate the maximum pumping rate. Also the evaluation of the well efficiency by means of a test, like the SDT (Step Drawdown Test), which needs different pumping rates and significant drawdowns, was not possible. At the allowed pumping rate, the maximum drawdown was only 45 cm, such conditions permitted just a constant yield-pumping test.

Drawdown versus time measurement were collected during 48 hours at a constant pumping rate of 3,8 L/s. The pumping test (Theis Method) showed a transmissivity of 9,12 x 10-3 m^2/s and a storativity of 6,30 x 10-2 339 . No 340 kind of barrier boundary or recharge effect has been highlighted during the pumping test. However, the results obtained from the elaboration of the pumping test, allow us to state that the maximum pumping rate of Ichnusa Well1 is definitely greater than 3.8 L/s. During the test, fluoride analysis of groundwater samples were carried out in situ. The fluoride content was 3.1 g/L.

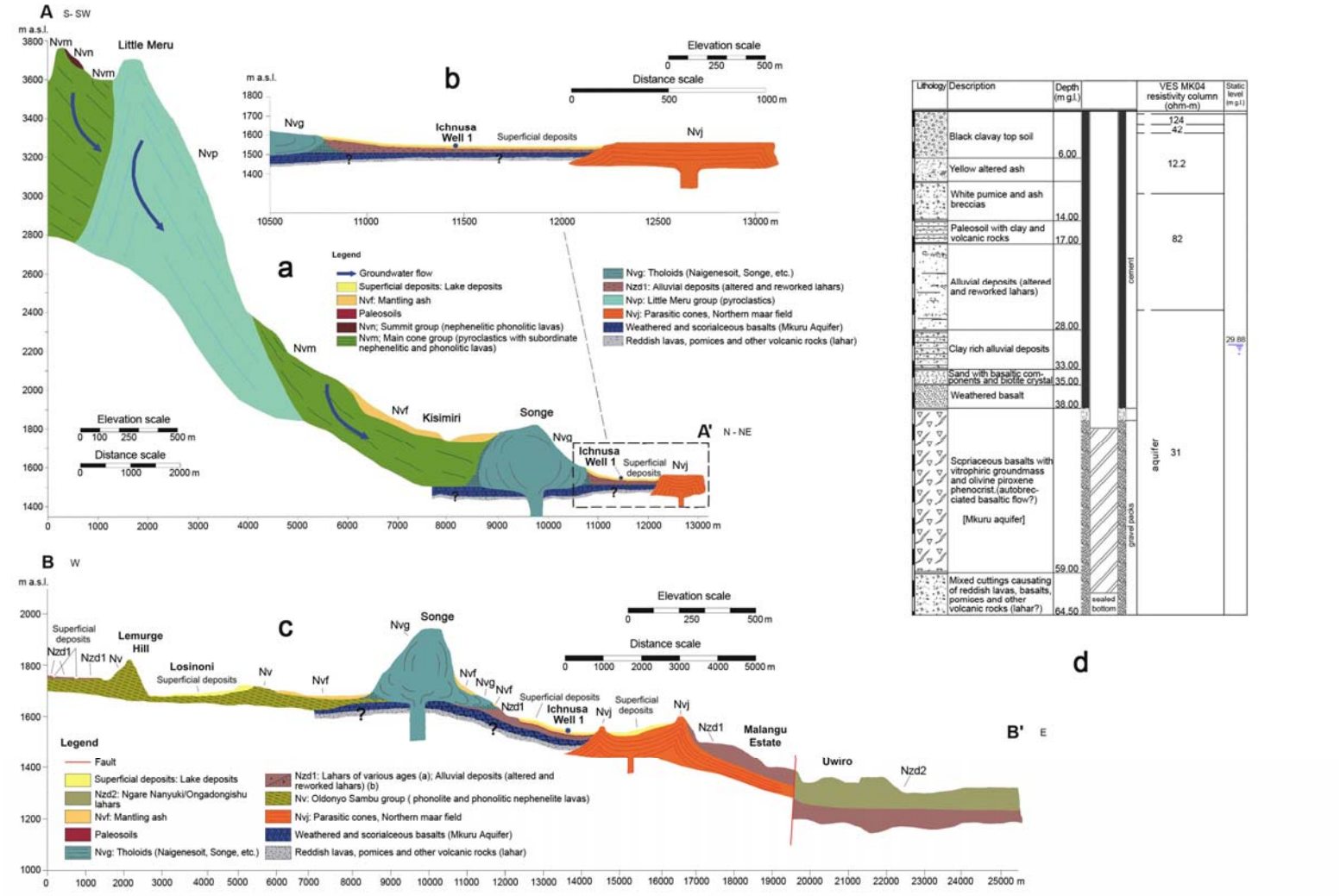

Figure 7.1 - Geolocical-Hydrogeological cross section A-A' (vertical exaggeration about x 4). b) Detail of the area surrounding the Ichnusa Well 1. c) Geological-Hydrogeological cross section B-B' (Vertical exaggeration about x7) d) – Ichnusa Well1: lithological log and well construction report. Comparison between the stratigraphy and the resistivity column of the electrical sounding MK04.

REFERENCES

Allmann R, Koritnig S, 1974. Fluorine. In: Wedepohl, KH (ed). Handbook of geochemistry. Springer, Berlin, 9-A-9-O.

Amini M., Mueller K., Abbaspour K. C ., Rosenberg T., Afyuni M. , Møller K. N., Sarr M., Johnson C.A., 2008. Statistical Modeling of Global Geogenic Fluoride Contamination in the XXVIIIth Conference of the International Society for Fluoride Research. Fluoride 41(3):233–258.

Anderson M. A., Zelazny L. W. and Bertsch P. M., 1991. Fluoro-Aluminium complexes on model and soil exchangers. Soil Sci. Soc. Am. J., 55: 71- 75.

Apambire W. B., Boyle D. R., Michel F. A., 1997. Geochemistry, genesis, and health implications of fluoriferous groundwaters in the upper regions of Ghana. Environmental Geology 33 (1).

Appelo CAJ, Postma D, 1994. Geochemistry, groundwater and pollution. Balkema, Rotterdam.

APHA, 1992. Standard methods for examination of water and wastewater. America Pubblic Health Association. Washington D.C.-APHA.

Ayenew, T, 2008. The distribution and hydrogeological controls of fluoride in the groundwater of central Ethiopian rift and adjacent highlands. Environ. Geol. 54:1313–1324. DOI 10.1007/s00254-007-0914-4.

Bagdasaryan G.P., Gerasimovskiy V.I., Polyakov A.I., Gukasyan R.K., 1973. Age of volcanic rocks in the rift zones of East Africa. Geochemistry International 10: 66–71.

Barbiero L., Valles V., Regeard A., 1995. Précipitation de la fluorine et contrôle géochimique du calcium dans des sols alcalins du Niger. Conséquences pour une estimation quantitative de l'évolution géochimique des sols. GÉOSCIENCES DE SURFACE, Comptes Rendue, 321. Academie des Sciences, Paris, pp. 1147–1154.

Banks D., Reimann C., Røyset O., Skarphagen H. and Sæther O.M., 1995. Natural concentrations of major and trace elements in some Norwegian bedrock groundwaters, *Appl. Geochem.* 10: 1–16.

Bardsen AK, Bjorvatn K, Selvig KA , 1996. Variability of fluoride content in subsurface water reservoirs. Acta Odontol Scand 54: 343–347.

Bhattacharji F. and Koide H., 1987. Theoretical and experimental studies of mantle upwelling, penetrative magmatism, and development of rifts in continental and oceanic crusts, Tectonophysics, 143: 13–30.

Boyle D.R.,1992. Effects of base exchange softening on fluoride uptake in groundwaters of the Moncton Sub-Basin, New Brunkswick, Canada. In: Kharaka YK, Maest AS (eds) Waterrock interaction. Proc 7th Int Symp Water-rock interaction. A.A. Balkema, Rotterdam, pp. 771–774.

Boyle D.R. and Chagnon M., 1995. An incidence of skeletal fluorosis associated with groundwaters of the maritime carboniferous basin, Gasp region, Quebec, Canada. *Environmental Geochemistry and Health* 17: 5-12.

Brehler B. and Fuge R., 1974. Chlorine. In: Wedepohl KH (ed) Handbook of geochemistry. Springer-Verlag, Berlin, 17-A–17-O.

Burke K. and Dewey J.F., 1973. An outline of Precambrian plate development in D.H. Tarling and S.K. Runcorn (editors) Implications of Continental Drift to the Earth Sciences. Academic Press, London, 2: 1035-45.

Carrillo-Rivera JJ, Cardona A, Edmunds WM, 2002. Using abstraction regime and knowledge of hydrogeological conditions to control high-fluoride concentration in abstracted groundwater: San Luis Potosi basin, Mexico. J Hydrol 261:24–47.

Chandra S., Thergaonkar V. P. and Sharma R.: 1981. Water quality and dental fluorosis, Ind. J. Publ. Health. 25: 47–51.

Charkes, N.D., Makler P.T., & Phillips C., 1978. Studies of skeletal tracer kinetics. I. Digital-computer solution of a five-compartment model of (18F) fluoride kinetics in humans. *J. nucl. Med.,* 19: 1301-1309.

Chaturvedi A. K., Yadava K. P., Pathak K. C. and Singh V. N. , 1990. Defluoridation of water by adsorption on fly ash

Chorowicz J., 2005. The East African rift system. Journal of African Earth Sciences 43, 379–410.

Clarke M.C.G., Woodhall D.G., Allen D. and Darling G., 1990. Geological, volcanological and hydrological controls on the occurrence of geothermal activity in the area surrounding Lake Naivasha, Kenya, *Ministry of Energy Report*, Nairobi, Kenya, 138 pp.

Coleman *et al*., 1982. Reduction of water with zinc for hydrogen isotope analysis. Anal. Chem., 54: 993-995.

Courtillot V., Arcache J., Landre F., Bonhommet N., Montigny R. and Féraud G., 1984. Episodic spreading and rift propagation: new paleomagnetic and geochronologic data from the Afar nascent passive margin. *J. Geophys. Res.* 89: 3315–3333.

Cronin S.J., Neall V.E., Lecointre J.A., Hedley M.J., Loganathan P., 2003. Environmental hazards of fluoride in volcanic ash: a case study from Ruapehu volcano, New Zealand. J Volcanol Geotherm Res 121:271–291

Datta P.S., Deb D.L., Tyagi S.K., 1996. Stable isotope ($^{18}0$) investigations on the processes controlling fluoride contamination of groundwater. Journal of Contamination Hydrology 24: 85-96.

Davidson A., Rex D.C. ,1980. Age of volcanism and rifting in southern Ethiopia. Nature 283: 657-658

Davies T.C., 1996. Chemistry and pollution of natural waters in western Kenya. Journal of African Earth Sciences 23, 4: 547-563.

Dawson J.B., 1992. Neogene tectonics and volcanicity in the North Tanzania sector of the Gregory Rift Valley: contrasts with the Kenya sector. Tectonophysics Volume 204, Issues 1-2: 1-195.

Dettman D.L., Palacios-Fest M.R., Nkotagu H., Cohen A.S. 2005. Paleolimnological investigations of anthropogenic environmental change in Lake Tanganyka: VII. Carbonate isotope geochemistry as a record of riverine runoff. Journal of Paleolimnology 34: 93-105.

Edmunds M. and Smedley P., 2005. Fluoride in natural waters. In O. Selinus, B. Alloway, J. Centano, R. Finkelman, R. Fuge, U. Lindh and P. Smedley, Editors. Book: Essential of medica geology – Impact of the natural environment on public health. Pp. 310-330. ISBN 0-12-36341-2.

Epstein S. and Mayeda T., 1953. Variation of ^{18}O content of waters from natural sources. Geochimica et Cosmochimica Acta, v. 4, n. 5: 213-224.

Fawell J., Bailey K., Chilton J., Dahi E., Fewtrell L. and Magara Y., 2006. Fluoride in Drinking-water. Published on behalf of the World Health Organization by IWA Publishing, Alliance House, 12 Caxton Street, London SW1H0QS, UK. ISBN 1900222965.

Fleischer M. and Robinson W.O., 1963. Some problems of the geochemistry of fluorine. In Studies in analytical geochemistry, the royal society of Canada special pubblications n°6, edited by Denis M. Shaw; pp. 58-75.

Fleischer M., Forbes R.M., Ozsvath D.L., 2006. Fluoride concentrations in a crystalline bedrock aquifer Marathon County, Wisconsin. Environ Geol, 50: 132–138 DOI 10.1007/s00254-006-0192-6.

Flühler, H., Polomski, J. and Blaser, P., 1982. Retention and Movement of Fluoride in Soils. J. Environ. Qual. 11/3: 461-468.

Foster A, Ebinger C., Mbede E. and Rex D., 1997. Tectonic development of the northern Tanzanian sector of the East African Rift System. *Journal of the Geological Society*; 154, 4: 689-700; DOI: 10.1144/gsjgs.154.4.0689.

Frengstad B., Banks D., Siewers U., 2001. The chemistry of Norwegian groundwaters: IV. The dependence of element concentrations in crystalline bedrock groundwaters. Sci. Total Environ. 277: 101–117.

Fuge R. and Andrews M.J., 1988. Fluoride in the UK environment. Environ. Geochem. Health 10: 96-104.

Gaciri S.J. and Davies T.C., 1993. The occurrence and geochemistry of fluoride in some natural waters of Kenya. *Journal of Hydrology,* 143: 395-412.

Gao X., Wang Y., Li Y., Guo Q., 2007. Enrichment of fluoride in groundwater under the impact of saline water intrusion at the salt lake area of Yuncheng basin, northern China. Environ Geol DOI 10.1007/s00254-007-0692-z.

Gaus I., Shand P., Gale I.N., Williams A.T., Eastwood J.C., 2002. Geochemical modeling of fluoride concentration changes during aquifer storage and recovery (ASR) in the Chalk aquifer, Wessex, England. Q J Eng Geol Hydrogeol 35(2):203–208.

Ghiglieri G., Balia R., Oggiano G., Ardau F., Pittalis D., 2008. Hydrogeological and geophysical investigations for groundwater in the Arumeru District (Northern Tanzania). Presentation at the 84° National Meeting of the Italian Geologic Society. Sassari 15 – 17 September 2008 (Conference Proceedings, pp. 431-433 vol.2).

Gittins M.J., 1985. Fluorine and Fluorides. Book Reviews: Environmental Health Criteria 36. Published by WHO, 1984. Pp. 136. ISBN: 92 4 154096 6.

Gizaw, B., 1996. The origin of high bicarbonate and fluoride in the Main Ethiopian Rift Valley, East African Rift system. J. Afr. Earth Sci. 22, 392–402.

Godwin F. Mollel , Swisher III C. C., Feigenson M. D., Carr M. J., 2008. Geochemical evolution of Ngorongoro Caldera, Northern Tanzania: Implications for crust–magma interaction Earth and Planetary Science Letters 271: 337–347.

Groth III E., 1975. Fluoride Pollution. Environment 17: 29-38.

Grynpas M., 2008. Fluoride effects on bone quality are influenced by genetics and environmental Factors. Conference abstracts Fluoride 41(3)233–258.

Handa BK 1975 Geochemistry and genesis of fluoride contains groundwater in India. Ground Water 13:275–281.

Hijmans R.J., Cameron S.E, Parra J.L., Jones P.G. and Jarvis A., 2005. Very high resolution interpolated climate surfaces for global land areas. *Int. J. Climatol.* 25: 1965–1978 (2005).

Isaacson R., 2008. Fluoride and the brain: dangers and diversities. Conference abstracts Fluoride 41, 3: 233–258. Abstracts from the XXVIIIth Conference of the International Society for Fluoride Research.

Jacks, G., Bhattacharya, P., Chaudhary, V., Singh, K.P., 2005. Controls on the genesis of some high-fluoride groundwater in India. Applied Geochemistry 20, 221–228.

Jones B.F., Eugster H.P. and Rettig S.L., 1977. Hydrochemistry of the Lake Magadi basin, Kenya. *Geochim. Cosmochim. Acta* 41: 53–72.

Kaseva M. E., 2006. Contribution of trona (magadi) study into excessive fluorosis – a case study in Maji ya Chai ward, northern Tanzania. Science of total environment, vol. 366, 1: 92-100

Kharb P., Susheela A.K., 1994. Fluoride ingestion in excess and its effect on organic and certain inorganic constituents of soft tissues. Med. Sci. Res. 22: 43–44.

Klaudius J. and Keller J., 2006 - Peralkaline silicate lavas at Oldoinyo Lengai, Tanzania. Lithos 91: 173–190.

Kilham P. and Hecky R.E., 1973. Fluoride: Geochemical and Ecological significance in East African waters and sediments. Limnology And Oceanography. November, V. 18(6).

Kim K. and Jeong G.Y., 2005. Factors influencing natural occurrence of fluoride-rich groundwaters: a case study in the southeastern part of the Korean Peninsula. Chemosphere 58: 1399–1408.

Koefoed O., 1972. A note on the linear filter method of interpreting resistivity sounding data. Geophysical Prospecting, 20: 403-405.

Koefoed O., 1979. Geosounding Principles, 1: Resistivity Sounding Measurements. Elsevier Science Publ. Co. Inc.

Le Gall B., Nonnotte P., Rolet J., Benoit M., Guillou H., Mousseau-Nonnotte M., Albaric J., Deverchère J., 2007. Rift propagation at craton margin. Distribution of faulting and volcanism in the North Tanzanian Divergence (East Africa) during Neogene times. Tectonophysics, Vol. 448, issues 1-4: 1-19.

Leone A, Brennan E G, Daines R H and Robbins W R, 1948. Some effects of fluorine on peach, tomato, and buckwheat when absorbed through roots. Soil Sci. 66, 259–266.

Lister G. S., Etheridge M. A. and Symonds P. A., 1986. Detachment faulting and the evolution of passive continental margins. *Geology,* v. 14; no. 3: 246-250; DOI: 10.1130/0091-7613.

Lundgren B. and Lundgren L., 1972. Comparison of some soil properties in one forest and two grassland ecosystems on mount Meru, Tanzania, *Geografiska Annaler. Series A, Physical Geography*, Vol. 54, 3/4. Studies of soil erosion and sedimentation in Tanzania, pp. 227-240. Published by: Blackwell Publishing on behalf of the Swedish Society for Anthropology and Geography. Stable URL: http://www.jstor.org/stable/520768

M.C. Latham and P. Grech, 1967. The effects of excessive fluoride intake, Am. J. Public Health, 57: 651-666.

Maalde M.J.K., Maage A., Macha E., Julsham K., 1997. Fluoride content in selected food items from five areas in Eastern Africa. Journal of Food Composition and Analysis 10: 233-45.

Madhavan N. and Subramanian V., 2001 Fluoride concentration in river waters of south Asia. Current science, vol. 80, no. 10.

Madhavan N. and Subramanian V., 2006. Environmental impact assessment including evolution of Fluoride and Arsenic contamination process in groundwater and remediation of contaminated groundwater system. In Sustainable Development and Management of Groundwater Resources, edited by M. Thangarajan, Capital Publishing Company, New Delhi (ISBN 81-85589-30-5). pp.128-155.

Mameri N., Yeddou A.R., Lo unici H., Grib H., Belhocine D., Bariou B., 1998. Defluoridation of septentrional Sahara water of North Africa by electrocoagulation process using bipolar aluminium electrodes, Water Res. 32 (5), 1604–1610.
Miller, G. W., *Fluoride*, 1993, 26, 3–22.

McClusky S., Reilinger R., Mahmoud S., Ben Sari D. and Tealeb A., 2003. GPS constraints on Africa (Nubia) and Arabia plate motions. Geophys. J. Int.. 155: 126-138.

McKenzie D.P., 1978. Some remarks on the development of sedimentary basins, *Earth Planet. Sci. Lett.* 40: 25–32.

Meenakshi M.R.C. and Maheshwari R.C., 2006. Fluoride in drinking water and its removal. Journal of Hazardous Materials 137 (1), 456–463.

Murray J.J. [Ed.] 1986 *Appropriate Use of Fluorides for Human Health*, World Health Organization, Geneva. National Plan for Oral Health 1988–2002, 1988. Ministry of Health and Social Welfare United Republic of Tanzania, pp. 14–15.

Nanyaro J. T., Aswathanarayana U., Mungure J. S. and Lahermo P. W., 1984. A geochemical model for the abnormal fluoride concentrations in waters in parts of northern Tanzania, J. African Earth Sci., 2: 129-140.

Nicholson K., 1993. Geothermal fluids, chemistry and exploration techniques. Springer, Berlin

Nielsen J.M., 1999. East African magadi (trona): fluoride concentration and mineralogical composition. Journal of African Earth Sciences 29: 423-428.

Nkotagu H.H. and Mwambo K., 2000. Hydrology of selected watersheds along the Lake Tanganyka shoreline. Lake Tanganyka Biodiversity project, Technical Research Report No. 11, RAF/92/G32, 111 pp.

Nordstrom DK, Ball JW, Donahoe RJ, Whittemore D., 1989. Groundwater chemistry and water–rock interactions at Stripa. Geochim Cosmochim Acta;53:1727–40.

Nordstrom DK, Jenne E.A., 1977. Fluoride solubility in selected geothermal waters. Geochimica Cosmochimica Acta 41:175–188.

O'Neill D.J. and Merrick N.P., 1984. A digital linear filter for resistivity sounding with a generalized electrode array: Geophysical Prospecting, 32: 105-123.

Omueti J. A. I. and Jones R. L., 1977. Fluoride adsorption by Illinois soils. *J. Soil Sci*., 28: 564-572.

Pauling L., 1960. The nature of the chemical bond and the structure of molecules and crystals: an introduction to modern structural chemistry. Cornell University Press, NY, p 644.

Pauwels H. and Ahmed S., 2007. Fluoride in groundwater: origin and health impacts. Géosciences - La revue du BRGM pour une terre durable 5: 68-73.

Pavoni N., 1993. Rifting of Africa and pattern of mantle convection beneath the African plate. Tectonophysics ISSN 0040-1951.

Peter Kilham P. and Hecky R.E., 1973. Fluoride: geochemical and ecological significance in east african waters and sediments. Limnology and Oceanography, V. 18 (6).

Raju N. J., Dey S., Das K., 2009. Fluoride contamination in groundwaters of Sonbhadra District, Uttar Pradesh, India. Current Science, Vol. 96, No. 7.

Rao S., 1997. The occurrences and behavior of fluoride in groundwater of the lower Vamsadhara River basin, India. J Hydrol Sci 42, 6: 877–891.

Rukah A.Y. and Alsokhny K., 2004. Geochemical assessment of groundwater contamination with special emphasis on fluoride concentration, North Jordan. Chemie der Erde 64: 171–181.

Saxena V.K. and Ahmed S., 2003. Inferring the chemical parameters for the dissolution of fluoride in groundwater. Environmental Geology 43:731–736.

Sebag D., Verrecchia E.P., Leed S.J., Durand A., 2001. The natural hydrous sodium silicates from the northern bank of Lake Chad: occurrance, petrology and genesis. Sedimentary geology, 139, 1: 15-31.

Smedley P.L., Nicollib H.B., Macdonalda D.M.J., Barrosb A.J., Tullioc J.O., 2002. Hydrogeochemistry of arsenic and other inorganic constituents in groundwaters from La Pampa, Argentina. Applied Geochemistry 17: 259–284.

Stollhofen H., Stanistreet I.G., McHenry L.J., Mollel G.F., Blumenschine R.J. and Masao F.T., 2008. Fingerprinting facies of the Tuff IF marker, catastrophe for early hominin palaeoecology, Olduvai Gorge, Tanzania, *Palaeogeography, Palaeoclimatology, Palaeoecology* 259: 382–409.

Teotia S.P.S, Teotia M., Singh R.K., 1981. Hydro-Geochemical Aspects of Endemic Skeletal Fluorosis in India - an Epidemiologic Study. Fluoride, Vol. 14, no. 2: 69-74.

Teotia SPS and Teotia M., 1988. Endemic skeletal fluorosis: clinical and radiological variants. Fluoride 21: 39-44 .

Todd D.K., 1980. Groundwater Hydrogeology.

Travi Y., 1993. Hydrogéologie et hydrochimie des aquifères du Sénégal, Sciences Géologiques, Mémoire 95, Université de Paris Sud.

UN, 2008 The Millennium Development Goals Report. UNITED NATIONS New York.

UN, 2009 The Millennium Development Goals Report. UNITED NATIONS New York.

U.S. DEPARTMENT OF ENERGY, Environmental Measurements Laboratory, 1997. Tritium in water – acid electrolysis – 3H – 01 – RC, HASL – 300, 28th Edition.

USNRC, 1993. National Research Council. Health Effects of Ingested Fluoride.

Vuhahulaa E.A.M ,. Masalua J.R.P, Mabelyaa L.,. Wandwib W.B.C, 2008. Dental fluorosis in Tanzania Great Rift Valley in relation to fluoride levels in water and in 'Magadi' (Trona). Desalination 252: 193–198.

Wang Y., Nahon D., Merino E., 1993. Geochemistry and dynamics of calcrete genesis in semi-arid regions. Chemical Geology 107, 349–351.

Wedepohl K.H., 1974. Handbook of geochemistry. Executive editor K.H. Wedepohl. Springer, Berlin, Heidelberg, New York.

Wedepohl K. H., 1978. Handbook of Geochemistry 11, Sections 73, B-G. Springer-Verlag.

Wernicke B. and Burchfield B.C., 1982. Modes of extensional tectonics. J. Struct. Geol., 4:105-115.

WHO World Health Organization, 1984. Guidelines for drinking water quality, vol 2. Health criteria and other supporting information. WHO, Geneva.

Williams L. A. J. , 1969 - Geochemistry and petrogenesis of the kilimanjaro volcanic rocks of the Amboseli area, Kenya. Volume 33, Number 3 / September. ISSN 0258-8900 (Print) 1432-0819 (Online)

Wood J. and Guth A., 2009. East Africa's Great Rift Valley: A Complex Rift System. http://geology.com/articles/east-africa-rift.shtml

Yoder K., Mabelya L., Robison V., Stookey G., Brizendine E. and Dunipace E., 1998. Severe dental fluorosis in a population, consuming water with negligible fluoride concentration, Commun. Dent. Oral. Epidemiol., 26, 382–393.

ACKNOWLEDGEMENTS

First and foremost, I would like to thank the Prof. Giorgio Ghiglieri (*Giorgio*) my tutor, for believing in me, for supporting this research activity, for, patiently, understand my difficult moments and because is a special person….*mzuri sana, cabisa*.

I am greatly indebted to Prof. Giacomo Oggiano for significantly supporting, facilitating and improving this research activity…..*siddai lavalè, tcul.*

I would like to thank my colleague Eng. Alberto Carletti (*Alberto*) for supporting our scientific common works (not only the "cross-section") and because is a trust friend.

I am thankful for the InTReGA's real friends as well as colleagues of a little dream that is becoming big….Ile, Giovanni and Tomoro always thank, also for supporting some personal "particular moments", and Massimo Iannetta a good and positive friend that believe in the dream like us.

I would also like to thank Prof. Roberto Balia, University of Cagliari, for the Geophysical activity.

I am also thankful to Prof. M. Dore for believing in me and for……. many things.

I sincerely thank the Geopedology and Applied Geology section staff (particularly Mariolino always prodigal of highly professional good advices and for supporting me in the analytical analyses, Prof. Gabriella Pulina for her gentle support and Dr. Giulia Urracci) and the Engeenering Territorial Department staff of Sassari University.

I am also thankful for Dr. Antonio Brundu, Department of Botanical, Ecological and Geological Sciences, University of Sassari for kindly carrying out the necessary XRF analyses.

I would also like Dr. Stefano Cuccuru, Department of Botanical, Ecological and Geological Sciences, University of Sassari, for providing rock sample preparation facilities.

I am grateful to NRD-UNISS (Desertification Research Group- University of Sassari), the financial grant for my professional experiences is gratefully acknowledged. Still I would like to thank all the staff members, particularly Valeria Sanna for supporting my bureacratic "incasinamenti", Roberta and Francesca.

Thanks are due also to Fondazione Banco di Sardegna for the financial support.

I am also thankful for Prof. Albert Soler Gil, Universitat de Barcelona, and his staff in supporting me referred to isotopic consultations, as well as the CSIC researchers Carlos Ayora y Enriquez Vasquez.

I am grateful to Dr. Massimo Marchesi, Universitat de Barcelona, for the support in the University and in the Barcelona experience.

I would also like to thank Dr. Elena Rossi for her valuable assistance in PhD question.

I would like to thank Dr. Rossella Rossi (OIKOS), Prof. Guido Tosi (University of Insubria) and all the OIKOS and OIKOS East Africa staff members for supporting my unforgettable Tanzanian Africa's experiences….thanks to Eng. Simon Kayala, Dr. Allesandra Confalonieri, Eng.Claudio Deola, Mzé Mr. Chambi (great), Mr. Mika, Makelala, Samueli, Adani, Jeremya, Abraham, Aimidiwe, Peter, Bere, Lily, Dr. Jean Mary, Mawala, Dr. Andrea Mandrici, Isa, the athari masai: Isaia Thomas and Joanna…."sorry for forgetting someone".

I am grateful to Georgy the athari buffalo driver Maasai….for the very long walk-climb and car tours in savana and in Mount Meru environment…*rafiki kubua*.

I am thankful to Georgy Nataely the maji discoverer and field guide in Oldonyosambu ward and the Ngarenanyuky ward staff, particularly Danieli (tendagi of Kisimiri Juu).

I wish to thank, strongly, Isaia the Magnakiti…*aljerallé*…for supporting me in a first and single difficult moment in Tanzania. I will not forget your friendship. *Sere*.

I would like greatly the Maasai people of Mkuru and the Meru people of Ngarenanyuky….and really that big land: the AFRICA……with its sun, smell, slow special time, people, its *ntotos* and fascinate *mamas*.

I also thank to all friends and colleagues who have accompanied and assisted me all along and my goddaughter Andrea Carlotta for her great peacefulness. I am very much thankful.

My deepest heartfelt gratitude goes to my family: Mamma e Babbo for believe in me ALWAYS and for belonging to your family, Andrea e Angelo my brothers with my sisters in law, my godson Alessandro and my nephew Francesca….I love you so much.